National Research FLAGSHIPS
Water for a Healthy Country

CSIRO

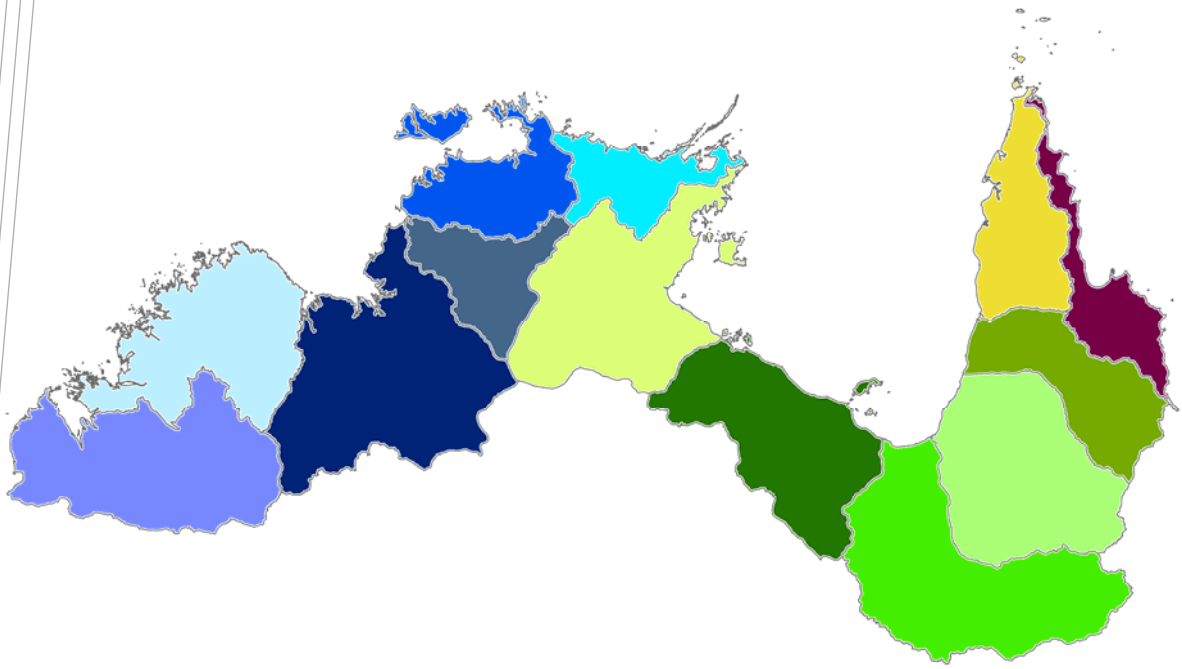

www.csiro.au

Diffuse groundwater recharge modelling across northern Australia

Russell S. Crosbie, James L. McCallum and Glenn A. Harrington

A report to the Australian Government from the CSIRO Northern Australia Sustainable Yields Project

December 2009

Northern Australia Sustainable Yields Project acknowledgments

Prepared by CSIRO for the Australian Government under the Raising National Water Standards Program of the National Water Commission (NWC). Important aspects of the work were undertaken by the Northern Territory Department of Natural Resources, Environment, The Arts and Sport (NRETAS); the Queensland Department of Environment and Resource Management (QDERM); the New South Wales Department of Water and Energy; Sinclair Knight Merz; Environmental Hydrology Associates and Jolly Consulting.

The Project was guided and reviewed by a Steering Committee (Kerry Olsson, NWC – co-chair; Chris Schweizer, Department of the Environment, Water, Heritage and the Arts (DEWHA) – co-chair; Tom Hatton, CSIRO; Louise Minty, Bureau of Meteorology (BoM); Lucy, Vincent, Bureau of Rural Sciences (BRS); Tom Crothers, QDERM; Lyall Hinrichsen, QDERM; Ian Lancaster, NRETAS; Mark Pearcey, DoW; Michael Douglas, Tropical Rivers and Coastal Knowledge (Strack); Dene Moliere, Environmental Research Institute of the Supervising Scientist (*eriss*); secretariat support by Angus MacGregor (DEWHA) and benefited from additional reviews by a Technical Reference Panel and other experts, both inside and outside CSIRO.

Citation

Crosbie RS, McCallum JL and Harrington GA (2009) Diffuse groundwater recharge modelling across northern Australia. A report to the Australian Government from the CSIRO Northern Australia Sustainable Yields Project. CSIRO Water for a Healthy Country Flagship, Australia. 56 pp.

Publication Details

ISSN 1835-095X

Preface

This is a report to the Australian Government from CSIRO. It is an output of the CSIRO Northern Australian Sustainable Yields Project which, together with allied projects for Tasmania and south-west Western Australia, provide a nation-wide expansion of the assessments that began with the CSIRO Murray-Darling Basin Sustainable Yields Project.

The projects are the first rigorous attempt to estimate the impacts of catchment development, changing groundwater extraction, climate variability and anticipated climate change on water resources at a whole-of-region scale, explicitly considering the connectivity of surface and groundwater systems. The CSIRO Northern Australian Sustainable Yields Project has undertaken the most comprehensive hydrological modelling ever attempted for the region, using rainfall-runoff models, groundwater recharge models, river system models and groundwater models, and considering all upstream-downstream and surface-subsurface connections.

Executive summary

The Northern Australia Sustainable Yields (NASY) Project aims to investigate the water resources across northern Australia now and into the future. Groundwater recharge is only a small component of the water balance but has an influence on the amount of groundwater available for consumptive use and sustaining groundwater dependant ecosystems. Prudent management of water resources requires that all threats to water availability are investigated and assessed for uncertainty. Climate change is one threat to our water resources and its impact upon groundwater recharge has been investigated here. This project follows on from the Murray-Darling Basin Sustainable Yields (MDBSY) Project and the methods used here are based upon those used in the MDBSY project.

Groundwater recharge was modelled at selected points using the WAVES (Zhang and Dawes, 1998) model for a variety of soil and vegetation types and is reported as a scaling factor that is the ratio of a given scenario to historical recharge rates. Recharge scaling factors were calculated for each climate scenario at those selected points. The point scale estimates of the recharge scaling factors were then upscaled to the entire NASY project area using soil type, vegetation type and rainfall as covariates to create rasters of recharge scaling factors for each scenario.

There are few field estimates of recharge across northern Australia so the model parameters were not calibrated. The estimates of historical recharge from this project were compared to estimates made using independent methods (chloride mass balance and baseflow separation). The results of the comparison were generally similar and so some confidence can be had that the historical estimates of recharge are appropriate. The impact of the uncertainty in the historical estimates of recharge was minimised by reporting the results as recharge scaling factors that are the scenario recharge relative to the historical recharge.

The climate scenarios investigated here are the historical climate (Scenario A), the recent climate (Scenario B) and three future climate scenarios (Scenario C) developed using 15 different global climate models (GCM) under high, medium and low global warming scenarios (i.e. 45 future climate sequences). The outputs of this modelling are a series of rasters for the change in recharge throughout the NASY project area at a resolution of 0.05° × 0.05° (~29 km^2) for each of these climate sequences. The results of Scenario C are presented as a composite of the different global climate models to create a wet extreme, median and dry extreme scenario. These rasters were aggregated to provide a single recharge scaling factor for each region. The recharge scaling factors were then used to assess the change in groundwater resources of northern Australia, as reported elsewhere.

Under the historical climate (Scenario A) results are very consistent between reporting regions with the median projection (Scenario Amid) for the next 23 years being a 2 to 3 percent decrease in recharge compared to the historical 77-year mean, and with the extremes (scenarios Awet and Adry) projecting between a 13 to 15 percent decrease in recharge to a 10 to 13 percent increase in recharge (Table 1).

Under the recent climate (Scenario B) the majority of the reporting regions show an increase in groundwater recharge with a maximum increase of 60 percent above the historical 77-year mean for the South-West Gulf region (Table 1). The South-East Gulf, Mitchell and Northern Coral are the only reporting regions to show a decrease in recharge under the recent climate.

Under the future climate (Scenario C), the majority of the 45 climate sequences project an increase in recharge for a 2030 climate relative to a 1990 climate. The median projection is for an increase in recharge of between 2 and 15 percent compared to the historical 77-year mean depending upon reporting region (Table 1). Under the wet extreme, the projections for all reporting regions show an increase in recharge of between 21 and 54 percent. Under the dry extreme, most reporting regions project a decrease in recharge of up to 13 percent except for the Western Cape and Northern Coral regions where the dry extreme projection is for a small increase in recharge.

The number of GCM-derived climate sequences projecting an increase or decrease in recharge is informative for evaluating trends. For the majority of northern Australia the trends in GCM outputs for rainfall show that between one-third and two-thirds of GCMs predict an increase under a 2030 climate relative to a 1990 climate. However for most of northern Australia recharge is projected to increase for a higher number of GCMs than rainfall. This counter-intuitive result is explained via a sensitivity analysis of the climate variables in WAVES which found that increased rainfall, temperature, CO_2 concentration and daily rainfall intensity lead to increased recharge and increased solar radiation and vapour pressure deficit lead to reduced recharge. After rainfall, recharge is most sensitive to changes in temperature and daily rainfall intensity when modelled using WAVES. Both temperature and daily rainfall intensity are projected to

increase under a future climate and so the results of the modelling show that recharge increases under more of the future climate sequences than does rainfall.

There is also the possibility that climate change can lead to ecological succession. Higher temperatures mean that the vegetation as modelled is pushed outside of its optimum temperature range; this presents an opportunity for different species to dominate. The implication of this observation is that the results presented here are for the current vegetation, there is the possibility that under a future climate the vegetation could change having an additional impact upon recharge.

Table 1. Recharge scaling factors (RSFs) for climate scenarios A, B and C aggregated to reporting region level

Region	Awet	Amid	Adry	B	Cwet	Cmid	Cdry
Fitzroy (WA)	1.11	0.98	0.87	1.50	1.26	1.06	0.87
Kimberley	1.10	0.98	0.87	1.33	1.21	1.08	0.91
Ord-Bonaparte	1.11	0.97	0.86	1.41	1.39	1.09	0.97
Daly	1.11	0.97	0.86	1.25	1.38	1.13	0.98
Van Diemen	1.12	0.97	0.86	1.18	1.37	1.11	0.93
Arafura	1.13	0.97	0.85	1.27	1.34	1.15	0.91
Roper	1.12	0.97	0.86	1.43	1.48	1.13	0.98
South-West Gulf	1.12	0.97	0.86	1.60	1.39	1.09	0.99
Flinders-Leichhardt	1.10	0.98	0.87	1.04	1.32	1.02	0.88
South-East Gulf	1.12	0.97	0.86	0.94	1.49	1.10	0.98
Mitchell	1.12	0.97	0.86	0.96	1.54	1.11	0.92
Western Cape	1.13	0.97	0.85	1.04	1.49	1.12	1.01
Northern Coral	1.13	0.97	0.86	0.98	1.37	1.11	1.02

Contents

Executive summary iii

1 Introduction 1
- 1.1 Project scope 1
- 1.2 Description of project area 1
- 1.3 Aims of project 2
- 1.4 Guidance on interpreting results 2

2 Methods 3
- 2.1 Point scale modelling 3
  - 2.1.1 Selection of model code 3
  - 2.1.2 Control points 3
  - 2.1.3 Climate 4
  - 2.1.4 Soil 6
  - 2.1.5 Vegetation 7
- 2.2 Upscaling 9
- 2.3 Aggregation 9
- 2.4 Recharge time series for groundwater modelling 9

3 Results 11
- 3.1 Point-scale modelling 11
- 3.2 Upscaling 16
  - 3.2.1 Scenario A 16
  - 3.2.2 Scenario B 17
  - 3.2.3 Scenario C 18
- 3.3 Aggregation 25
- 3.4 Recharge time series for groundwater modelling 26
  - 3.4.1 Daly model 26
  - 3.4.2 Howard East model 28

4 Discussion 29
- 4.1 A comparison of recharge estimates derived from WAVES to other methods 29
  - 4.1.1 Chloride mass balance 29
  - 4.1.2 Baseflow separation of streamflow 31
  - 4.1.3 Assessment of method 32
- 4.2 A sensitivity analysis of recharge to WAVES climate inputs 33
  - 4.2.1 Rainfall 35
  - 4.2.2 Carbon dioxide 36
  - 4.2.3 Temperature 37
  - 4.2.4 Vapour pressure deficit 39
  - 4.2.5 Solar radiation 40
  - 4.2.6 Daily rainfall intensity 41
  - 4.2.7 Relationship to Scenario C 42
- 4.3 An assessment of the results in light of the performance of the GCMs 45
- 4.4 An assessment of the methodology 47
  - 4.4.1 Limitations of the methodology 47
  - 4.4.2 Further work required 47

5 Conclusions 48

References 49

List of figures

Figure 1. Location of project area region showing the 13 reporting regions 1
Figure 2. Control points for WAVES modelling. These were selected to cover the rainfall gradient with a bias toward the priority catchments 4
Figure 3. Mean monthly rainfall (bars) and potential evapotranspiration (PET) (line) at each of the control points 5
Figure 4. Soil types across northern Australia, simplified from Johnston et al. (2003) 7
Figure 5. Vegetation types across northern Australia simplified from BRS (2003) 8
Figure 6. Example annual time series of recharge for a low rainfall control point (D) with perennial vegetation on a Kandasol soil also showing the 10th (red line), 50th (green line) and 90th (blue line) percentiles of the 23-year means of recharge 11
Figure 7. Example annual time series of recharge for a medium rainfall control point (Q) with perennial vegetation on a Kandasol soil also showing the 10th (red line), 50th (green line) and 90th (blue line) percentiles of the 23-year means of recharge 12
Figure 8. Example annual time series of recharge for a high rainfall control point (E) with perennial vegetation on a Kandasol soil also showing the 10th (red line), 50th (green line) and 90th (blue line) percentiles of the 23-year means of recharge 12
Figure 9. Relationships between mean annual rainfall and recharge for each combination of soil and vegetation types used for upscaling to create the Scenario A recharge raster 13
Figure 10. Frequency of start year selected for 23-year periods of scenarios Awet, Amid and Adry 14
Figure 11. Example of regression equations developed for the 23-year (R23) scenarios Awet, Amid and Adry with the 77-year historical modelled recharge (R77) 15
Figure 12. Scatterplot of change in mean annual rainfall versus change in mean annual recharge under scenarios A and C for all GCMs, soil and vegetation types lumped together for the high, medium and low global warming scenarios 15
Figure 13. Mean annual recharge under Scenario A (1930 to 2007) 16
Figure 14. Recharge scaling factors for scenarios Awet, Amid and Adry compared to the 77-year historical period (1930 to 2007) 17
Figure 15. Recharge scaling factor (RSF) raster for Scenario B; and rainfall under Scenario B expressed as the 11-year rainfall (P11) as a proportion of the 77-year rainfall (P77) 17
Figure 16. Rasters of recharge scaling factors (RSFs) from each GCM for the low global warming scenario 18
Figure 17. Rasters of recharge scaling factors (RSFs) from each GCM for the medium global warming scenario 19
Figure 18. Rasters of recharge scaling factors (RSFs) from each GCM for the high global warming scenario 20
Figure 19. Composite rasters of recharge scaling factors (RSFs) for scenarios Cwet, Cmid and Cdry 26
Figure 20. Daly model recharge zones overlaid on the NASY region map (Figure 1), showing its overlap with five reporting regions 27
Figure 21. Howard East model recharge zones overlaid on the NASY region map (Figure 1), showing that the Howard East model is within the Van Diemen region 28
Figure 22. Relationship between chloride deposition and distance from the coast, displayed with chloride deposition on (a) a linear scale and (b) a logarithmic scale 30
Figure 23. Chloride mass balance across northern Australia showing the chloride deposition, the concentration of chloride in groundwater and baseflow, and the resultant net recharge 31
Figure 24. Baseflow in gauged catchments that have measurements of dry season chloride concentration in surface water 32
Figure 25. A comparison between gross recharge estimated as the 77-year mean under Scenario A, net recharge as determined by chloride mass balance, and baseflow as determined by digital filter for each reporting region 33
Figure 26. Number of GCM-derived climate scenarios that predict an increase in recharge for the low, medium and high global warming scenarios and compared to the number of GCMs which predict an increase in rainfall 34
Figure 27. Sensitivity of recharge estimates for perennial and savannah vegetation on Kandasol soils to changes in daily rainfall (P) 35
Figure 28. Sensitivity of recharge estimates for perennial and savannah vegetation on Kandasol soils to changes in concentration of carbon dioxide in the atmosphere 36
Figure 29. Sensitivity of recharge estimates for perennial and savannah vegetation on Kandasol soils to changes in temperature 37
Figure 30. Sensitivity of recharge estimates for perennial and savannah vegetation on Kandasol soils to changes in temperature if the vegetation's optimum growth temperature is allowed to increase at the same rate as the atmospheric temperature 38
Figure 31. Sensitivity of recharge estimates for perennial and savannah vegetation on Kandasol soils to changes in vapour pressure deficit 39
Figure 32. Sensitivity of recharge estimates for perennial and savannah vegetation on Kandasol soils to changes in solar radiation 40
Figure 33. Sensitivity of recharge estimates for perennial and savannah vegetation on Kandasol soils to changes in daily rainfall intensity 41
Figure 34. Probability of exceedance curves for daily rainfall and recharge for perennial grasses on Kandasol soils for the high global warming scenario for the 15 GCMs at control points D (low rainfall), E (high rainfall) and Q (medium rainfall) 43
Figure 35. Probability of exceedance curves for daily rainfall and recharge for perennial grasses on Kandasol soils for the high global warming scenario for the 15 GCMs at control points D, E and Q 44
Figure 36. A comparison of the weighted and unweighted RSF rasters after being fitted to a Pearson Type III distribution. The plot shows the 10th and 90th percentile exceedance rasters for the high global warming scenario and the 50th percentile exceedance for the medium global warming scenario. The difference plots are the weighted minus the unweighted 46

List of tables

Table 1. Recharge scaling factors (RSFs) for climate scenarios A, B and C aggregated to reporting region level iv
Table 2. Soil parameters used in the WAVES modelling 7
Table 3. Vegetation parameters for WAVES model taken from the user manual (Dawes et al., 2004) 8
Table 4. Recharge (A77 R) and recharge scaling factors (RSFs) for Scenario A and B aggregated to reporting region level 16
Table 5. Changes in rainfall and recharge for the 13 reporting regions for each GCM and global warming scenario expressed as a percent difference from the 77-year historical mean 21
Table 6. Recharge scaling factors (RSFs) for scenarios Cwet, Cmid and Cdry aggregated to reporting region level 25
Table 7. Recharge scaling factors (RSFs) for each recharge zone in the Daly model for scenarios A, B and C 27
Table 8. Recharge scaling factors (RSFs) for each recharge zone in the Howard East model for scenarios A, B and C 28
Table 9. Literature values of chloride deposition used for estimating relationship between chloride deposition and distance from the coast 30
Table 10. Weights for each GCM for use in weighted Pearson Type III distribution. The weights are 1 minus the failure rate identified by Post et al. (2009) 45
Table 11. Comparison of the average RSFs calculated for each reporting region from the RSFs as output from the Pearson Type III distribution for the weighted and unweighted cases 46

1 Introduction

1.1 Project scope

In March 2008 the Council of Australian Governments (COAG) asked CSIRO to extend the work that was done in the Murray-Darling Basin Sustainable Yields (MDBSY) Project to other areas of Australia. The Northern Australia Sustainable Yields (NASY) Project was one of three new sustainable yields projects undertaken by CSIRO. This project was tasked with investigating the water availability across northern Australia under a range of current and future climate and development scenarios.

1.2 Description of project area

The NASY project area covers 1,200,000 km^2 across Northern Australia. This area is sub-divided into 13 reporting regions based upon Australian Water Resource Council surface water catchments (Figure 1). In comparison to the Murray-Darling Basin, northern Australia is largely undeveloped with a low population. It has high seasonal rainfall and is internationally renowned for its pristine tropical environments.

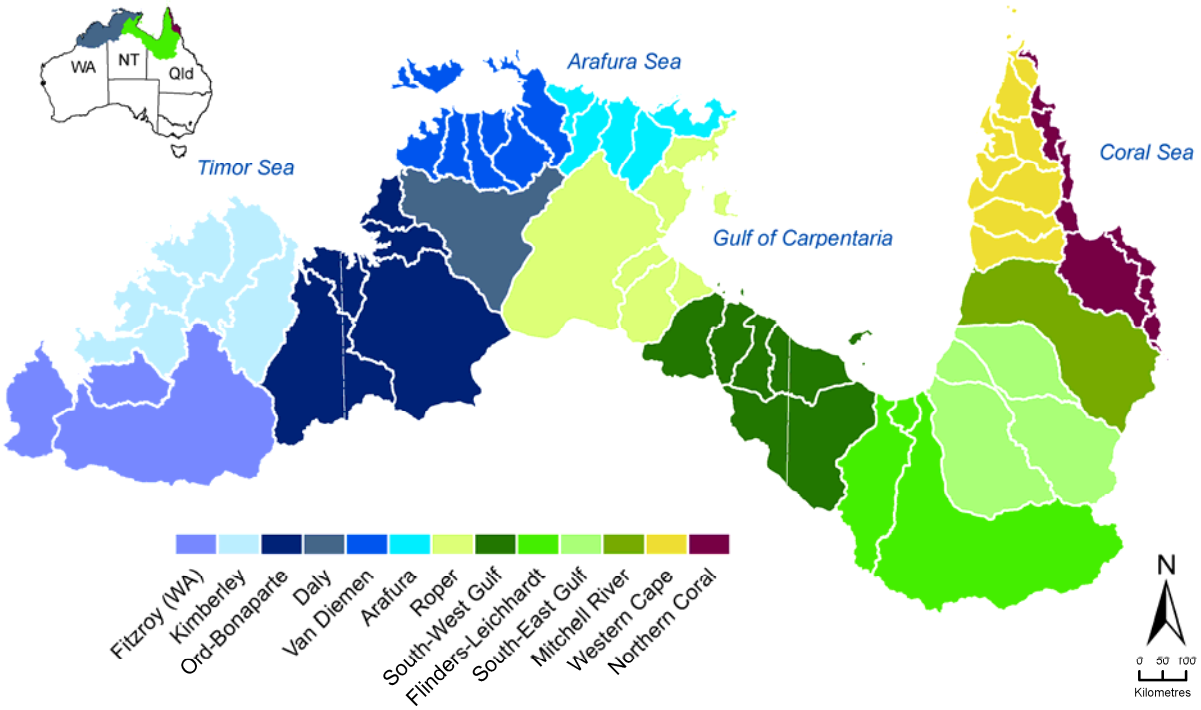

Figure 1. Location of project area region showing the 13 reporting regions

1.3 Aims of project

This technical report describes the recharge component of the NASY Project that estimated the amount of water available throughout the project area for every catchment and aquifer under a series of historical and future climate scenarios. It provides the technical background to the recharge results reported in the three NASY drainage division reports (CSIRO, 2009b; CSIRO, 2009c; CSIRO, 2009d).

The aims of the recharge modelling component of the project were to:

- use a similar methodology to that used in the Murray-Darling Basin Sustainable Yields (MDBSY) project for estimating the change in dryland diffuse groundwater recharge with a change in climate
- provide scaling factors for the change in recharge caused by a change in climate for all reporting regions in the project area.

1.4 Guidance on interpreting results

There is a great deal of uncertainty when predicting the impact of climate change upon groundwater recharge in the NASY project area. The first source of uncertainty is in climate change itself; this has been addressed through modelling three global warming scenarios – high, medium and low. The second source of uncertainty is in the impact of increased global temperatures upon climate; this has been addressed through the use of 15 different global climate models (GCMs). The third source of uncertainty is in our ability to determine groundwater recharge; this has been addressed by reporting the change in recharge for a future climate relative to the historical climate. The fourth source of uncertainty is in climate variability and its ability to mask a climate change effect.

The approach taken by this project for reporting the fourth source of uncertainty is to present a range of estimates of the impact of climate change and climate variability upon recharge. The range of estimates incorporates the extremes and the median of the historical climate, the recent climate and the likely extremes in a wet future climate and a dry future climate.

2 Methods

The method used for the recharge modelling in the NASY project is based upon that used in the MDBSY project (Crosbie et al., 2008a). It is based around modelling recharge at a series of points using WAVES (Zhang and Dawes, 1998) and then upscaling the outputs to the entire area using soil type, vegetation type and mean annual rainfall as covariates. The results are reported as recharge scaling factors (RSFs) giving the scenario recharge as a proportion of the historical recharge.

2.1 Point scale modelling

2.1.1 Selection of model code

The model chosen for the unsaturated zone modelling in this project was WAVES (Zhang and Dawes, 1998) which is a SVAT model that can be used to estimate the components of an unsaturated zone water balance at a daily timestep. The WAVES model achieves a balance in its modelling complexity between soil physics, plant physiology, energy and solute balances. WAVES has been shown to be able to reproduce the water balance of field experiments in many studies in the Murray-Darling Basin (Crosbie et al., 2008b; Slavich et al., 1999; Zhang et al., 1999), the rest of Australia (Dawes et al., 2002; Salama et al., 1999; Xu et al., 2008) and throughout the world (Wang et al., 2001; Yang et al., 2003; Zhang et al., 1996). Some changes were made to the model code to tailor its use for simulating future climate scenarios, specifically to make CO_2 concentration a variable rather than a constant (Crosbie et al., 2008a).

The WAVES model requires three input datasets: climate, soil and vegetation. These were generated automatically using a simple FORTRAN program developed for this project. Similarly the output files from WAVES were summarised using another simple program.

A 4 m soil profile was modelled with a free-draining lower-boundary condition. It was assumed that deep drainage from the bottom of the model became groundwater recharge and did not become lateral flow. The assumption was also made that diffuse recharge in dryland areas was not affected by groundwater; noting that this assumption would result in under- and over-estimation where the watertable is close to the surface. Recharge would be underestimated where the watertable is close to the surface but does not reach the surface because the water has less distance to travel to reach the watertable and therefore less chance of being evaporated or transpired. Recharge would be overestimated where the watertable intersects the surface because there is no storage available for additional recharge and the water will become overland flow.

The output of the point scale modelling was 38,088 model runs of WAVES. This was comprised of 23 control point locations, 3 vegetation types, 12 soils and 46 climate scenarios. These are described below.

2.1.2 Control points

With each run of the WAVES model taking up to two minutes to complete, it was impractical to model the entire NASY project area at the same scale as the climate data (~5 km grid). A set of control points was selected across the NASY project area to reflect the rainfall gradient and with a bias toward the five priority reporting regions (Fitzroy (WA), Daly, Flinders, Leichhardt, Mitchell). These control points were used to develop regression equations between mean annual rainfall and mean annual recharge that were used to upscale the mean annual recharge to the SILO grid (Jeffrey et al., 2001). The 23 control points selected are labelled A to W in Figure 2.

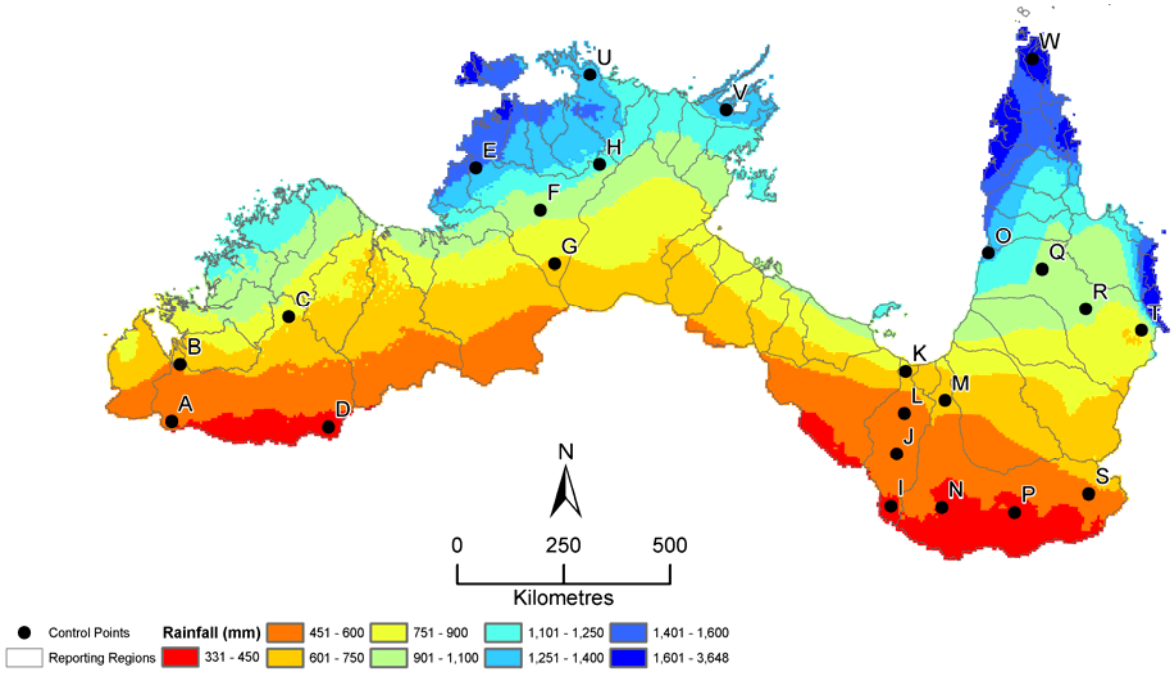

Figure 2. Control points for WAVES modelling. These were selected to cover the rainfall gradient with a bias toward the priority catchments

Figure 3 shows the mean monthly rainfall and potential evapotranspiration (PET) for each of the control points. These all show similar patterns of very low rainfall during winter and high rainfall during summer. At every point PET exceeds rainfall over winter and only in the wetter areas of northern Australia does rainfall exceed PET during the summer months.

2.1.3 Climate

The climate across northern Australia is very seasonal with wet summers and dry winters (Figure 3). The mean annual rainfall varies greatly from less than 400 mm/year to over 3000 mm/year with a strong rainfall gradient toward the coast (Figure 2). Three climate scenarios were modelled for recharge as part of the NASY project (CSIRO, 2009a):

- Scenario A – historical climate
- Scenario B – recent climate
- Scenario C – future climate (~2030).

The time frame modelled for the A and C scenarios was 77 years, beginning 1 September 1930 and ending 30 August 2007. Scenario B is a subset of Scenario A comprising the last 11 years of the model run.

For Scenario A the interpolated historical climate sequence was extracted from the Queensland government SILO website (Jeffrey et al., 2001) (<http://www.nrw.qld.gov.au/silo/ppd/index.html>) for each of the 23 control points. The CO_2 concentration used was 378 ppm as the scenario was for current conditions, this concentration was used as a constant even though the CO_2 concentrations have been increasing throughout the historical period used for Scenario A (IPCC, 2007). As a point of difference to the MDBSY project, for the NASY project there were three variants of Scenario A used for forward modelling of groundwater conditions to 2030. These are a subset of the historical modelled recharge and were defined as:

- Awet – the 90th percentile 23 year period from within the 77-year modelled record
- Amid – the 50th percentile 23 year period from within the 77-year modelled record
- Adry – the 10th percentile 23 year period from within the 77-year modelled record.

Scenario B is taken as a subset of the Scenario A modelled recharge record, and represents the last 11 years (i.e. 1 September 1996 to 31 August 2007). This 11-year recharge record was implemented in the numerical models by repeating the record 2.1 times to produce a 23-year time series.

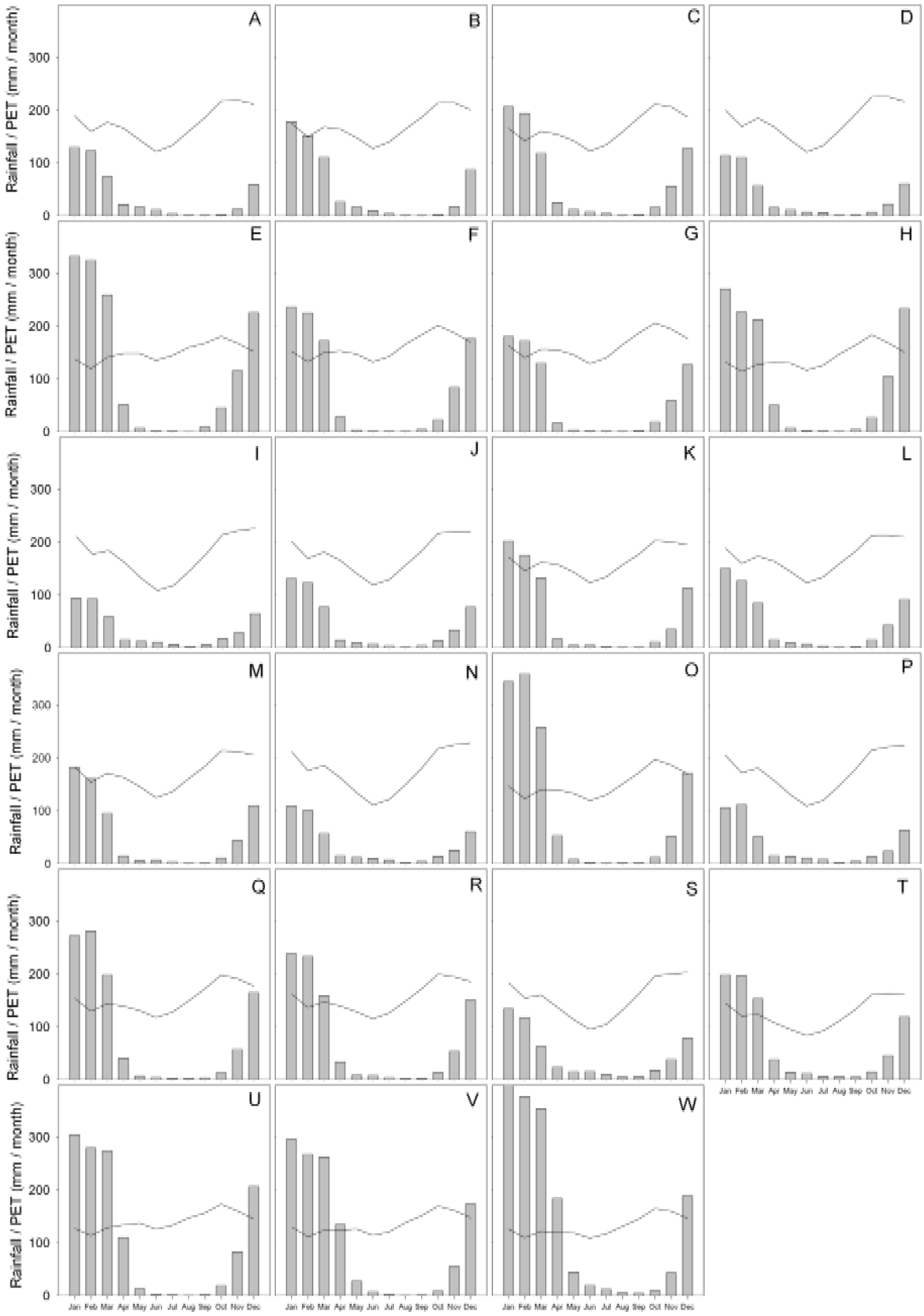

Figure 3. Mean monthly rainfall (bars) and potential evapotranspiration (PET) (line) at each of the control points

For Scenario C there were three climate scenarios (scenarios Cwet, Cmid and Cdry) produced from 15 global climate models (GCMs) under high, medium and low global warming scenarios of 1.3, 1.0 and 0.7 °C increases in temperature respectively. The CO_2 concentrations used in the WAVES modelling for the high, medium and low global warming

scenarios were 455, 446 and 437 ppm respectively. The outputs from the three global warming scenarios for 15 GCMs produced a total of 45 climate scenarios for modelling. Each of the 45 scenarios produced climate modifiers that were applied to the historical 77-year climate sequence (Scenario A). Full details of the climate generation procedure can be found in Li et al. (2009).

The 45 Scenario C recharge scenarios were aggregated to three scenarios at a reporting region level for further modelling. These were:

- Cwet – the 90th percentile (rank 2 of 15 GCM outputs) under high global warming
- Cmid – the 50th percentile (rank 8 of 15 GCM outputs) under medium global warming
- Cdry – the 10th percentile (rank 14 of 15 GCM outputs) under high global warming

Scenario D as defined for the NASY project (future climate, future development) was not considered for recharge modelling because only one region (Daly) was flagged as having potential future land use change (African Mahogany plantations) that could affect recharge rates, and there was no information on the vegetation parameters for this species.

2.1.4 Soil

The Broadbridge-White equation (Broadbridge and White, 1998) for soil moisture retention is used in WAVES. To calculate hydraulic conductivity (K) and matric potential (Ψ) as a function of moisture content (θ) five parameters are required: saturated hydraulic conductivity (K_s, m/d), saturated moisture content (θ_s , cm^3/cm^3), residual moisture content (θ_r , cm^3/cm^3), inverse capillary length scale (α, m) and an empirical constant based on soil properties (C, unitless).

$$\Theta = \frac{\theta - \theta_r}{\theta_s - \theta_r} \tag{1}$$

where Θ is the relative moisture content (scaled between 0 and 1).

$$K(\Theta) = K_s \frac{(C-1)\Theta^2}{C - \Theta} \tag{2}$$

$$\Psi(\Theta) = \frac{1}{\alpha}\left[\frac{1-\Theta}{\Theta} + \frac{1}{C}\ln\left(\frac{C-\Theta}{\Theta(C-1)}\right)\right] \tag{3}$$

The ASRIS 1 database (Johnston et al., 2003) is the best dataset that covers the entire NASY project area. There is more detailed soil mapping available through ASRIS v1.5 for parts of the Northern Territory but this was not used as a consistent database for the entire area was preferred. ASRIS has data layers for soil type (Isbell, 2002), K_s and plant available water capacity (PAWC) for two soil layers. The PAWC is defined as the difference in volumetric moisture content between matric potentials of 0.1 and 15 bar. A map of soil types is shown in Figure 4.

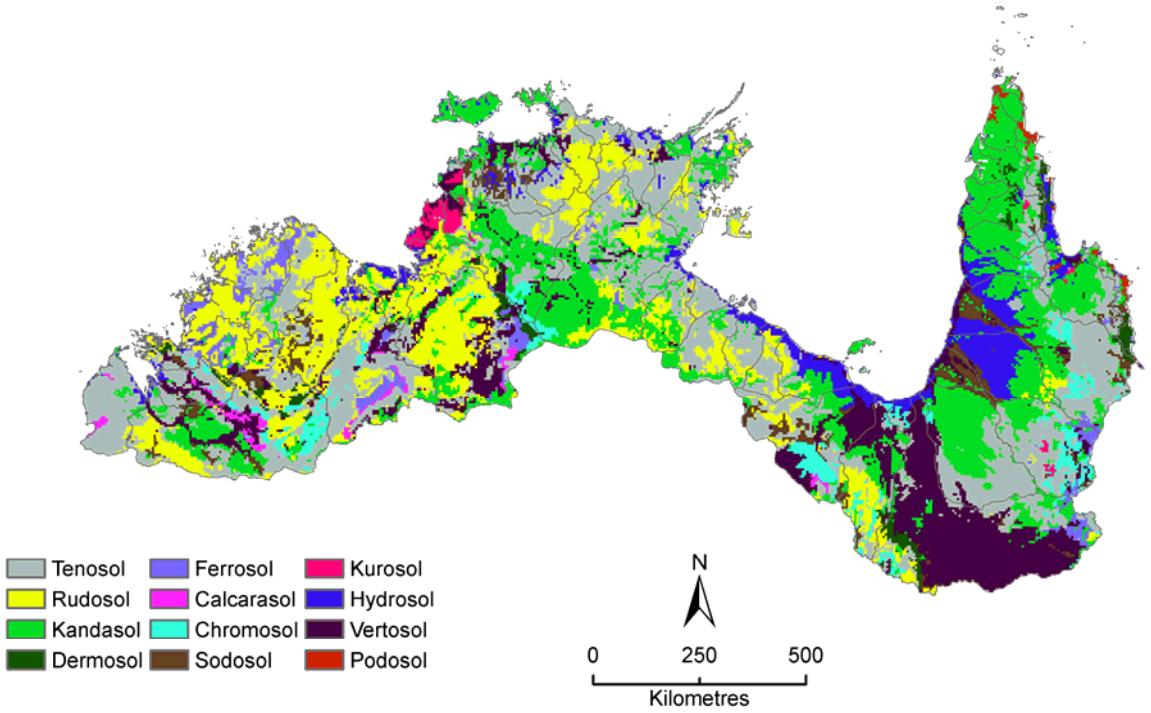

Figure 4. Soil types across northern Australia, simplified from Johnston et al. (2003)

The K_s and PAWC of the topsoils and subsoils were averaged across the NASY project area by soil type, and θ_s and θ_r were determined using equations (1) and (3). The C and α parameters were estimated based on soil texture and K_s. The soil parameters used are shown in Table 2.

Table 2. Soil parameters used in the WAVES modelling

Soil Type	K_s (m/d)	θ_s (v/v)	θ_r (v/v)	α (m)	C (-)
	Topsoil/subsoil				
Calcarosol	0.97 / 0.18	0.35 / 0.33	0.2 / 0.2	0.05 / 0.20	1.002 / 1.300
Chromosol	2.19 / 0.59	0.34 / 0.28	0.2 / 0.2	0.04 / 0.10	1.015 / 1.200
Dermosol	2.25 / 0.84	0.37 / 0.33	0.2 / 0.2	0.04 / 0.07	1.015 / 1.060
Ferrosol	3.70 / 0.93	0.35 / 0.33	0.2 / 0.2	0.03 / 0.06	1.015 / 1.050
Hydrosol	0.25 / 0.05	0.35 / 0.31	0.2 / 0.2	0.15 / 0.35	1.300 / 1.300
Kandosol	3.03 / 0.90	0.37 / 0.35	0.2 / 0.2	0.03 / 0.06	1.015 / 10.50
Kurosol	3.26 / 0.52	0.34 / 0.32	0.2 / 0.2	0.03 / 0.10	1.015 / 1.200
Podosol	5.47 / 0.92	0.35 / 0.33	0.2 / 0.2	0.01 / 0.06	1.010 / 1.020
Rudosol	3.70 / 1.58	0.34 / 0.34	0.2 / 0.2	0.03 / 0.05	1.015 / 1.020
Sodosol	1.32 / 0.22	0.34 / 0.27	0.2 / 0.2	0.05 / 0.20	1.015 / 1.300
Tenosol	3.95 / 3.05	0.35 / 0.33	0.2 / 0.2	0.03 / 0.03	1.010 / 1.015
Vertosol	0.012 / 0.006	0.36 / 0.36	0.2 / 0.2	0.45 / 1.00	1.500 / 2.00

2.1.5 Vegetation

Because it was computationally unfeasible to model every point within the NASY project area, it was necessary to simplify the number of vegetation classes. The Integrated Vegetation Coverage (BRS, 2003) was used and reclassified to three vegetation classes:

- annuals
- perennials
- savannah.

The vegetation parameters required by WAVES were taken from the User Manual (Dawes et al., 2004). The annuals (including crops) were modelled as a C4 annual pasture, the perennials were modelled as a C4 perennial pasture and the savannah (including any land cover with trees) was modelled as an overstorey of Eucalypts with an understorey of C4 perennial grasses. The simplified vegetation groupings are shown in Figure 5 and the parameters used in the WAVES modelling are shown in Table 3.

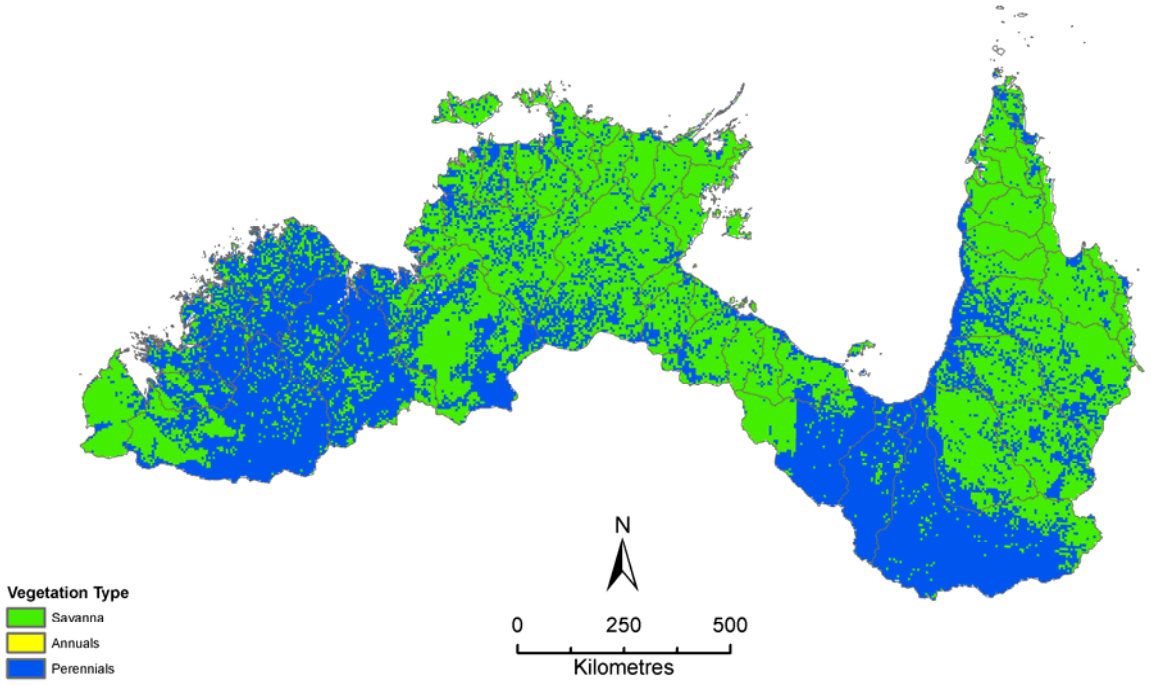

Figure 5. Vegetation types across northern Australia simplified from BRS (2003)

Table 3. Vegetation parameters for WAVES model taken from the user manual (Dawes et al., 2004)

Parameter	Units	Annuals	Perennials	Savannah (overstorey)	Savannah (understorey)
1 minus albedo of the canopy	-	0.85	0.85	0.80	0.85
1 minus albedo of the soil	-	0.85	0.85	0.85	0.85
Rainfall interception coefficient	m d^{-1} LAI^{-1}	0.0005	0.0008	0.001	0.0008
Light extinction coefficient	-	-0.65	-0.85	-0.45	-0.85
Maximum carbon assimilation rate	Kg C m^{-2} d^{-1}	0.02	0.03	0.03	0.03
Slope parameter for the conductance model	-	0.9	1	0.9	1
Maximum plant available water potential	m	-150	-150	-150	-150
IRM weighting of water	m	1.5	2	2.1	2
IRM weighting of nutrients	m	0.5	0.5	0.3	0.5
IRM weighting of CO_2	m	1.42	1.42	1.42	1.42
Ratio of stomatal to mesophyll conductance	m	0.8	0.8	0.2	0.8
Temperature when growth is half optimum	°C	20	20	20	20
Temperature when growth is optimum	°C	25	25	25	25
Year day of germination	d	330	-1	-1	-1
Degree-daylight hours of growth	°C h	35000	-1	-1	-1
Saturation light intensity	μmoles m^{-2} d^{-1}	1500	1800	1000	1800
Maximum rooting depth	m	1	1.5	3.9	1.5
Specific leaf area	LAI kg C^{-1}	48	24	13	24
Leaf respiration coefficient	kg C kg C^{-1}	0.002	0.0002	0.001	0.0002
Stem respiration coefficient	kg C kg C^{-1}	-1	-1	0.0006	-1
Root respiration coefficient	kg C kg C^{-1}	0.0002	0.0002	0.0001	0.0002
Leaf mortality rate	Fraction of C d^{-1}	0.001	0.001	0.0001	0.001
Above ground portioning factor	-	0.4	0.4	0.4	0.4
Aerodynamic resistance	s d^{-1}	30	30	10	30

2.2 Upscaling

The output of the WAVES modelling was used to create regression equations between mean annual rainfall and mean annual recharge for each combination of soil, vegetation and climate. The form of the relationship was an exponential rise in recharge with rainfall. For simplicity in automating the calculation of the regression equations the logarithm of the recharge was taken to enable a linear relationship between mean annual rainfall and mean annual recharge:

$$\log(R_s) = a\,P_s + b \tag{4}$$

where R_S is the recharge for a given scenario, P_S is the rainfall for a given scenario and a and b are fitting parameters. The fitting parameters were determined using a least squares routine between the 23 model runs (i.e. one for each 23 control points) for every combination of soil, vegetation and climate. The regression equations were applied with a rainfall limit of 1651 mm (the highest mean annual rainfall of the control points) to prevent recharge being predicted to be greater than rainfall when the regression equation was applied to areas that had rainfall greater than the control points.

Using the set of regression equations (4) and the set of mean annual rainfall rasters, a series of mean annual recharge rasters on a 0.05° grid were developed for the 77-year Scenario A, the 11-year Scenario B and the 45 different outputs for the 77-year Scenario C. These are reported as a recharge scaling factor (RSF):

$$RSF = \frac{R_S}{R_A} \tag{5}$$

where R_S is the recharge for a given scenario and R_A is the mean annual recharge for the 77-year Scenario A.

For the three 23-year variants of Scenario A, a different upscaling approach had to be taken. As a time series of recharge is only calculated at the 23 control points, these are the only points where the 23-year mean annual recharge series can be ranked and the 10th, 50th and 90th percentiles evaluated. There is a poor relationship between annual rainfall and annual recharge so the 10th, 50th and 90th percentiles of 23-year series of rainfall were not an appropriate covariate for upscaling. A relationship was found between the 23-year Scenario A variants (R_{A23}) and the 77-year Scenario A (R_{A77}) to enable the 23-year Scenario A variants to be upscaled across the entire NASY project area:

$$R_{A23} = a\,R_{A77} \tag{6}$$

These Scenario A variant rasters were then expressed as RSFs using Equation (5).

2.3 Aggregation

The 45 different Scenario C outputs were used to investigate the differences between GCMs and their predictions of how the future climate will impact upon groundwater recharge. For reporting and further detailed groundwater modelling only scenarios Cwet, Cmid and Cdry were modelled. As each GCM was ranked differently in each reporting region, composite rasters were created for these scenarios by stitching together the scenarios selected in each reporting region.

The mean RSFs were also reported at the reporting region scale. The calculated recharge varied greatly depending upon soil type and land use but could give very similar RSFs. Therefore the mean RSF over a reporting region was calculated as the mean of the recharge for the scenario divided by the area-weighted mean recharge under Scenario A:

$$\overline{RSF} = \frac{\overline{R_s}}{\overline{R_A}} \tag{7}$$

2.4 Recharge time series for groundwater modelling

There were only two numerical groundwater models used to investigate the impacts of change in recharge rates upon groundwater in the NASY project, they were in the Daly and Van Diemen regions. The recharge time series for the future climate scenarios in these models was obtained by scaling the WAVES-derived recharge time series to the recharge used in the existing calibrated numerical models.

It is only at the control points where a time series of recharge has been calculated by WAVES and so the new recharge time series for the model regions use the shape of the time series from the nearest control point and the average from the existing recharge calibrated in the model multiplied by the RSF for that scenario.

$$R_{MS,i} = \frac{R_{WS,i}}{\overline{R_{WS}}} . \overline{R_{MC}} . RSF_S \quad (8)$$

where $R_{MS,i}$ is the new recharge to go into the model for a given scenario at stress period i, $R_{WS,i}$ is the recharge from WAVES for the nearest control point at stress period *i*, $\overline{R_{WS}}$ is the average recharge from WAVES for the scenario from the nearest control point, $\overline{R_{MC}}$ is the average recharge from the model calibration for the model recharge zone and $\overline{RSF_S}$ is the average RSF for the scenario calculated for the model zone.

For the Scenario A variants the recharge time series from the nearest control point was used in Equation (8) for the appropriate 23-year period along with the RSF. For Scenario B the 11-year time series was looped 2.1 times to create a 23-year time series. Scenario C was considered relative to Scenario Amid. This means that for the numerically modelled areas the mean recharge for the model zone derived through model calibration was multiplied by the RSF for Scenario Amid and the RSF for the scenario under investigation e.g. $\overline{R_{MC}} \times \overline{RSF_{Amid}} \times \overline{RSF_C}$.

3 Results

3.1 Point-scale modelling

The WAVES model produces a daily time series as output. When the control point modelling is aggregated to an annual series it is clear that recharge is more variable than rainfall (Figure 6, Figure 7 and Figure 8).

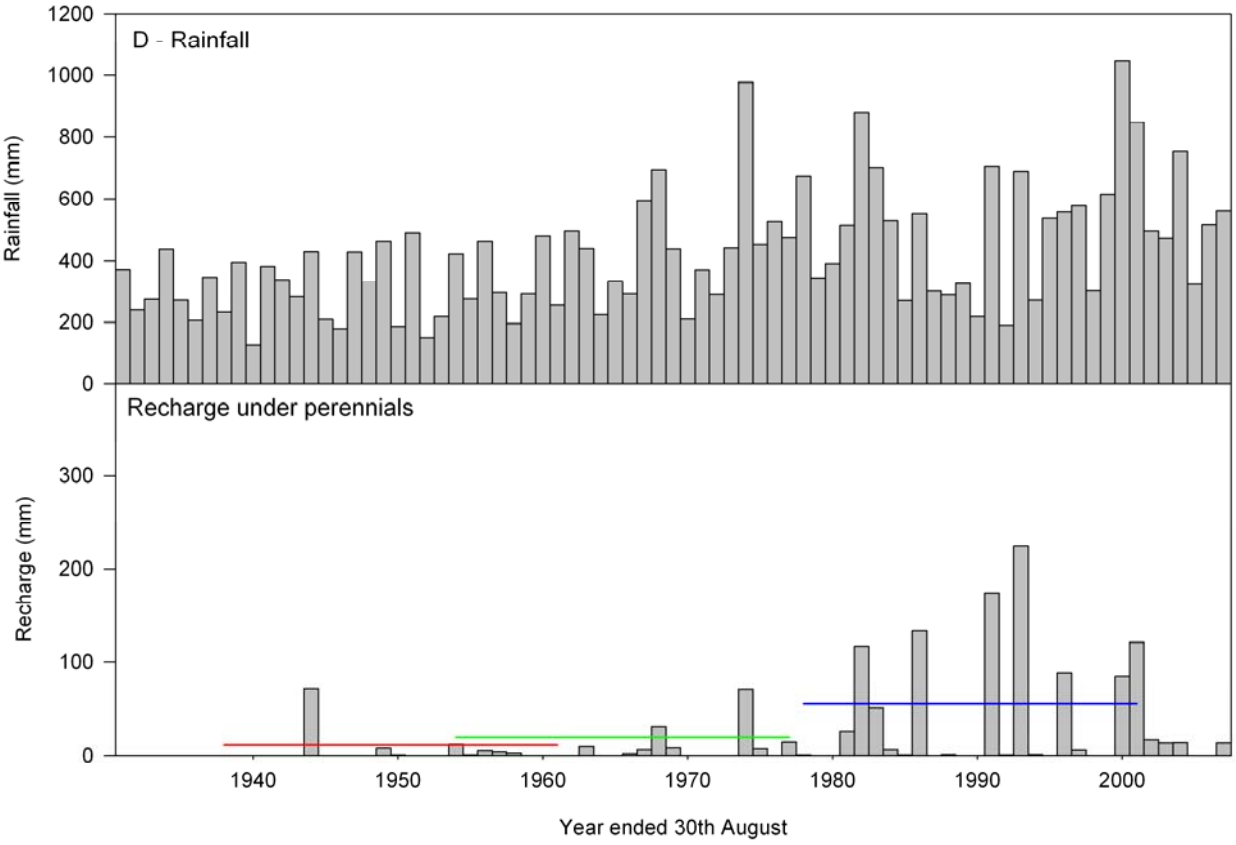

Figure 6. Example annual time series of recharge for a low rainfall control point (D) with perennial vegetation on a Kandasol soil also showing the 10th (red line), 50th (green line) and 90th (blue line) percentiles of the 23-year means of recharge

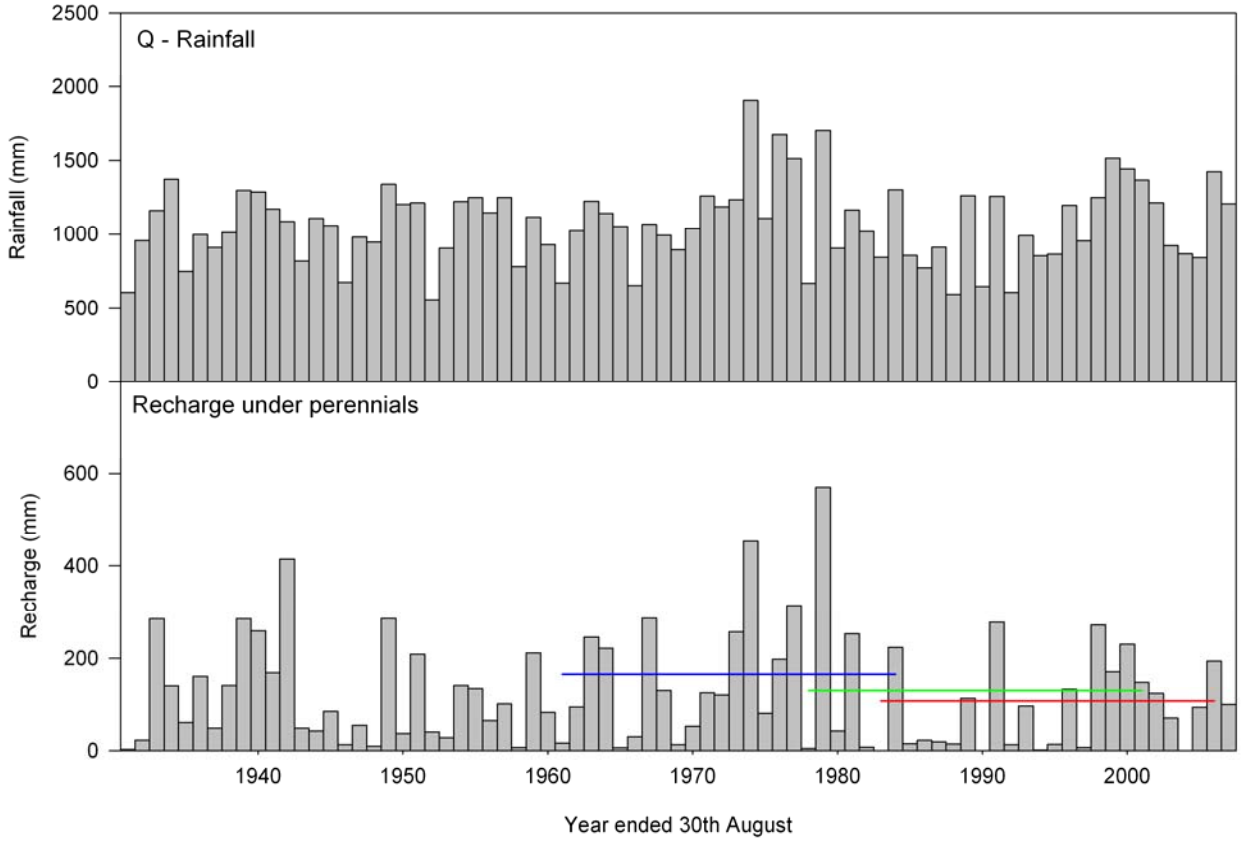

Figure 7. Example annual time series of recharge for a medium rainfall control point (Q) with perennial vegetation on a Kandasol soil also showing the 10th (red line), 50th (green line) and 90th (blue line) percentiles of the 23-year means of recharge

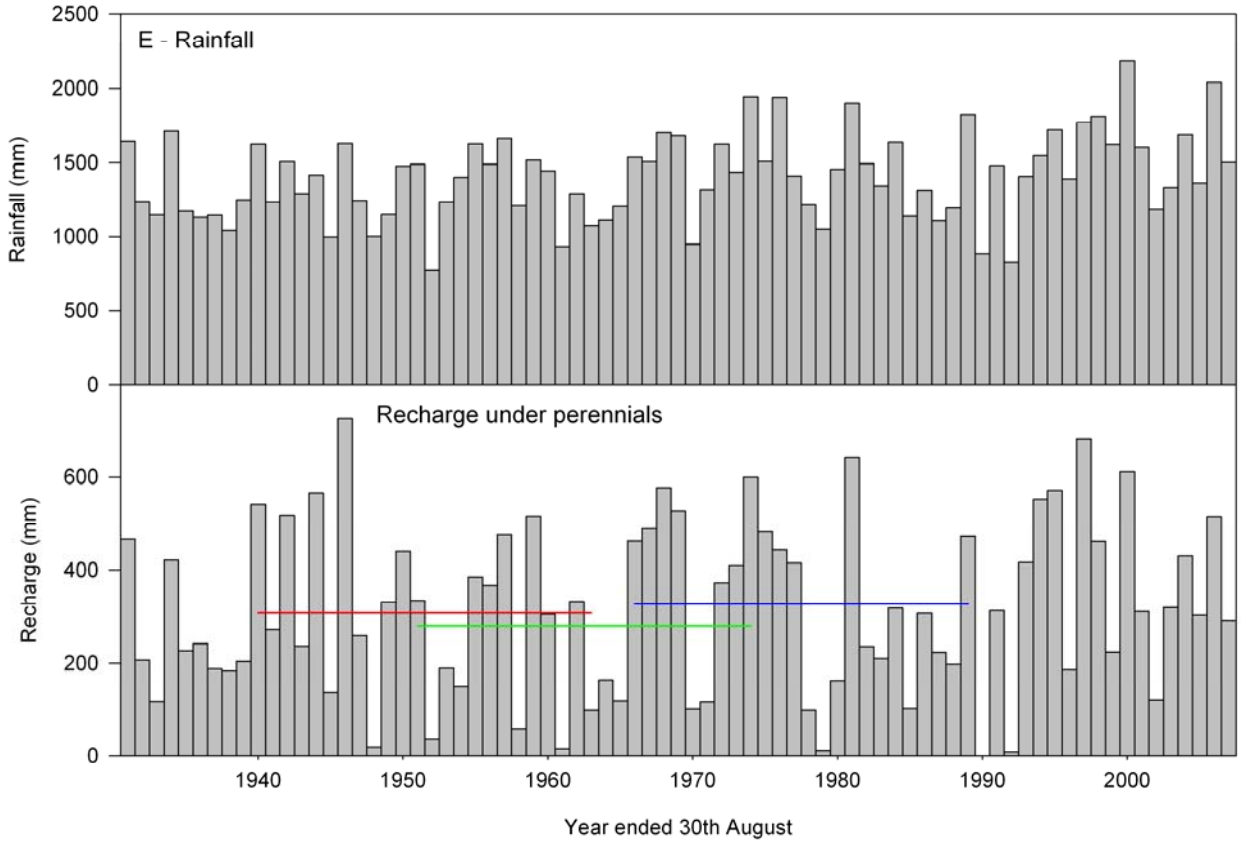

Figure 8. Example annual time series of recharge for a high rainfall control point (E) with perennial vegetation on a Kandasol soil also showing the 10th (red line), 50th (green line) and 90th (blue line) percentiles of the 23-year means of recharge

The point-scale modelling was used to create regression equations between mean annual rainfall and mean annual recharge for each combination of soil, vegetation and climate scenario. The results of these regression equations are shown in Figure 9 for Scenario A. The plots for Scenario B and the 45 Scenario C variants are very similar to that shown for Scenario A (data for other scenarios not shown).

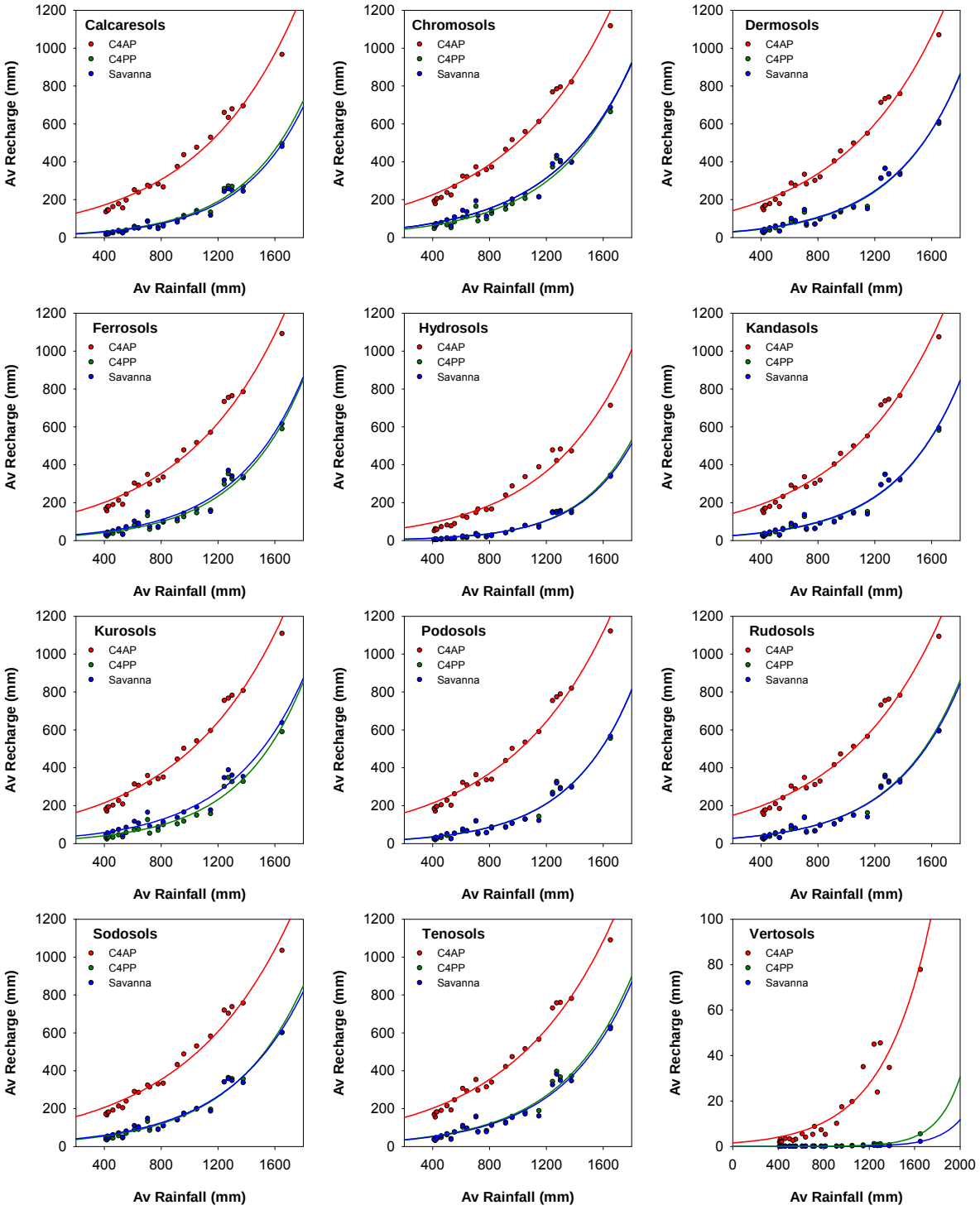

Figure 9. Relationships between mean annual rainfall and recharge for each combination of soil and vegetation types used for upscaling to create the Scenario A recharge raster

For scenarios Awet, Amid and Adry, the 10th, 50th and 90th percentiles of the 23-year mean annual recharge were extracted from the 77-year time series (Figure 6, Figure 7 and Figure 8). For each of the priority reporting regions there

were four control points that each had 12 soil types and three vegetation types modelled, giving a total of 144 model runs. There was significant variability in the 23-year periods selected depending upon the model scenario being investigated (Figure 10). However some patterns did emerge from the analysis. The Daly and Fitzroy (WA) regions showed that Scenario Adry was more often selected from the early part of the 77-year time period under investigation and Scenario Awet was selected from the more recent times. This is indicative of an increasing trend in recharge through time. The three Queensland priority regions displayed similar patterns as expected due to their geographic proximity.

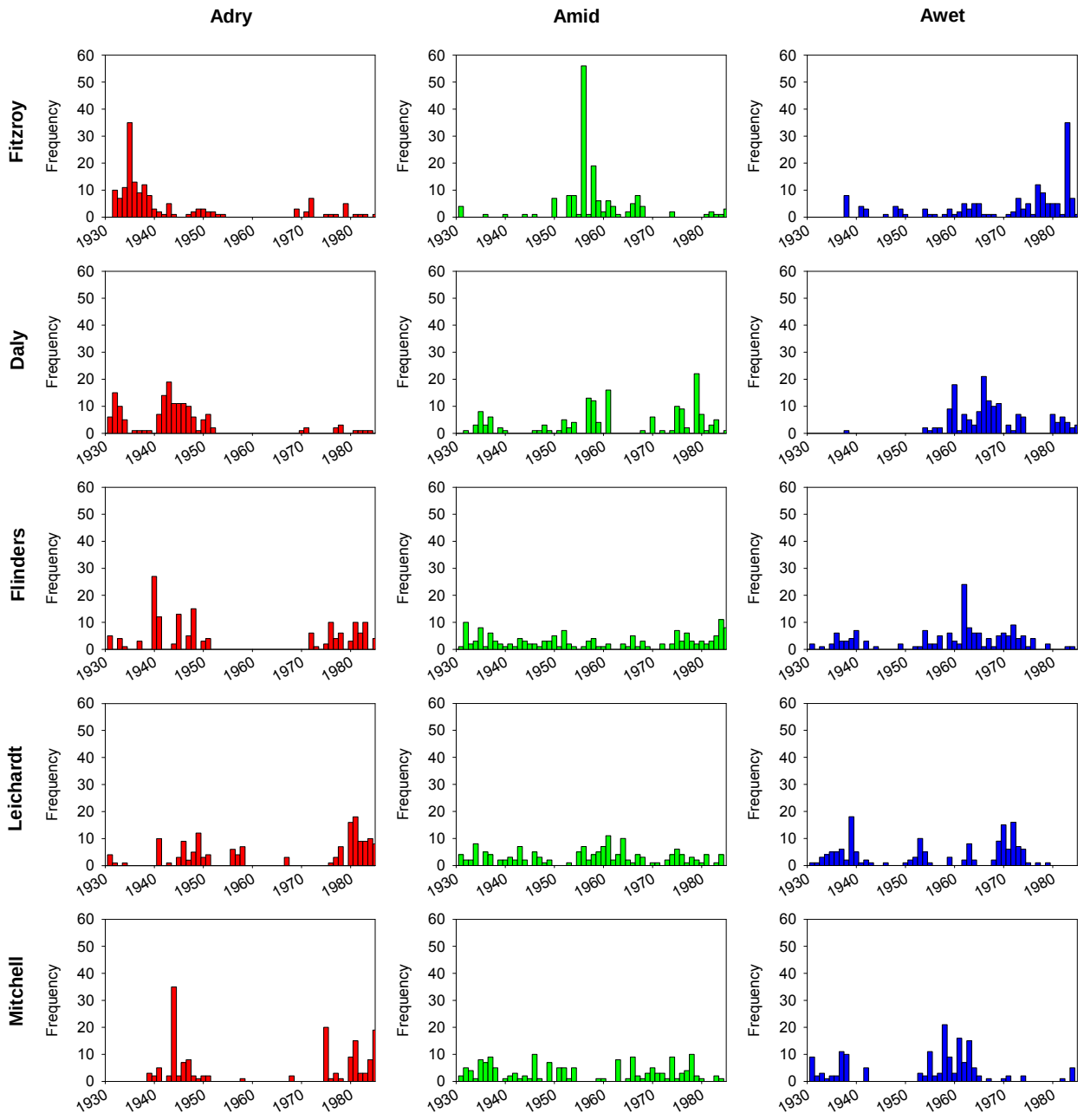

Figure 10. Frequency of start year selected for 23-year periods of scenarios Awet, Amid and Adry

The regression equations developed for scenarios Awet, Amid and Adry show that rainfall under Scenario Adry is drier than the 77-year mean and that rainfall under Scenario Awet is wetter than the 77-year mean and that rainfall under Scenario Amid is most often slightly drier than average. An example of the relationships obtained is shown in Figure 11 for the three vegetation types on a Kandasol soil type. The other 11 soil types show very similar relationships (data not shown).

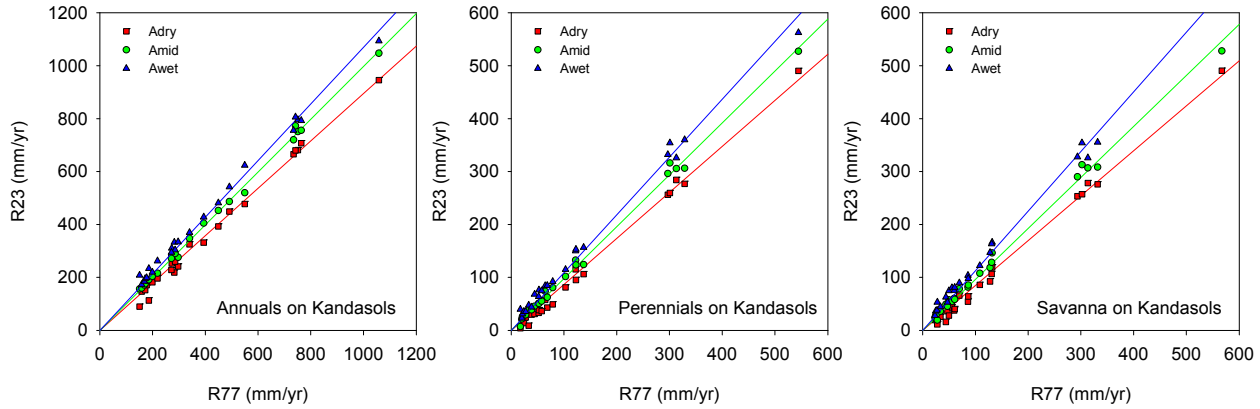

Figure 11. Example of regression equations developed for the 23-year (R23) scenarios Awet, Amid and Adry with the 77-year historical modelled recharge (R77)

The point modelling for Scenario C shows very similar results to that obtained from the MDBSY project, i.e. the change in recharge is disproportionately large when compared to the change in rainfall. When all 45 scenarios are plotted together (without accounting for different soil or vegetation types) as a change in rainfall versus change in recharge, it is clear that a regression line fitted through all the points shows the three global warming scenarios are parallel to each other with a difference in intercept [Figure 12, Equation (9)]. The intercept in all three cases is positive which indicates that the modelling predicts an increase in recharge due to climate change without a change in rainfall. This observation is explored further in Section 4.2.

$$\begin{aligned} &High: && \Delta R = 2.04 \times \Delta P + 13 && r^2 = 0.46 \\ &Medium: && \Delta R = 2.02 \times \Delta P + 9 && r^2 = 0.46 \\ &Low: && \Delta R = 1.99 \times \Delta P + 6 && r^2 = 0.42 \end{aligned} \qquad (9)$$

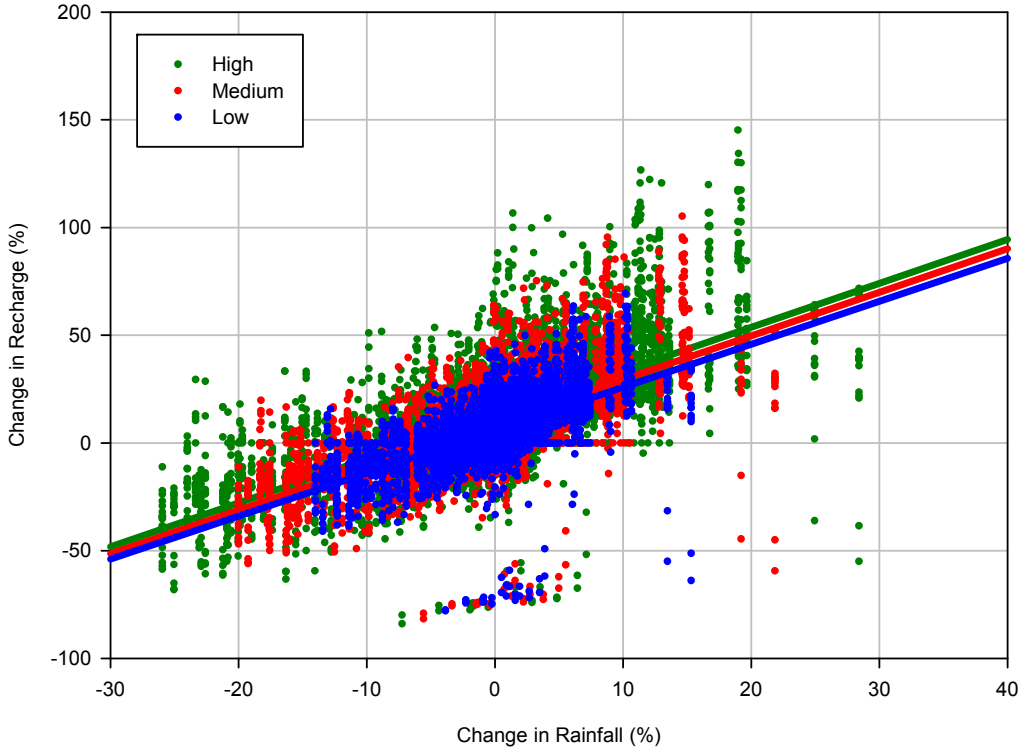

Figure 12. Scatterplot of change in mean annual rainfall versus change in mean annual recharge under scenarios A and C for all GCMs, soil and vegetation types lumped together for the high, medium and low global warming scenarios

3.2 Upscaling

3.2.1 Scenario A

The regression equations developed between mean annual rainfall and mean annual recharge (Figure 9) along with rasters of mean annual rainfall (Figure 2), soil type (Figure 4) and vegetation type (Figure 5) allow a raster of mean annual recharge to be developed (Figure 13). The mean annual recharge follows the general trend of mean annual rainfall with the exception of areas of Vertosol soils. The Vertosol soils have a very low hydraulic conductivity (Table 2) which means that vertical water flow is restricted and consequently recharge is very low (Figure 9). When the mean annual recharge is expressed as a percentage of rainfall it is clear that proportionately high recharge areas are also the high rainfall areas.

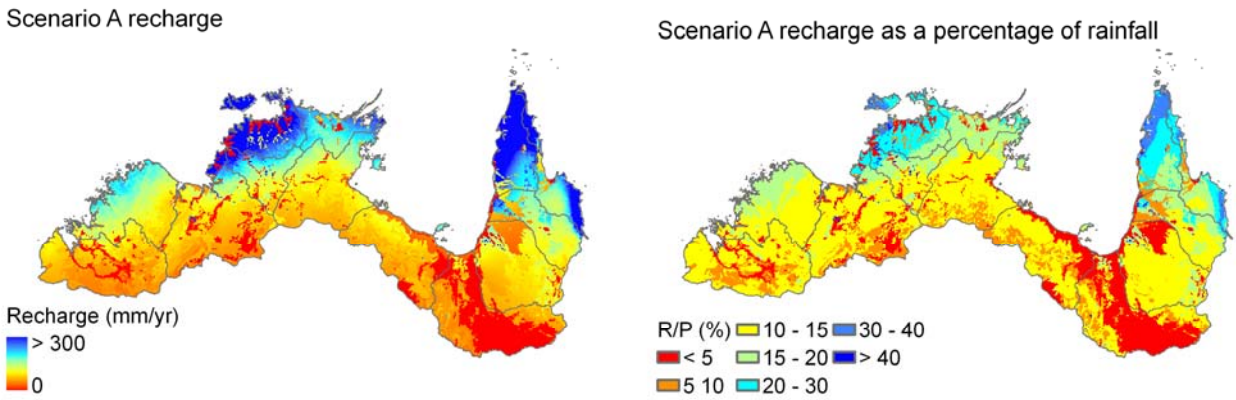

Figure 13. Mean annual recharge under Scenario A (1930 to 2007)

Rasters of recharge under scenarios Awet and Adry were created in a similar way to that for recharge under Scenario Amid (Figure 14). For the different reporting regions, compared to the 77-year mean, recharge under Scenario Awet increases 10 to 13 percent (), under Scenario Amid it decreases 2 to 3 percent and under Scenario Adry it decreases 13 to 15 percent.

Table 4. Recharge (A77 R) and recharge scaling factors (RSFs) for Scenario A and B aggregated to reporting region level

Region	A77 R (mm/y)	Awet RSF	Amid RSF	Adry RSF	B RSF
Fitzroy (WA)	50	1.11	0.98	0.87	1.50
Kimberley	120	1.10	0.98	0.87	1.33
Ord-Bonaparte	70	1.11	0.97	0.86	1.41
Daly	153	1.11	0.97	0.86	1.25
Van Diemen	307	1.12	0.97	0.86	1.18
Arafura	196	1.13	0.97	0.85	1.27
Roper	95	1.12	0.97	0.86	1.43
South-West Gulf	54	1.12	0.97	0.86	1.60
Flinders-Leichhardt	19	1.10	0.98	0.87	1.04
South-East Gulf	68	1.12	0.97	0.86	0.94
Mitchell	122	1.12	0.97	0.86	0.96
Western Cape	346	1.13	0.97	0.85	1.04
Northern Coral	271	1.13	0.97	0.86	0.98

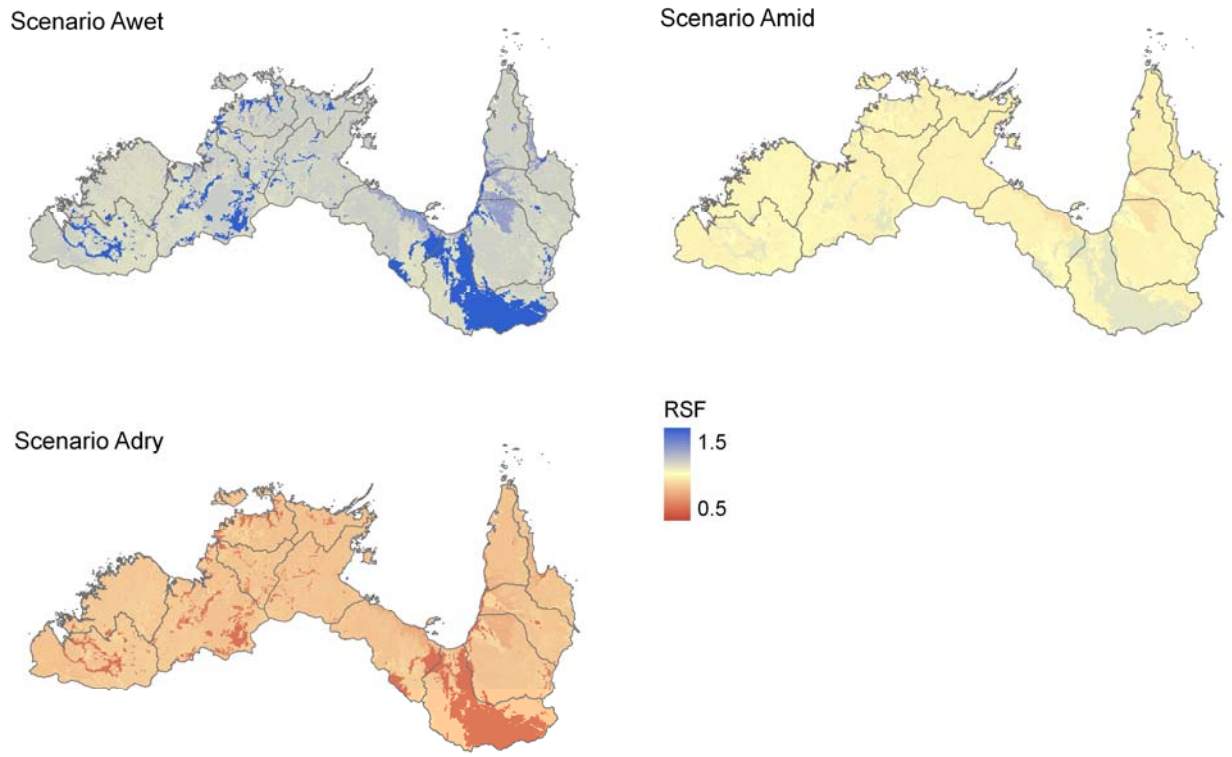

Figure 14. Recharge scaling factors for scenarios Awet, Amid and Adry compared to the 77-year historical period (1930 to 2007)

3.2.2 Scenario B

The RSF raster for Scenario B was created similarly to the rasters for Scenario A RSF (Figure 15). The changes in recharge closely follow the patterns of changes in rainfall except for the Vertosol soil type which showed a decrease in recharge in areas where rainfall increased. The only regions to show a decrease in recharge over the recent past are the South-East Gulf, Mitchell and Northern Coral regions with a maximum decrease in recharge of 6 percent in the South-East Gulf region (). The rest of the reporting regions showed an increase in recharge with the South-West Gulf region having the greatest increase in recharge at 60 percent.

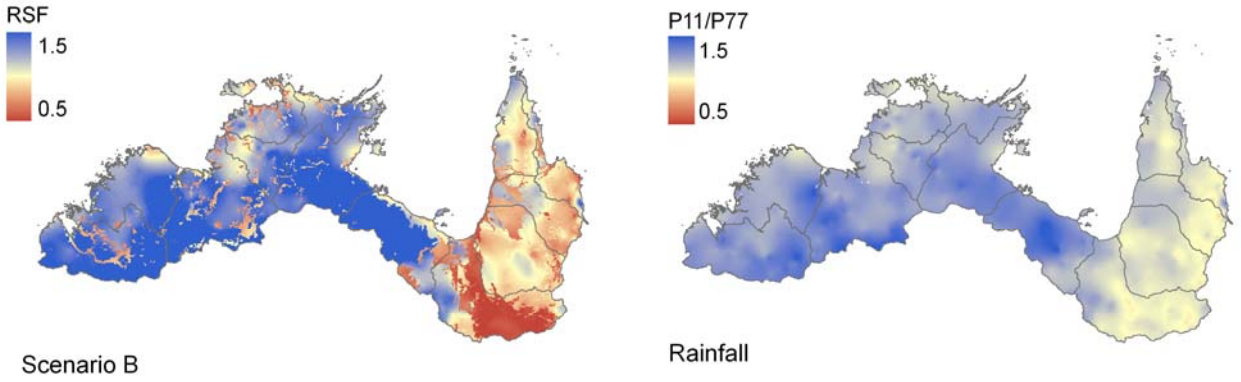

Figure 15. Recharge scaling factor (RSF) raster for Scenario B; and rainfall under Scenario B expressed as the 11-year rainfall (P11) as a proportion of the 77-year rainfall (P77)

3.2.3 Scenario C

The 45 rasters for Scenario C were created similarly to the rasters for scenarios A and B and are shown in Figure 16 for the low global warming scenario, Figure 17 for the medium global warming scenario and Figure 18 for the high global warming scenario. The patterns under the global warming scenarios are very similar but become more extreme in either increasing or decreasing recharge with the high global warming scenario when compared to the low global warming scenario. The linear features in these figures are caused by a coarser discretisation of the GCM grid compared to the distributed soil and vegetation type data used to develop the RSF rasters.

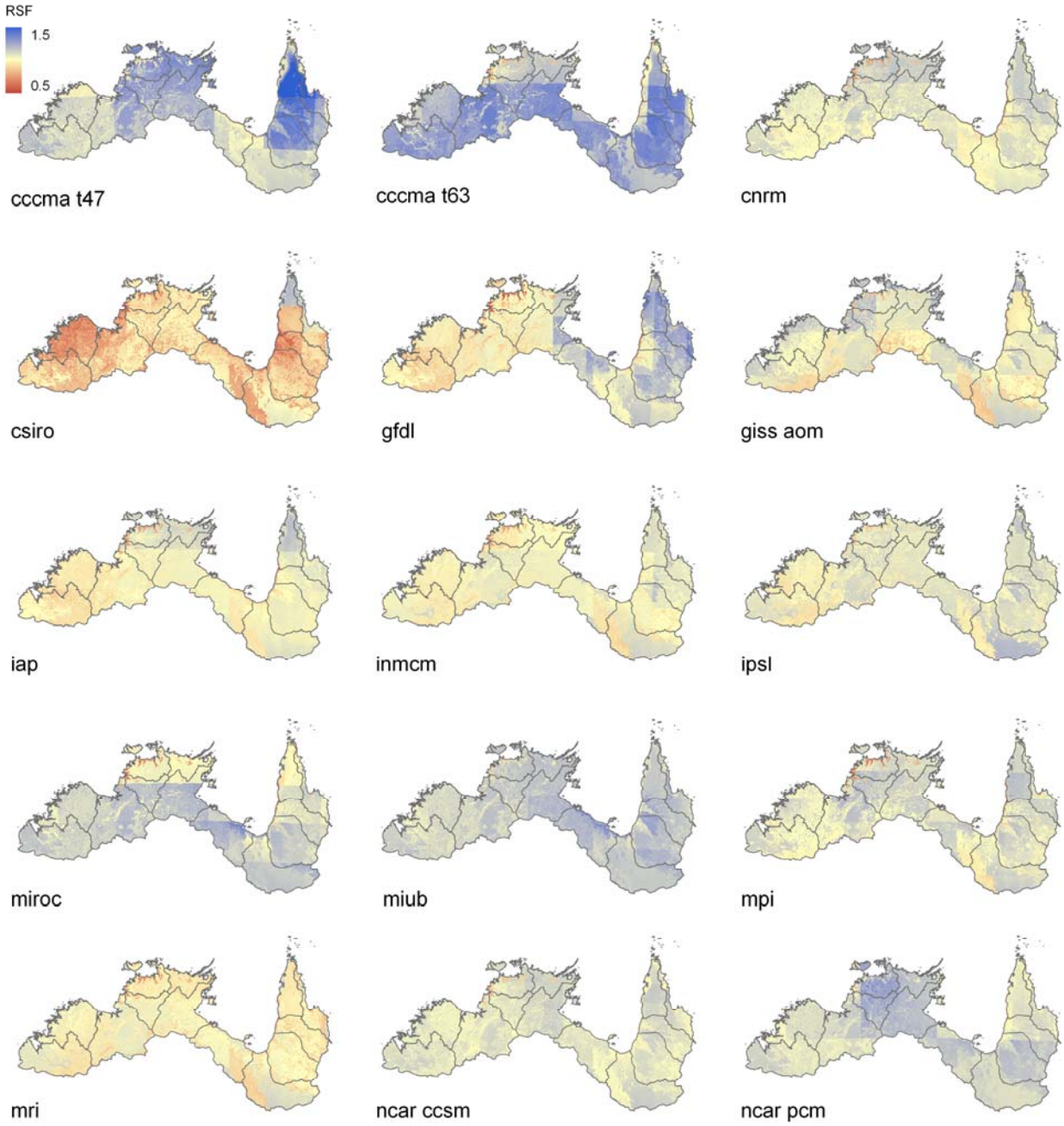

Figure 16. Rasters of recharge scaling factors (RSFs) from each GCM for the low global warming scenario

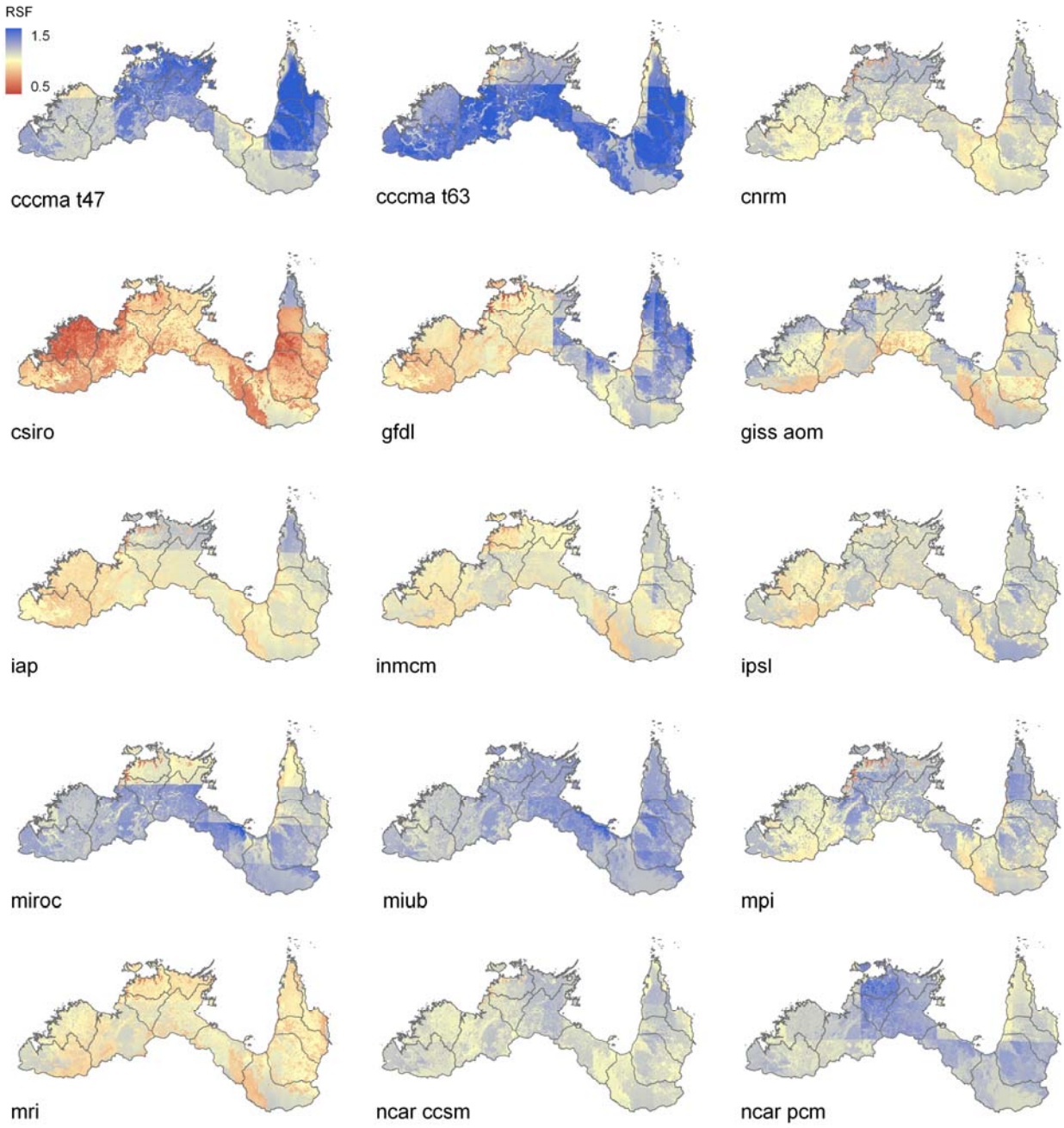

Figure 17. Rasters of recharge scaling factors (RSFs) from each GCM for the medium global warming scenario

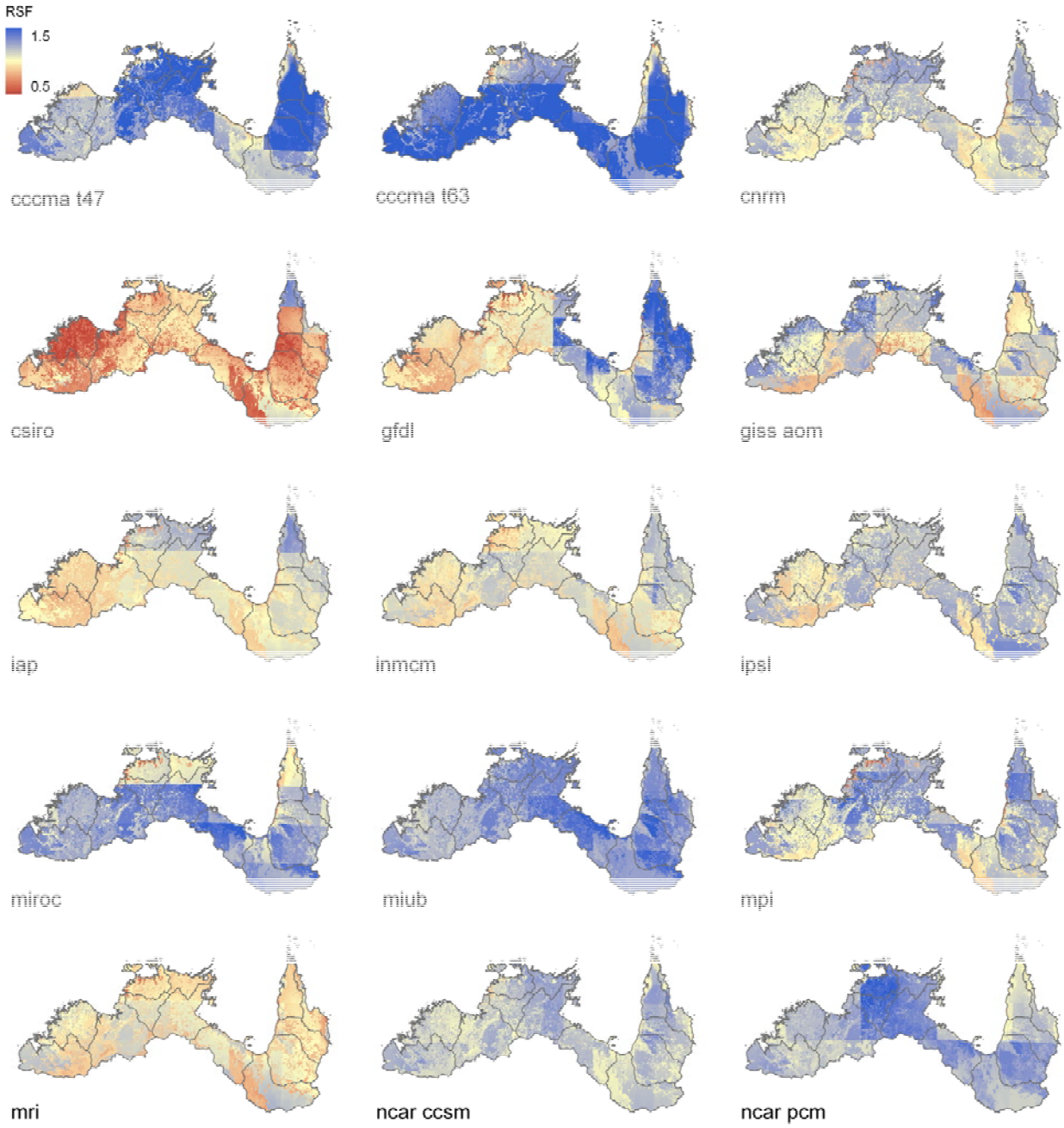

Figure 18. Rasters of recharge scaling factors (RSFs) from each GCM for the high global warming scenario

The changes in rainfall and recharge were aggregated to the reporting region level for each GCM and global warming scenario and are listed in Table 5. The changes in recharge show a large variation between different GCMs and the inconsistency between the change in rainfall and change in recharge. It is not uncommon for a GCM to predict a decrease in rainfall for a particular region when the recharge modelling predicts an increase in recharge. This apparent contradiction is explored further in Section 4.2.

Table 5. Changes in rainfall and recharge for the 13 reporting regions for each GCM and global warming scenario expressed as a percent difference from the 77-year historical mean

High global warming			Medium global warming			Low global warming		
GCM	Rainfall	Recharge	GCM	Rainfall	Recharge	GCM	Rainfall	Recharge
	percent			percent			percent	
Fitzroy								
csiro	-19	-24	csiro	-15	-19	csiro	-10	-14
gfdl	-19	**-13**	gfdl	-14	-10	gfdl	-10	-6
iap	-10	-9	iap	-8	-7	iap	-5	-5
inmcm	0	0	inmcm	0	-1	inmcm	0	-1
mri	-1	1	mri	-1	1	mri	0	0
ipsl	-2	5	ipsl	-2	2	ipsl	-1	1
giss_aom	2	8	giss_aom	1	5	giss_aom	1	2
cnrm	-2	8	**cnrm**	-2	**6**	cnrm	-1	4
mpi	0	12	mpi	0	9	mpi	0	5
ncar_ccsm	5	16	ncar_ccsm	4	11	ncar_ccsm	3	7
ncar_pcm	2	18	ncar_pcm	2	13	ncar_pcm	1	9
miub	1	22	miub	1	16	miub	1	11
cccma_t47	5	25	cccma_t47	4	18	cccma_t47	3	12
miroc	6	**26**	miroc	5	20	miroc	3	13
cccma_t63	10	51	cccma_t63	8	39	cccma_t63	5	26
Kimberley								
csiro	-23	-44	csiro	-18	-37	csiro	-12	-27
iap	-6	**-9**	iap	-4	-7	iap	-3	-5
gfdl	-13	-7	gfdl	-10	-5	gfdl	-7	-4
inmcm	1	-1	inmcm	1	-1	inmcm	1	-1
ipsl	0	1	ipsl	0	0	ipsl	0	0
mri	0	1	mri	0	1	mri	0	0
cnrm	1	9	cnrm	1	6	cnrm	1	5
ncar_ccsm	4	11	**ncar_ccsm**	3	**8**	ncar_ccsm	2	5
mpi	1	12	mpi	1	9	mpi	1	6
cccma_t47	4	14	cccma_t47	3	11	cccma_t47	2	8
giss_aom	6	16	giss_aom	5	12	giss_aom	3	8
ncar_pcm	4	16	ncar_pcm	3	12	ncar_pcm	2	8
miub	2	19	miub	1	14	miub	1	10
miroc	5	**21**	miroc	4	16	miroc	3	10
cccma_t63	8	34	cccma_t63	6	27	cccma_t63	5	18
Ord-Bonaparte								
csiro	-18	-26	csiro	-14	-21	csiro	-10	-15
gfdl	-13	**-3**	gfdl	-10	-2	gfdl	-7	-1
iap	-5	-2	iap	-4	-1	iap	-3	-1
mri	-2	3	mri	-1	2	mri	-1	1
inmcm	2	6	inmcm	2	4	inmcm	1	2
ipsl	0	11	ipsl	0	7	ipsl	0	5
giss_aom	1	13	giss_aom	1	9	giss_aom	1	5
ncar_ccsm	3	13	**ncar_ccsm**	2	**9**	ncar_ccsm	2	6
cnrm	0	14	cnrm	0	11	cnrm	0	8
mpi	2	21	mpi	2	16	mpi	1	10
ncar_pcm	5	24	ncar_pcm	4	17	ncar_pcm	3	12
miub	3	28	miub	2	21	miub	2	14
miroc	7	31	miroc	6	23	miroc	4	15
cccma_t47	10	**39**	cccma_t47	7	29	cccma_t47	5	21
cccma_t63	14	58	cccma_t63	11	44	cccma_t63	8	30

High global warming			Medium global warming			Low global warming		
Daly								
gfdl	-14	**-2**	gfdl	-11	-1	gfdl	-7	-1
mri	-4	0	mri	-3	0	mri	-2	-1
inmcm	0	4	inmcm	0	2	inmcm	0	1
iap	-2	6	iap	-2	5	iap	-1	3
ncar_ccsm	3	14	ncar_ccsm	2	10	ncar_ccsm	2	7
ipsl	1	15	ipsl	1	10	ipsl	1	6
cnrm	1	17	**cnrm**	1	**13**	cnrm	1	9
giss_aom	2	20	giss_aom	1	13	giss_aom	1	9
miroc	4	22	miroc	3	17	miroc	2	11
miub	3	28	miub	2	21	miub	2	14
mpi	2	29	mpi	2	21	mpi	1	13
cccma_t63	9	38	cccma_t63	7	29	cccma_t63	5	20
ncar_pcm	11	**38**	ncar_pcm	8	28	ncar_pcm	6	20
cccma_t47	12	45	cccma_t47	9	34	cccma_t47	6	24
Van Diemen								
csiro	-12	-16	csiro	-9	-13	csiro	-6	-9
gfdl	-15	**-7**	gfdl	-11	-5	gfdl	-8	-4
mri	-6	-7	mri	-5	-5	mri	-3	-4
inmcm	-4	-5	inmcm	-3	-5	inmcm	-2	-4
miroc	-1	6	miroc	-1	5	miroc	-1	3
ipsl	1	13	ipsl	1	9	ipsl	0	6
iap	0	14	iap	0	11	iap	0	7
ncar_ccsm	4	16	**ncar_ccsm**	3	**11**	ncar_ccsm	2	8
cccma_t63	5	18	cccma_t63	4	14	cccma_t63	3	10
cnrm	3	22	cnrm	3	16	cnrm	2	12
mpi	-1	23	mpi	0	17	mpi	0	10
giss_aom	3	24	giss_aom	2	17	giss_aom	2	11
miub	3	29	miub	2	22	miub	2	14
ncar_pcm	10	**37**	ncar_pcm	8	29	ncar_pcm	6	21
cccma_t47	12	40	cccma_t47	9	33	cccma_t47	6	25
Arafura								
mri	-8	-10	mri	-6	-8	mri	-4	-6
csiro	-11	**-9**	csiro	-8	-8	csiro	-6	-5
inmcm	-2	2	inmcm	-2	1	inmcm	-1	0
miroc	-4	3	miroc	-3	3	miroc	-2	1
gfdl	-11	10	gfdl	-8	8	gfdl	-6	5
ipsl	0	15	ipsl	0	9	ipsl	0	6
iap	2	20	**iap**	2	**15**	iap	1	10
giss_aom	2	21	giss_aom	1	14	giss_aom	1	9
mpi	-1	22	mpi	-1	16	mpi	0	9
ncar_ccsm	6	24	ncar_ccsm	5	17	ncar_ccsm	3	11
cnrm	3	24	cnrm	3	18	cnrm	2	13
cccma_t63	5	27	cccma_t63	4	21	cccma_t63	3	14
ncar_pcm	7	29	ncar_pcm	6	22	ncar_pcm	4	16
miub	4	**34**	miub	3	25	miub	2	16
cccma_t47	13	57	cccma_t47	10	43	cccma_t47	7	30

High global warming			Medium global warming			Low global warming		
Roper								
mri	-5	**-2**	mri	-4	-1	mri	-3	-2
inmcm	0	6	inmcm	0	3	inmcm	0	2
iap	-2	10	iap	-1	8	iap	-1	5
giss_aom	-3	10	giss_aom	-2	6	giss_aom	-1	3
gfdl	-9	14	gfdl	-7	10	gfdl	-5	7
ipsl	0	14	ipsl	0	8	ipsl	0	5
cnrm	0	18	**cnrm**	0	**13**	cnrm	0	9
ncar_ccsm	5	22	ncar_ccsm	4	15	ncar_ccsm	3	10
mpi	1	24	mpi	1	17	mpi	1	10
miroc	5	26	miroc	4	20	miroc	3	12
ncar_pcm	9	33	ncar_pcm	7	24	ncar_pcm	5	17
miub	5	35	miub	4	26	miub	3	17
cccma_t47	11	**48**	cccma_t47	9	35	cccma_t47	6	25
cccma_t63	11	50	cccma_t63	9	38	cccma_t63	6	25
South-West Gulf								
csiro	-20	-20	csiro	-15	-16	csiro	-10	-11
mri	-6	**-1**	mri	-4	-1	mri	-3	-1
iap	-5	1	iap	-3	1	iap	-2	0
inmcm	-1	4	inmcm	0	2	inmcm	0	1
cnrm	-4	9	cnrm	-3	6	cnrm	-2	4
giss_aom	-1	11	giss_aom	0	7	giss_aom	0	4
ipsl	0	12	ipsl	0	7	ipsl	0	4
ncar_ccsm	1	14	**ncar_ccsm**	1	**9**	ncar_ccsm	1	6
mpi	-1	17	mpi	0	12	mpi	0	7
cccma_t47	1	22	cccma_t47	1	16	cccma_t47	1	11
ncar_pcm	7	27	ncar_pcm	5	19	ncar_pcm	4	13
gfdl	0	27	gfdl	0	20	gfdl	0	13
miroc	10	36	miroc	7	27	miroc	5	18
miub	8	**39**	miub	6	29	miub	4	19
cccma_t63	10	52	cccma_t63	8	39	cccma_t63	6	26
Flinders-Leichhardt								
csiro	-22	-30	csiro	-17	-24	csiro	-12	-17
mri	-8	**-12**	mri	-6	-9	mri	-4	-7
giss_aom	-8	-11	giss_aom	-6	-9	giss_aom	-4	-7
inmcm	-3	-8	inmcm	-2	-7	inmcm	-2	-5
iap	-5	-4	iap	-4	-3	iap	-2	-2
mpi	-3	2	mpi	-3	1	mpi	-2	1
ipsl	1	3	ipsl	1	1	ipsl	0	0
cnrm	-4	3	**cnrm**	-3	**2**	cnrm	-2	2
ncar_ccsm	1	9	ncar_ccsm	1	6	ncar_ccsm	1	4
gfdl	-1	10	gfdl	0	8	gfdl	0	6
cccma_t47	3	19	cccma_t47	2	14	cccma_t47	2	9
ncar_pcm	8	25	ncar_pcm	6	19	ncar_pcm	4	12
miroc	11	32	miroc	8	24	miroc	6	16
miub	8	**32**	miub	7	24	miub	5	16
cccma_t63	12	55	cccma_t63	9	41	cccma_t63	6	28

High global warming			Medium global warming			Low global warming		
South-East Gulf								
csiro	-22	-24	csiro	-17	-19	csiro	-12	-14
mri	-7	**-2**	mri	-5	-2	mri	-4	-2
inmcm	-2	4	inmcm	-1	2	inmcm	-1	1
giss_aom	-5	4	giss_aom	-4	2	giss_aom	-2	1
iap	-3	5	iap	-2	4	iap	-1	2
cnrm	-2	12	cnrm	-2	8	cnrm	-1	6
ncar_ccsm	2	15	ncar_ccsm	1	10	ncar_ccsm	1	6
ipsl	1	16	**ipsl**	1	**10**	ipsl	0	6
mpi	-1	18	mpi	-1	13	mpi	-1	8
gfdl	0	28	gfdl	0	20	gfdl	0	14
miroc	4	28	miroc	3	21	miroc	2	13
ncar_pcm	7	28	ncar_pcm	5	21	ncar_pcm	4	14
miub	6	35	miub	4	26	miub	3	17
cccma_t47	14	**49**	cccma_t47	11	37	cccma_t47	8	25
cccma_t63	14	62	cccma_t63	11	46	cccma_t63	8	31
Mitchell								
csiro	-21	-29	csiro	-16	-23	csiro	-11	-17
mri	-8	**-8**	mri	-6	-6	mri	-4	-5
iap	-1	7	iap	-1	5	iap	-1	3
giss_aom	-2	8	giss_aom	-1	5	giss_aom	-1	3
inmcm	1	11	inmcm	1	7	inmcm	1	4
cnrm	0	15	cnrm	0	11	cnrm	0	8
miroc	1	16	miroc	0	12	miroc	0	8
ncar_ccsm	3	16	**ncar_ccsm**	2	**11**	ncar_ccsm	2	7
ipsl	2	17	ipsl	1	11	ipsl	1	7
mpi	-2	17	mpi	-1	13	mpi	-1	8
ncar_pcm	4	18	ncar_pcm	3	13	ncar_pcm	2	9
miub	4	31	miub	3	23	miub	2	15
gfdl	0	36	gfdl	0	26	gfdl	0	17
cccma_t63	14	**54**	cccma_t63	11	41	cccma_t63	7	28
cccma_t47	17	58	cccma_t47	13	44	cccma_t47	9	30
Western Cape								
mri	-7	-7	mri	-5	-5	mri	-3	-3
giss_aom	-5	**1**	giss_aom	-3	-1	giss_aom	-2	0
miroc	-2	2	miroc	-2	2	miroc	-1	0
csiro	-9	2	csiro	-8	0	csiro	-5	1
ncar_pcm	2	7	ncar_pcm	1	6	ncar_pcm	1	5
inmcm	1	15	inmcm	1	11	inmcm	1	7
ncar_ccsm	5	17	ncar_ccsm	4	12	ncar_ccsm	3	9
ipsl	2	17	**ipsl**	2	**12**	ipsl	1	9
cnrm	2	19	cnrm	2	13	cnrm	1	11
iap	2	22	iap	2	17	iap	1	12
cccma_t63	11	24	cccma_t63	8	20	cccma_t63	6	15
miub	3	28	miub	2	22	miub	2	13
mpi	0	30	mpi	0	23	mpi	0	13
gfdl	-3	**49**	gfdl	-3	36	gfdl	-2	22
cccma_t47	26	53	cccma_t47	20	47	cccma_t47	14	37

High global warming			Medium global warming			Low global warming		
Northern Coral								
mri	-7	-7	mri	-5	-6	mri	-3	-4
csiro	-8	**2**	csiro	-6	1	csiro	-4	1
ncar_pcm	4	8	ncar_pcm	4	7	ncar_pcm	3	5
giss_aom	0	10	giss_aom	1	7	giss_aom	1	5
miroc	1	10	miroc	2	8	miroc	2	5
ncar_ccsm	5	11	ncar_ccsm	4	7	ncar_ccsm	4	5
inmcm	3	13	inmcm	3	10	inmcm	2	6
ipsl	4	16	**ipsl**	3	**11**	ipsl	3	8
iap	3	16	iap	3	13	iap	2	8
cnrm	4	17	cnrm	3	12	cnrm	3	9
mpi	0	23	mpi	0	18	mpi	1	11
miub	4	26	miub	4	20	miub	3	12
cccma_t63	15	28	cccma_t63	12	22	cccma_t63	9	16
cccma_t47	19	**37**	cccma_t47	15	30	cccma_t47	11	23
gfdl	1	59	gfdl	1	41	gfdl	2	26

3.3 Aggregation

Three Scenario C rasters (Cwet, Cmid and Cdry) were selected from the 45 future recharge simulations for further analysis. The GCMs associated with the three adopted rasters were selected on a reporting region basis; these are highlighted in bold type in Table 5. Scenario Cwet is the 2nd ranked from the high global warming scenario, Scenario Cmid is the 8th ranked from the medium global warming scenario and Scenario Cdry is the 14th ranked from the high global warming scenario. The results of this aggregation process are: recharge is projected to increase in all reporting regions under scenarios Cwet and Cmid, while recharge is projected to decrease under Scenario Cdry in all reporting regions except Western Cape and Northern Coral (Figure 19, Table 6).

Table 6. Recharge scaling factors (RSFs) for scenarios Cwet, Cmid and Cdry aggregated to reporting region level

Region	Cwet	Cmid	Cdry
Fitzroy (WA)	1.26	1.06	0.87
Kimberley	1.21	1.08	0.91
Ord-Bonaparte	1.39	1.09	0.97
Daly	1.38	1.13	0.98
Van Diemen	1.37	1.11	0.93
Arafura	1.34	1.15	0.91
Roper	1.48	1.13	0.98
South-West Gulf	1.39	1.09	0.99
Flinders-Leichhardt	1.32	1.02	0.88
South-East Gulf	1.49	1.10	0.98
Mitchell	1.54	1.11	0.92
Western Cape	1.49	1.12	1.01
Northern Coral	1.37	1.11	1.02

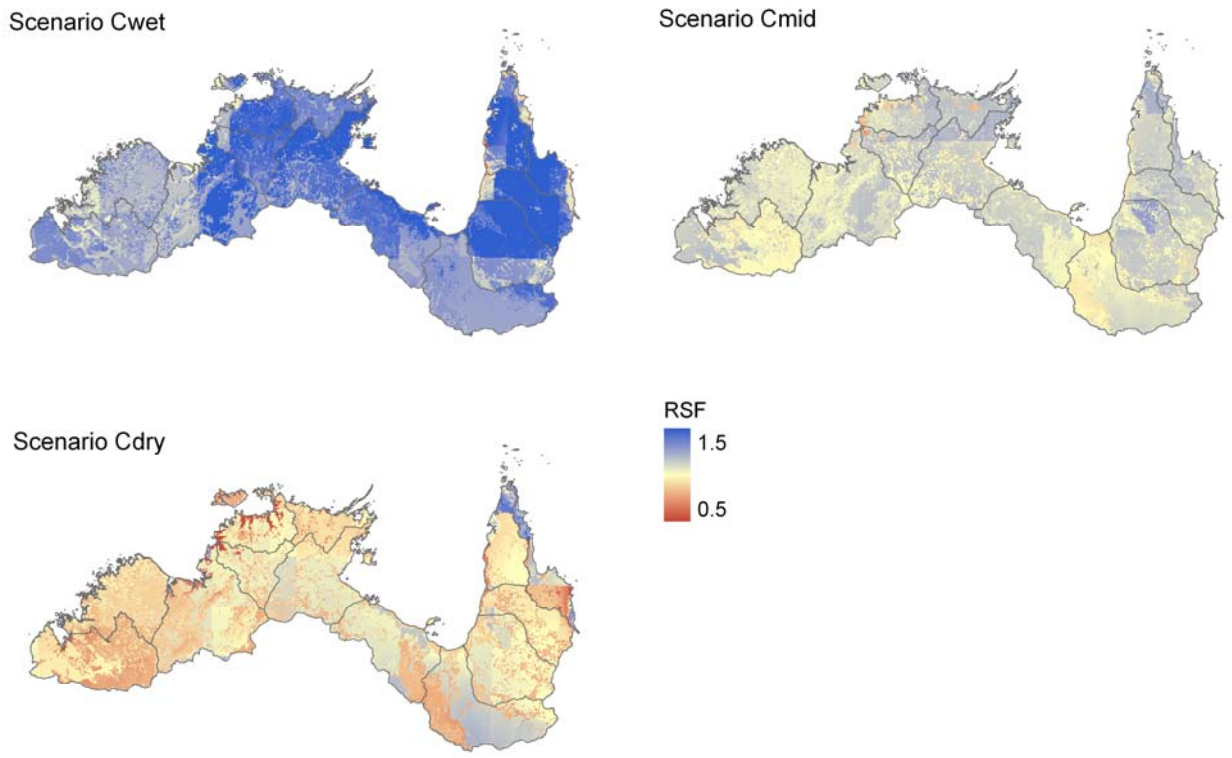

Figure 19. Composite rasters of recharge scaling factors (RSFs) for scenarios Cwet, Cmid and Cdry

3.4 Recharge time series for groundwater modelling

3.4.1 Daly model

The Daly model (Knapton, 2010) is a large regional model that incorporates parts of five reporting regions (Figure 20). The model has 44 recharge zones and each zone has a RSF calculated for each scenario (). These RSFs were used to calculate a time series for numerical modelling in FEFLOW. The time series was determined from the nearest control point (F) for the 23-year period that corresponded to that scenario.

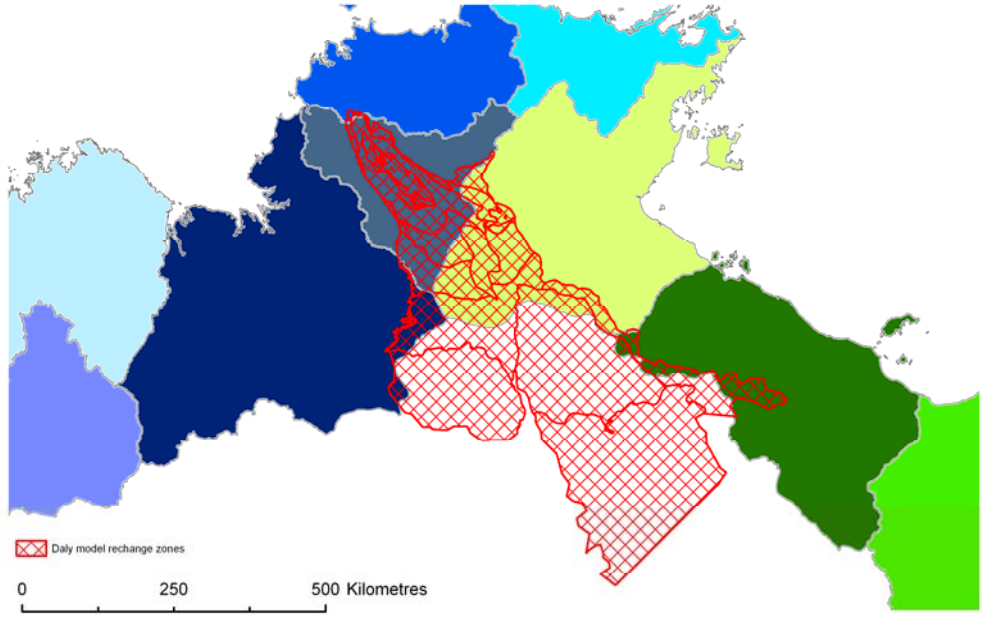

Figure 20. Daly model recharge zones overlaid on the NASY region map (Figure 1), showing its overlap with five reporting regions

Table 7. Recharge scaling factors (RSFs) for each recharge zone in the Daly model for scenarios A, B and C

Zone	Awet	Amid	Adry	B	Cwet	Cmid	Cdry
0	1.12	0.97	0.86	1.66	1.26	1.04	0.98
1	1.11	0.97	0.87	1.77	1.16	0.98	0.88
2	1.10	0.98	0.87	1.42	1.30	1.04	0.87
3	1.12	0.97	0.85	1.54	1.33	1.07	0.95
4	1.12	0.97	0.86	1.67	1.28	1.06	1.10
5	1.10	0.98	0.87	1.44	1.32	1.05	0.90
6	1.10	0.98	0.87	1.42	1.30	1.04	0.87
7	1.10	0.98	0.87	1.44	1.32	1.05	0.90
8	1.11	0.97	0.86	1.53	1.35	1.08	0.95
9	1.12	0.97	0.86	1.56	1.36	1.08	0.96
10	1.12	0.97	0.85	1.51	1.37	1.10	0.99
11	1.12	0.97	0.85	1.53	1.36	1.08	0.96
12	1.11	0.97	0.86	1.46	1.35	1.08	0.96
13	1.11	0.97	0.86	1.28	1.39	1.07	0.95
14	1.09	0.98	0.88	1.54	1.29	1.01	0.87
15	1.12	0.97	0.86	1.37	1.36	1.12	1.01
16	1.12	0.97	0.86	1.37	1.36	1.12	1.01
17	1.12	0.97	0.85	1.53	1.36	1.08	0.96
18	1.12	0.97	0.86	1.29	1.37	1.09	0.97
19	1.13	0.97	0.85	1.37	1.40	1.12	0.99
20	1.13	0.96	0.85	1.36	1.41	1.13	1.00
21	1.12	0.97	0.85	1.33	1.39	1.09	0.96
22	1.13	0.96	0.85	1.31	1.41	1.12	1.00
23	1.13	0.96	0.85	1.31	1.41	1.12	1.00
24	1.13	0.97	0.85	1.64	1.38	1.12	1.01
25	1.13	0.96	0.85	1.31	1.41	1.12	1.00
26	1.13	0.96	0.85	1.31	1.41	1.12	1.00
27	1.11	0.97	0.86	1.24	1.38	1.02	0.90
28	1.13	0.96	0.85	1.36	1.42	1.12	1.00
29	1.11	0.98	0.86	1.47	1.37	1.07	0.94
30	1.11	0.97	0.86	1.24	1.38	1.02	0.90
31	1.13	0.96	0.85	1.36	1.42	1.12	1.00

Zone	Awet	Amid	Adry	B	Cwet	Cmid	Cdry
32	1.11	0.97	0.86	1.24	1.38	1.02	0.90
33	1.12	0.97	0.85	1.63	1.42	1.07	0.95
34	1.12	0.97	0.85	1.63	1.42	1.07	0.95
35	1.11	0.97	0.86	1.27	1.42	1.04	0.92
36	1.09	0.98	0.87	1.28	1.40	0.97	0.85
37	1.09	0.98	0.87	1.28	1.40	0.97	0.85
38	1.12	0.97	0.86	1.52	1.38	1.10	1.02
39	1.11	0.97	0.86	1.28	1.39	1.07	0.95
40	1.10	0.98	0.87	1.06	1.39	1.08	0.94
41	1.11	0.97	0.86	1.15	1.43	1.13	0.96
42	1.12	0.97	0.86	1.29	1.40	1.09	0.97
43	1.12	0.97	0.85	1.01	1.49	1.13	0.98

3.4.2 Howard East model

The Darwin Rural Area – McMinn's – Howard East Section groundwater system model (Evans et al., 2009) is a small model that lies within the Van Diemen region (Figure 21). The model has three recharge zones and each zone has a RSF calculated for each scenario (Table 8). These RSFs were used to calculate a time series for numerical modelling in FEFLOW. The shape of the time series was determined from the nearest control point (E) for the 23-year period that corresponded to that scenario.

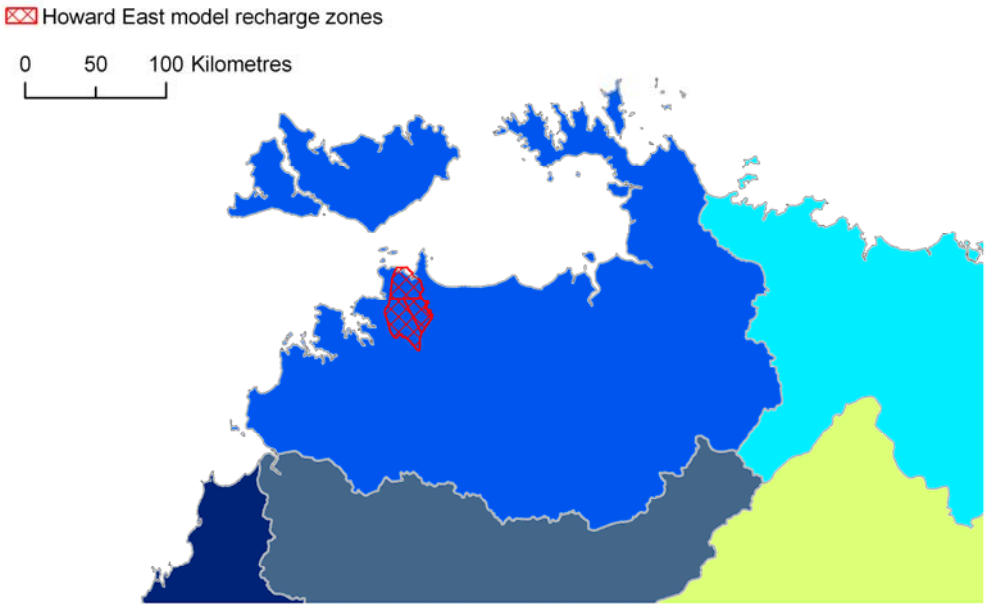

Figure 21. Howard East model recharge zones overlaid on the NASY region map (Figure 1), showing that the Howard East model is within the Van Diemen region

Table 8. Recharge scaling factors (RSFs) for each recharge zone in the Howard East model for scenarios A, B and C

Zone	Awet	Amid	Adry	B	Cwet	Cmid	Cdry
2	1.11	0.98	0.86	1.07	1.07	1.05	0.89
3	1.11	0.97	0.86	1.10	1.15	1.06	0.97
1	1.11	0.98	0.87	1.21	1.10	1.04	0.98

4 Discussion

4.1 A comparison of recharge estimates derived from WAVES to other methods

There are few methods available to estimate groundwater recharge and discharge over very large, data-poor areas. The method used for this project (i.e. upscaling WAVES point estimates) is effective for quantifying the changes in recharge due to different climate change scenarios; however the historical estimates have not been calibrated or tested against field data. Modelling recharge is not like modelling runoff where models can be calibrated to observed data. Instead estimations of recharge vary widely in magnitude and in the spatial and temporal resolution.

To evaluate the upscaled WAVES estimates of recharge, model results were compared with estimates of recharge from a chloride mass balance and estimates of discharge from the separation of baseflow from stream gauge records. While the methods employed here are suited to large data-poor areas it is important to understand that they are not estimating the same quantity and so cannot be directly compared.

Gross recharge (R_g) is water that passes the root zone and crosses the plane of the watertable, net recharge (R_n) is that proportion of groundwater recharge that is not subject to evapotranspiration, and groundwater discharge is groundwater that leaves the saturated zone as baseflow (B) to streams or evapotranspiration. Gross recharge has been estimated as the 77-year means under Scenario A. Net recharge is estimated using a steady state chloride mass balance. Groundwater discharge has been estimated using a digital filter on stream gauging data; thus only estimating the baseflow component of groundwater discharge. A relative comparison of each method is presented at the scale of the 13 reporting regions.

4.1.1 Chloride mass balance

The steady state chloride mass balance (CMB) approach is based upon the fact that evapotranspiration removes water but not chloride and hence chloride is concentrated in the groundwater compared to rainfall. Knowing the chloride deposition and concentration of chloride in groundwater enables an estimate of the net recharge to be made. Eriksson (1985) showed that it is the arithmetic mean of the deposition (D) and the harmonic mean of the groundwater chloride concentrations (C_{gw}) that are used in the CMB:

$$\overline{R_n} = \overline{D}\,\overline{\left(1/C_{gw}\right)} \tag{10}$$

Literature values of chloride deposition across northern Australia were collated and a regression equation was fitted with chloride deposition versus distance from the coast. The double exponential form of the regression equation has previously been used by Keywood et al. (1997). The use of the regression equation enabled chloride deposition to be modelled on a 0.05° grid across northern Australia. The chloride deposition as used for this study does not make any allowance for chloride lost in overland flow or chloride dry deposited by impingement and entrainment on vegetation. As these two processes act in different directions on the estimates of chloride to be used in the chloride mass balance it has been assumed that they are of approximately the same order of magnitude and therefore cancel each other out.

The chloride concentration of groundwater was estimated from all measurements recorded in the state databases for bores drilled less than 20 m deep. In some areas there were very little data so the chloride concentration of streams during the dry season was also used. Using the stream concentrations of chloride assumes that the stream is entirely groundwater fed during the dry season. Where stream chloride concentrations have been used they are treated as a point estimate in the same way as the chloride measurements of groundwater.

There were 23 locations with chloride deposition estimates collated from the literature over the past few decades (Table 9); this is spatially variable and conspicuous by the complete lack of data from within the study region in Queensland (Figure 23). There is a lot of scatter in the relationship between chloride deposition (D) and the distance from the coast (x) resulting in a wide confidence interval around the line of best fit ().

The regression equation fitted was:

$$D = 44.2e^{-0.0288x} + 2.83e^{-4.05*10^{-11}x} \quad (11)$$

Table 9. Literature values of chloride deposition used for estimating relationship between chloride deposition and distance from the coast

Latitude	Longitude	Cl deposition	Distance from coast	Reference	Site	Year
		kg/ha/y	km			
-12.68	132.42	8.1	36	(Keywood et al., 1997)	Kapalga	1992-1994
-14.45	132.3	1.7	235	(Wetselaar and Hutton, 1963)	Katherine	1958-1960
-14.63	132.45	2.5	258	(Keywood et al., 1997)	Katherine	1992-1994
-14.44	132.27	5.0	240	(Wilson et al., 2006)	Katherine	2005-2006
-13.83	131.19	6.7	122	(Wilson et al., 2006)	Douglas	2005-2006
-14.92	133.13	6.0	250	(Wilson et al., 2006)	Mataranka	2005-2006
-15.5	128.75	9.9	55	(Hingston and Gailitis, 1976)	Wyndham	1973
-15.8	128.75	4.3	70	(Hingston and Gailitis, 1976)	Kununara	1973
-17.97	122.15	13.0	0	(Hingston and Gailitis, 1976)	Broome	1973
-18	124.18	3.5	78	(Hingston and Gailitis, 1976)	Camballin	1973
-18.18	125.55	2.4	205	(Hingston and Gailitis, 1976)	Fitzroy Crossing	1973
-18.22	127.65	6.5	315	(Hingston and Gailitis, 1976)	Halls Creek	1973
-12.65	132.8	10.1	54	(Noller et al., 1985)	1,3,4	1982-1983
-12.5	132.85	10.4	40	(Noller et al., 1985)	5,6,9	1982-1983
-12.8	132.8	13.5	65	(Noller et al., 1985)	10,11	1982-1983
-14.02	136.6	56.0[2]	20	(Langkamp and Dalling, 1983)	Groote Eylandt	1979-1980
-19.08	121.67	13.3	0	(Hingston and Gailitis, 1976)	Nita Downs[1]	1973
-19.3	146.8	51.0	9	(Probert, 1976)	Townsville[1]	1972-73
-19.63	146.83	23.5	40	(Probert, 1976)	Lansdown[1]	1972-73
-19.91	134.36	2.7	530	(Keywood et al., 1997)	Tennant Creek[1]	1992-1994
-20.3	118.57	99.6	0	(Hingston and Gailitis, 1976)	Port Hedland[1]	1973
-20.33	119.22	4.6	30	(Hingston and Gailitis, 1976)	Goldsworthy[1]	1973
-16.79	133.45	1.8	300	(Keywood et al., 1997)	Dunmarra[1]	1992-1994

[1] This site is outside the NASY project area but was included because it was close
[2] The chloride deposition was estimated at this site from an ion balance

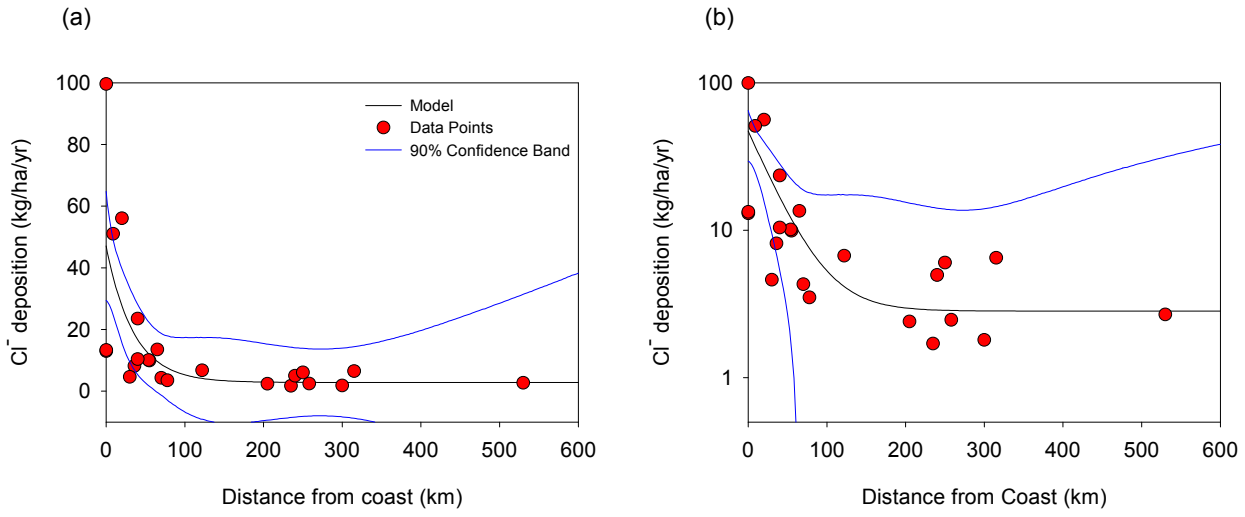

Figure 22. Relationship between chloride deposition and distance from the coast, displayed with chloride deposition on (a) a linear scale and (b) a logarithmic scale

The amount of data available for the estimation of chloride in groundwater is less than ideal. In total there were 2759 bores with data and 210 surface water locations with dry season chloride measurements. The most data-poor area was the Kimberley (KI) with no estimates of chloride in groundwater and only 11 gauging stations with measurements of dry season chloride concentration in surface water. The most data-rich area was Van Diemen (VD) region which had 1527 bores with measurements of chloride in groundwater and 56 gauging stations with measurements of dry season chloride concentration in surface water.

The individual estimates of net recharge from a single bore or surface water sampling site were quite variable (Figure 23) ranging from 1 to >1000 mm/year from the surface water estimates and from 0.1 to >1000 mm/year from the groundwater estimates. The extreme values are recorded from locations with very little data and on occasion only a single estimate of chloride concentration. When all the observations from a reporting region are combined an average estimate of the net recharge is always less than the mean annual rainfall.

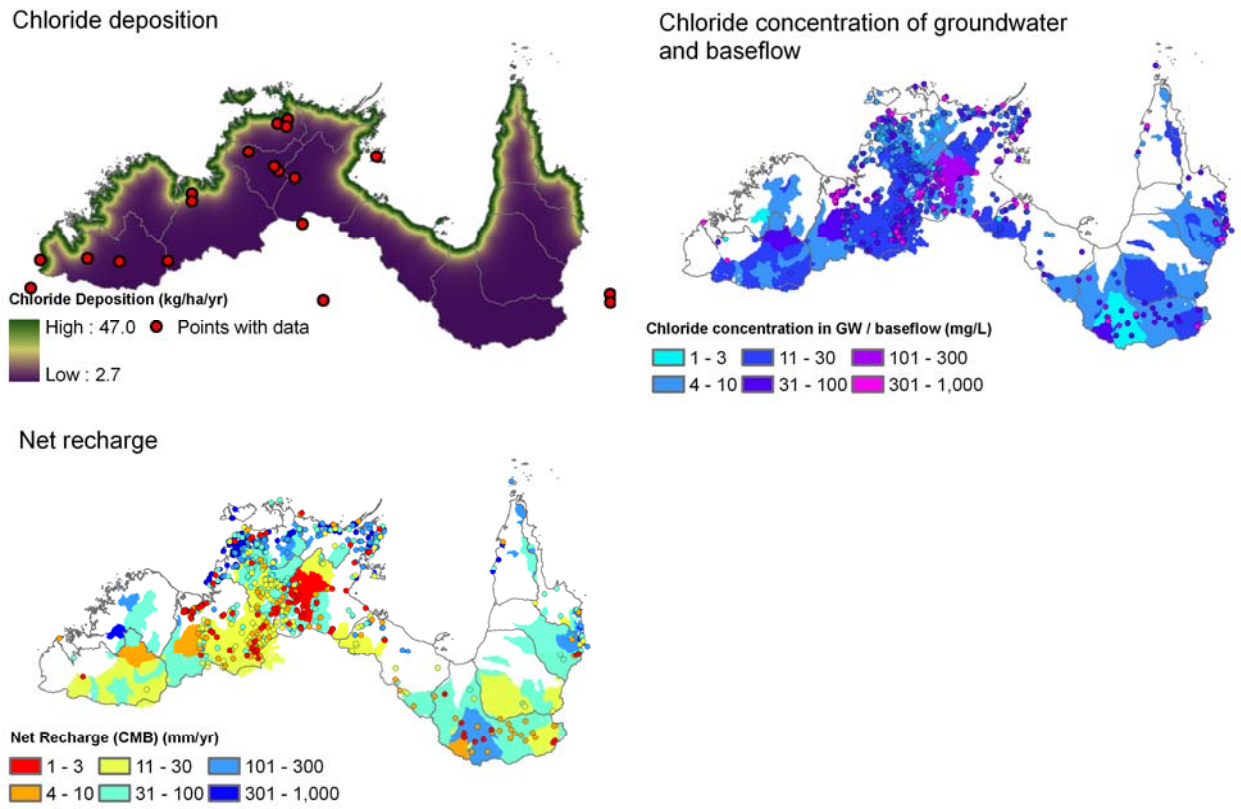

Figure 23. Chloride mass balance across northern Australia showing the chloride deposition, the concentration of chloride in groundwater and baseflow, and the resultant net recharge

4.1.2 Baseflow separation of streamflow

A recursive digital filter was used to separate the baseflow from the total flow at all the gauging stations where chloride measurements were available across northern Australia. Although the most widely used filter in Australia is still the one proposed by Lynne and Hollick (1979), this has no physical basis and has been criticised for not being able to match tracer studies (Grayson et al., 1996). The form of the filter used for this study is as suggested by Eckhardt (2005):

$$b_k = \frac{(1 - BFI_{\max})\, a\, b_{k-1} + (1-a) BFI_{\max}\, y_k}{1 - a\, BFI_{\max}} \qquad (12)$$

where b_k is baseflow at time k, y_k is total flow at time k, BFI_{max} and a are fitting parameters. The values used for the fitting parameters are parameters recommended by Eckhardt (2005) as appropriate for an ephemeral stream with a porous aquifer; BFI_{max} = 0.5, and a = 0.925. These parameters make this filter equivalent to the one proposed by Chapman and Maxwell (1996).

The baseflow was averaged over the time of gaugings to obtain a mean annual; this was divided by the area of the gauged subcatchment to get the baseflow as a depth which can then be readily compared to the estimates of gross and net recharge. It was assumed that the effect of missing values in the gauging record would be minimal across the timeframe of investigation.

To aggregate results to a reporting region, an area-averaged baseflow depth was used. In nested catchments, the area used is the area that is not measured by another gauge. In this way an area is only counted once no matter how many gauges are downstream of that point.

The results of the baseflow separation were also spatially variable (Figure 24) with a highest value of 1700 mm and a lowest of <1 mm. As has been found in other studies the baseflow index increased with increasing catchment size (Petheram et al., 2008). It is hard to determine whether this is due to increased groundwater discharge in the lower parts of a catchment or peak flow attenuation.

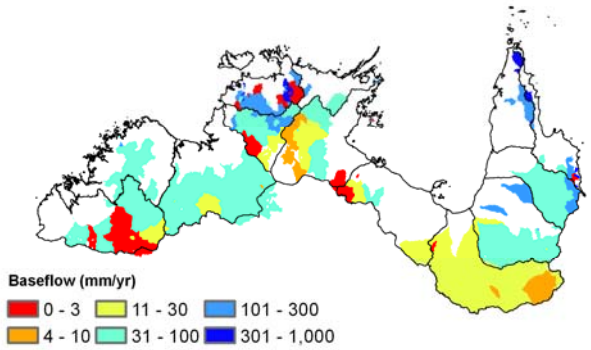

Figure 24. Baseflow in gauged catchments that have measurements of dry season chloride concentration in surface water

4.1.3 Assessment of method

When the different methods are aggregated to a common reporting level they can be compared. Care needs to be taken as the three methods are not estimating the same quantity and the estimates used in the aggregation are not spatially consistent between methods (Figure 13, Figure 23 and Figure 24). The working hypothesis was that gross recharge should be the highest and baseflow the lowest. However, this occurred in only 3 of the 13 reporting regions (Figure 25). Generally the gross recharge estimates were greater than the net recharge estimates (9 of the13) and the baseflow estimates (12 of the 13). The calculation of net recharge allowed error estimates to be calculated from the 90 percent confidence limits in the chloride deposition and the chloride concentration. These error estimates are very wide due to uncertainty in the chloride deposition estimates, and in 9 of the 13 reporting regions, the error bars on the net recharge encompass the estimates of gross recharge and baseflow.

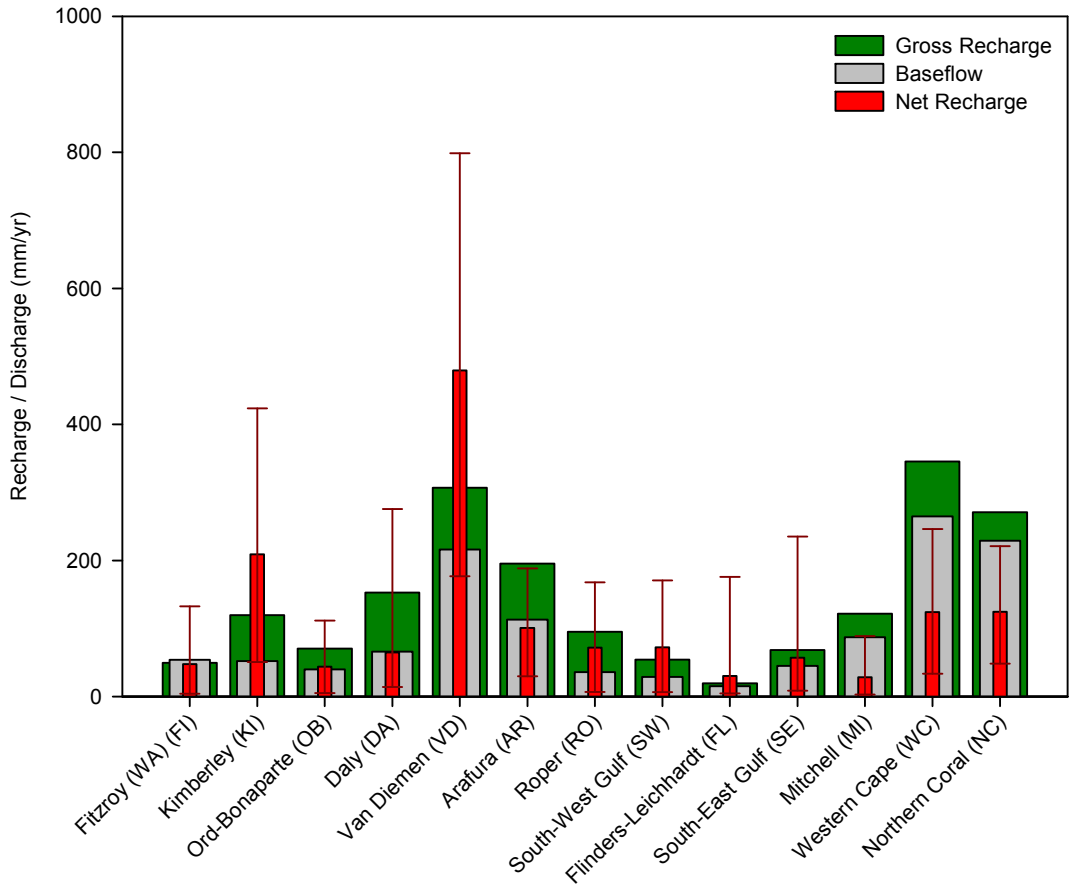

Figure 25. A comparison between gross recharge estimated as the 77-year mean under Scenario A, net recharge as determined by chloride mass balance, and baseflow as determined by digital filter for each reporting region

Further, at the broad scale, spatial patterns of recharge and discharge are as expected, with the highest recharge and discharge in the highest rainfall areas of the Van Diemen, Western Cape and Northern Coral regions and the lowest recharge and discharge estimated to be in the low rainfall areas of the Flinders-Leichhardt and South-West Gulf regions. This analysis gives some confidence that the recharge estimates from upscaling WAVES modelling are appropriate for Scenario A and therefore appropriate to be using for Scenarios B and C.

4.2 A sensitivity analysis of recharge to WAVES climate inputs

The Scenario C modelling produced some counter-intuitive results whereby the mean annual recharge increased from a decrease in mean annual rainfall. At a pixel level these trends were investigated for rainfall and each of the global warming scenarios for recharge (Figure 26). For the majority of northern Australia the trends in GCM outputs for rainfall show that between one-third and two-thirds of GCMs predict an increase. This is different to recharge where for most of northern Australia recharge is projected to increase for more GCMs than rainfall. To investigate the cause of these results a sensitivity analysis of the climate inputs to WAVES was undertaken in a similar manner to that used to investigate the MDBSY project results (McCallum et al., 2009).

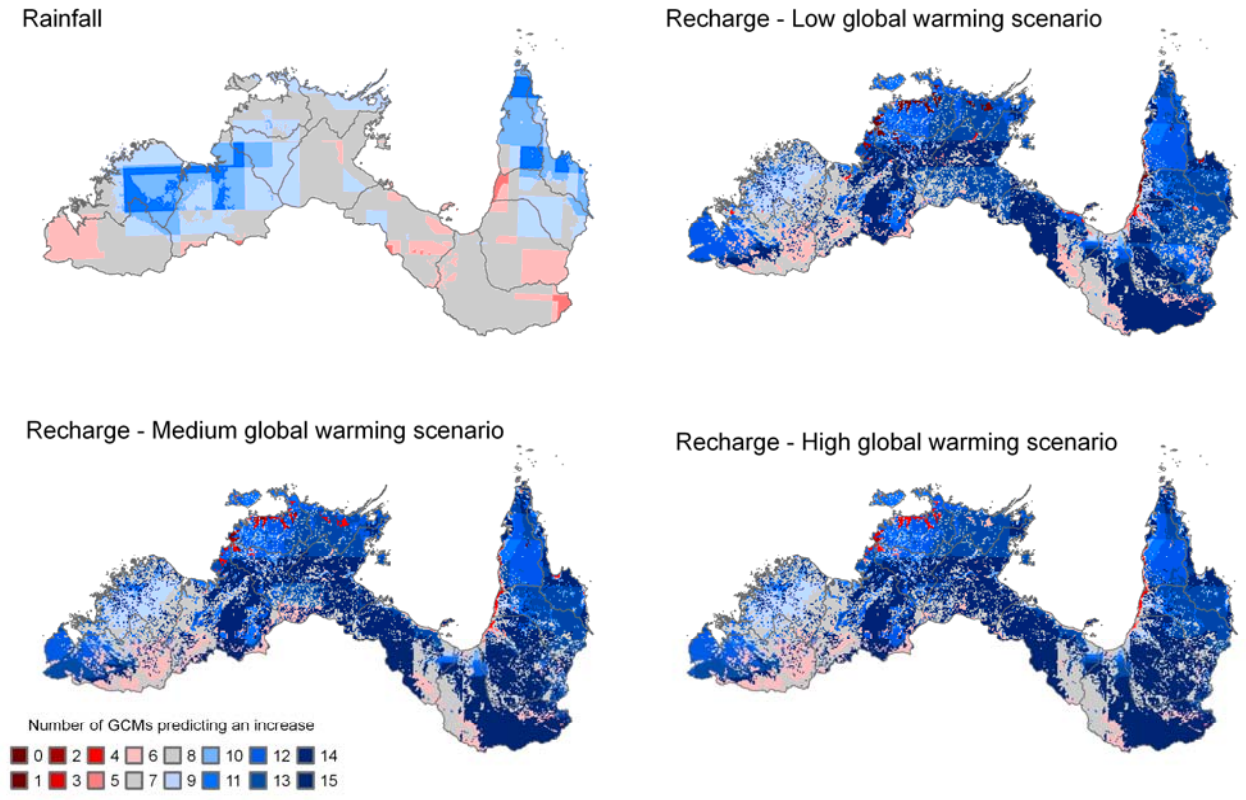

Figure 26. Number of GCM-derived climate scenarios that predict an increase in recharge for the low, medium and high global warming scenarios and compared to the number of GCMs which predict an increase in rainfall

Three control points were selected to reflect the rainfall gradient; the climate variables at each site were then systematically altered to investigate their impact upon recharge. This was done for the most common soil type across northern Australia (Kandasols) and the two most common vegetation types (savannah and perennial grasslands). The control points selected were: D for the low rainfall example; E for the high rainfall example; and, Q for the medium rainfall example.

The variables under investigation were:

- Rainfall – a 10 percent increase or decrease in daily rainfall
- CO_2 concentration – a baseline of 380 ppm and 437, 446 and 455 ppm which are the concentrations used for the low, medium and high global warming scenarios respectively
- Temperature – a baseline and increases of 0.7°C, 1.0°C and 1.3°C which are the temperatures used for the low, medium and high global warming scenarios respectively
- Vapour pressure deficit – a 10 percent increase or decrease in the daily VPD
- Solar radiation – a 10 percent increase or decrease in the daily solar radiation
- Daily rainfall intensity either increasing or decreasing.

Changes to the daily rainfall intensity were made by ranking the daily rainfall from highest to lowest and then multiplying the daily rainfall total with a multiplier that varied linearly between 1.5 for the highest daily rainfall and 0.5 for the lowest. The total rainfall was then scaled back to that of the original time series. In this way the high intensity rainfall events were increased and the low rainfall events were decreased but the total amount of rainfall over the 77 years was identical. The multipliers were reversed to get the low intensity scenario.

The results of the sensitivity analysis are reported as percentage changes in recharge (ΔR), transpiration (ΔT), evaporation (ΔE) and leaf area index (ΔLAI).

4.2.1 Rainfall

The results of the investigation into the sensitivity of recharge estimates to changes in total rainfall amounts are as expected (Figure 27). When rainfall increases so too does recharge, and vice versa. The change in recharge is greater than the change in rainfall, being between 2.3 and 3.7 times greater depending upon the scenario. The changes in evaporation and transpiration also reflect the changes in water availability; they change in the same direction as the change in rainfall.

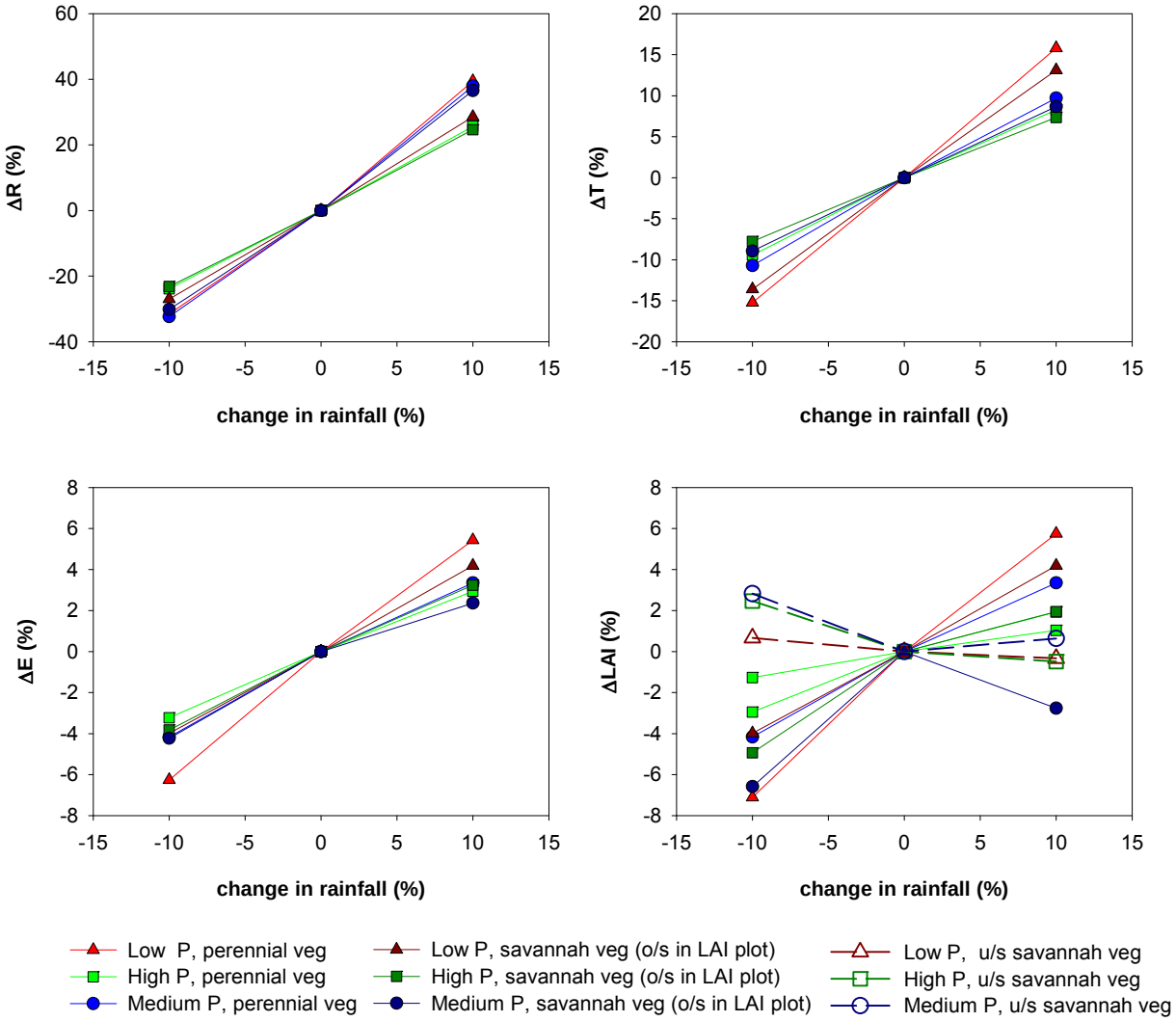

Figure 27. Sensitivity of recharge estimates for perennial and savannah vegetation on Kandasol soils to changes in daily rainfall (P)

4.2.2 Carbon dioxide

Under a high CO_2 atmosphere vegetation is able to assimilate carbon more efficiently and therefore less water is required. However the increased carbon assimilation leads to increased leaf area and consequently more interception of rainfall on the plant canopy, much of which is subsequently evaporated. The change in recharge will be dependent upon the relative balance of the changes in transpiration and evaporation. In the cases modelled here the change in recharge due to increases in CO_2 concentration is quite small and generally increases except for the savannah vegetation at the low rainfall climate point (Figure 28).

Of interest here is that the leaf area index (LAI) of the understorey (u/s) in the savannah (S) vegetation is decreasing under increasing CO_2 concentration while that of the overstorey (o/s) in increasing in the low and medium rainfall scenarios. The modelling is suggesting that increasing CO_2 concentrations favour the overstorey at the expense of the understorey. The modelling is predicting more trees. There has been an increase in woody vegetation across Australia over the last few decades that has been attributed to increased CO_2 concentration (Donohue et al., 2009), this sensitivity analysis is consistent with these observations.

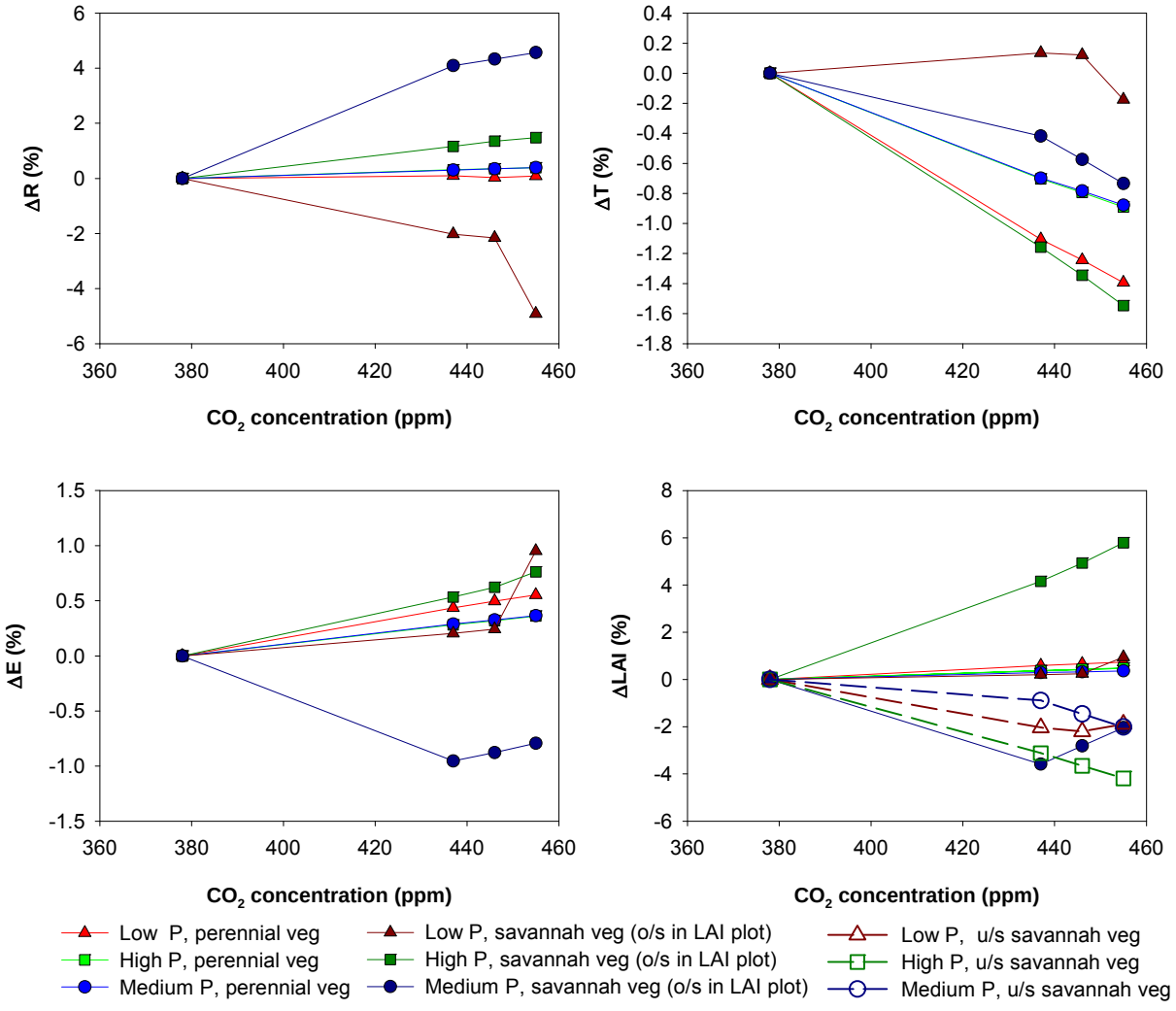

Figure 28. Sensitivity of recharge estimates for perennial and savannah vegetation on Kandasol soils to changes in concentration of carbon dioxide in the atmosphere

4.2.3 Temperature

The results of this sensitivity analysis show that increased temperature leads to increased recharge. This is counter-intuitive as increased temperature increases potential ET and would be expected to decrease recharge. The answer lies in the LAI plot (Figure 29). The increased temperature leads to decreased LAI because the vegetation is not able to assimilate carbon as efficiently. Transpiration is increased but carbon assimilation is reduced, the reduced canopy area leads to less rainfall interception and ultimately wetter soil and more recharge.

Cartwright and Simmonds (2008) speculated that increased temperature could lead to less vegetation and ultimately more recharge, the modelling undertaken here adds some credence to this argument.

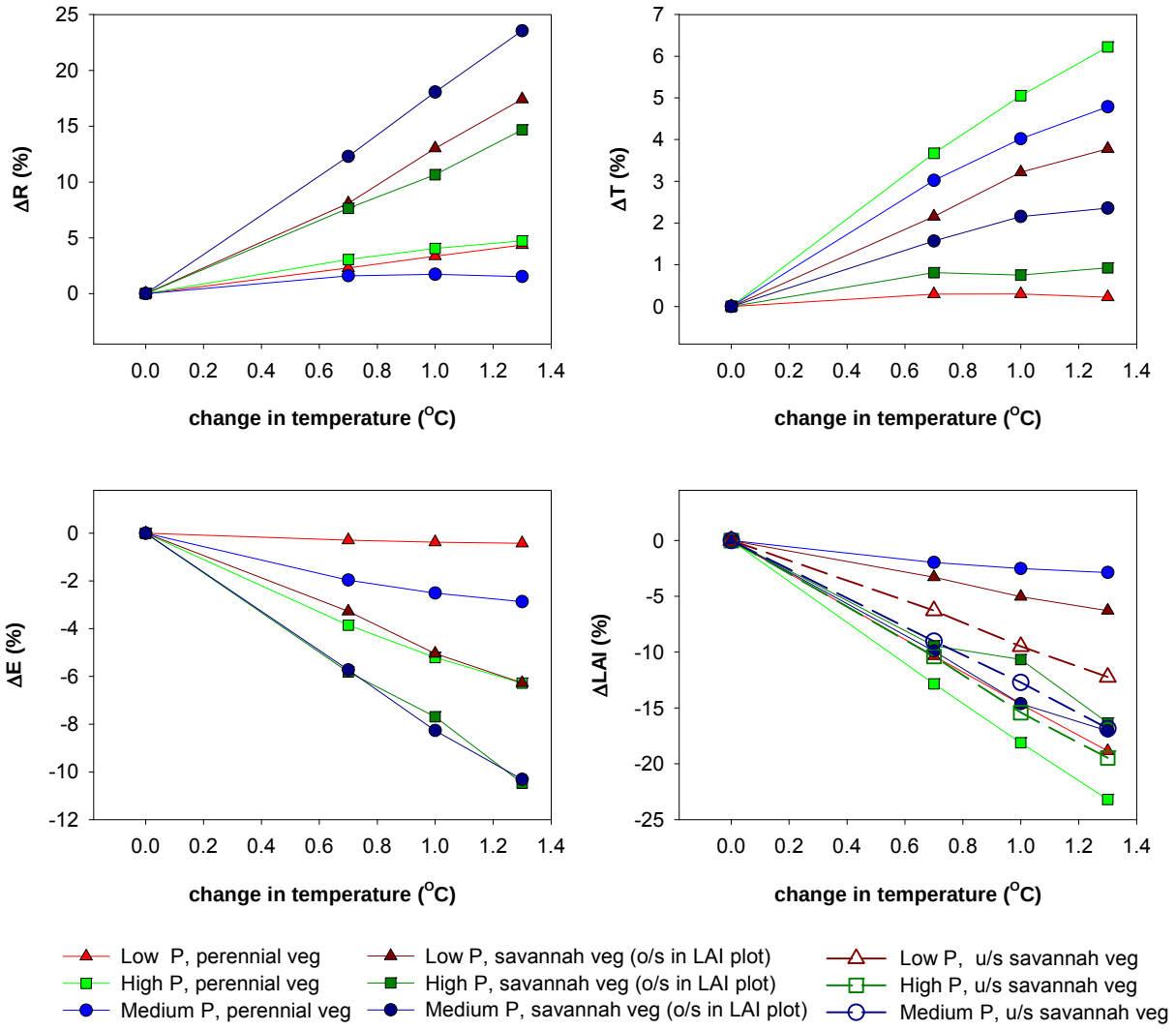

Figure 29. Sensitivity of recharge estimates for perennial and savannah vegetation on Kandasol soils to changes in temperature

There is also the possibility that climate change could lead to ecological succession. Higher temperatures mean that the vegetation as modelled is pushed outside of its optimum temperature range; this presents an opportunity for different species to dominate. To test the effect that optimum vegetation growth temperatures have upon modelling recharge, the vegetation parameters relating to optimum temperature were increased at the same rate as the atmospheric temperature. The results of this process show that recharge still increases under a future climate but the magnitude is greatly reduced (Figure 30). Investigating the impact of climate change on vegetation is beyond the scope of this project but this demonstration highlights how important changes in vegetation could be to groundwater recharge.

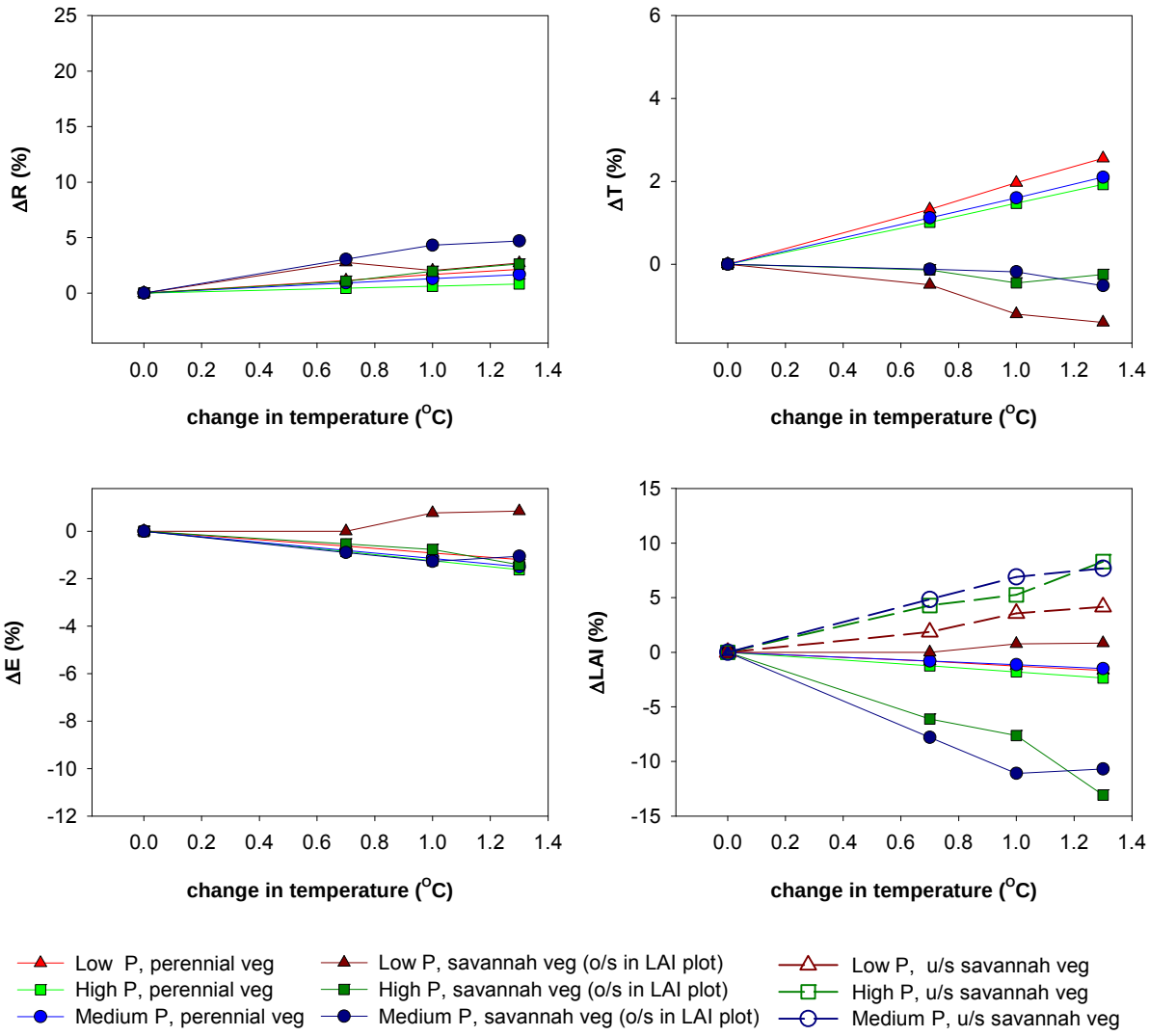

Figure 30. Sensitivity of recharge estimates for perennial and savannah vegetation on Kandasol soils to changes in temperature if the vegetation's optimum growth temperature is allowed to increase at the same rate as the atmospheric temperature

4.2.4 Vapour pressure deficit

Changes in vapour pressure deficit have a small effect upon recharge with increased vapour pressure deficit resulting in less recharge (Figure 31). The small changes are due to more water (i.e. higher transpiration) being required to assimilate the same amount of CO_2. This results in small changes in LAI and evaporation. The changes predicted in vapour pressure deficit (calculated via changes in relative humidity and temperature) by the GCMs are small and so the impact of these changes will be negligible.

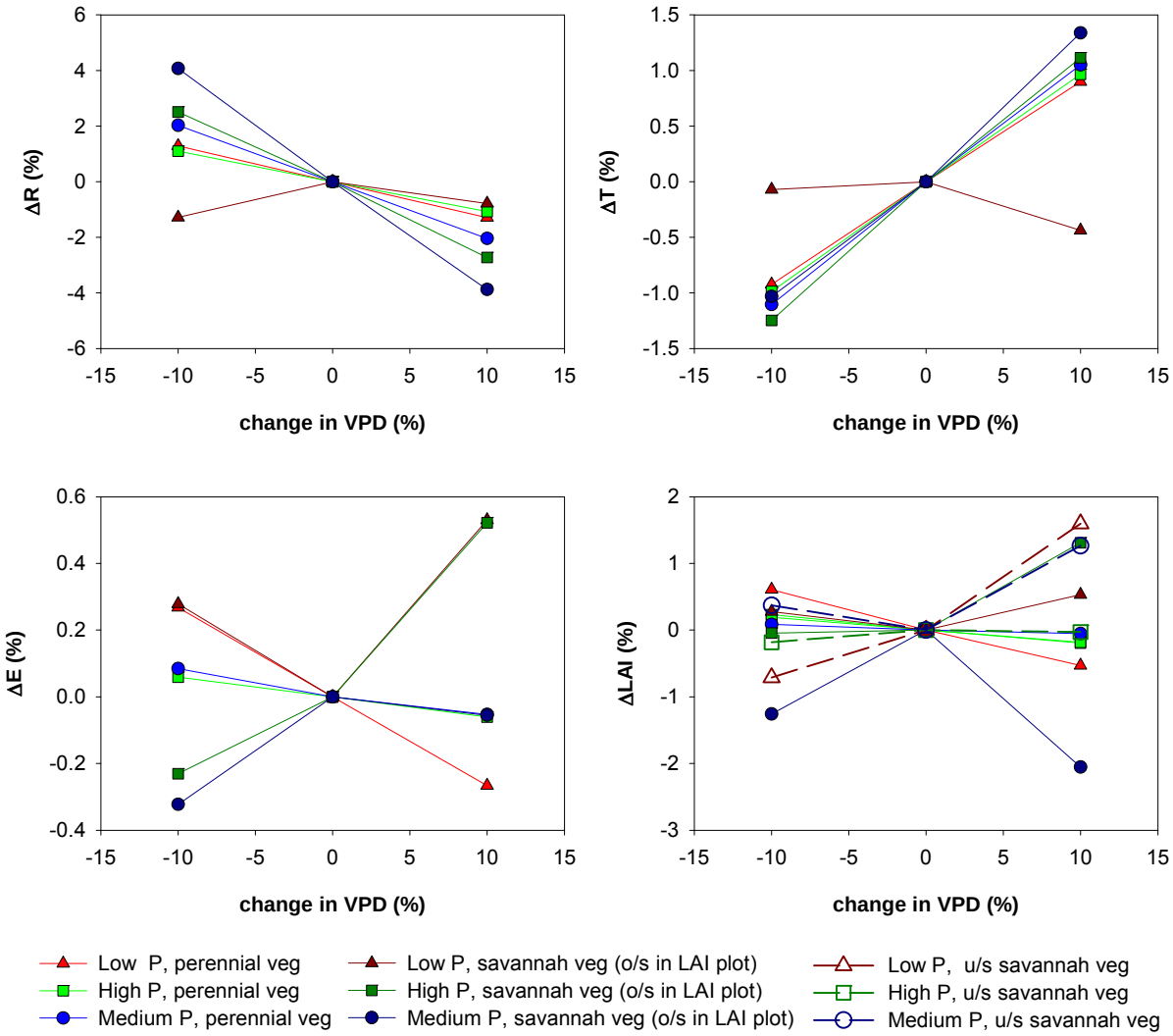

Figure 31. Sensitivity of recharge estimates for perennial and savannah vegetation on Kandasol soils to changes in vapour pressure deficit

4.2.5 Solar radiation

Solar radiation is the driving force for evapotranspiration and so has a large effect upon recharge with increases in solar radiation resulting in decreases in recharge (Figure 32). However, the changes to modelled solar radiation from the GCMs are generally less than one percent and so have very little effect upon recharge.

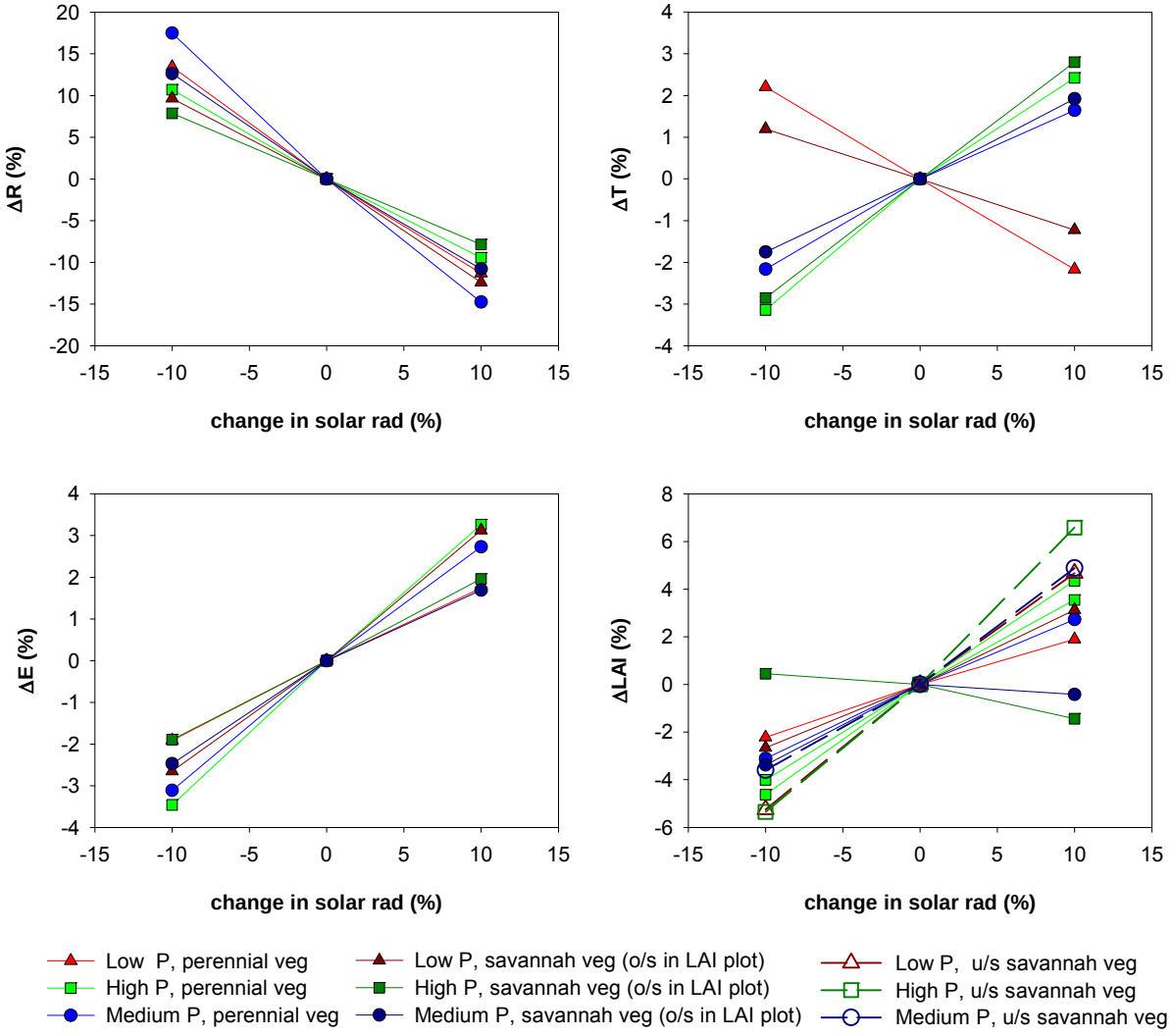

Figure 32. Sensitivity of recharge estimates for perennial and savannah vegetation on Kandasol soils to changes in solar radiation

4.2.6 Daily rainfall intensity

Recharge is very sensitive to changes in rainfall intensity, increases in rainfall intensity result in increased recharge (Figure 33). This is due to the reduction in frequency of small rainfall events that are intercepted by the vegetation canopy and evaporated before reaching the soil moisture store. This means that even if the total amount of rainfall does not change, an increase in rainfall intensity would result in more rainfall entering the soil moisture store and, in turn, being available for transpiration or recharge. Change in rainfall intensity has been shown to be an important driver of changes in recharge, however GCMs are not particularly good at estimating rainfall intensity and so there is considerable uncertainty about this parameter in the modelling (Sun et al., 2006).

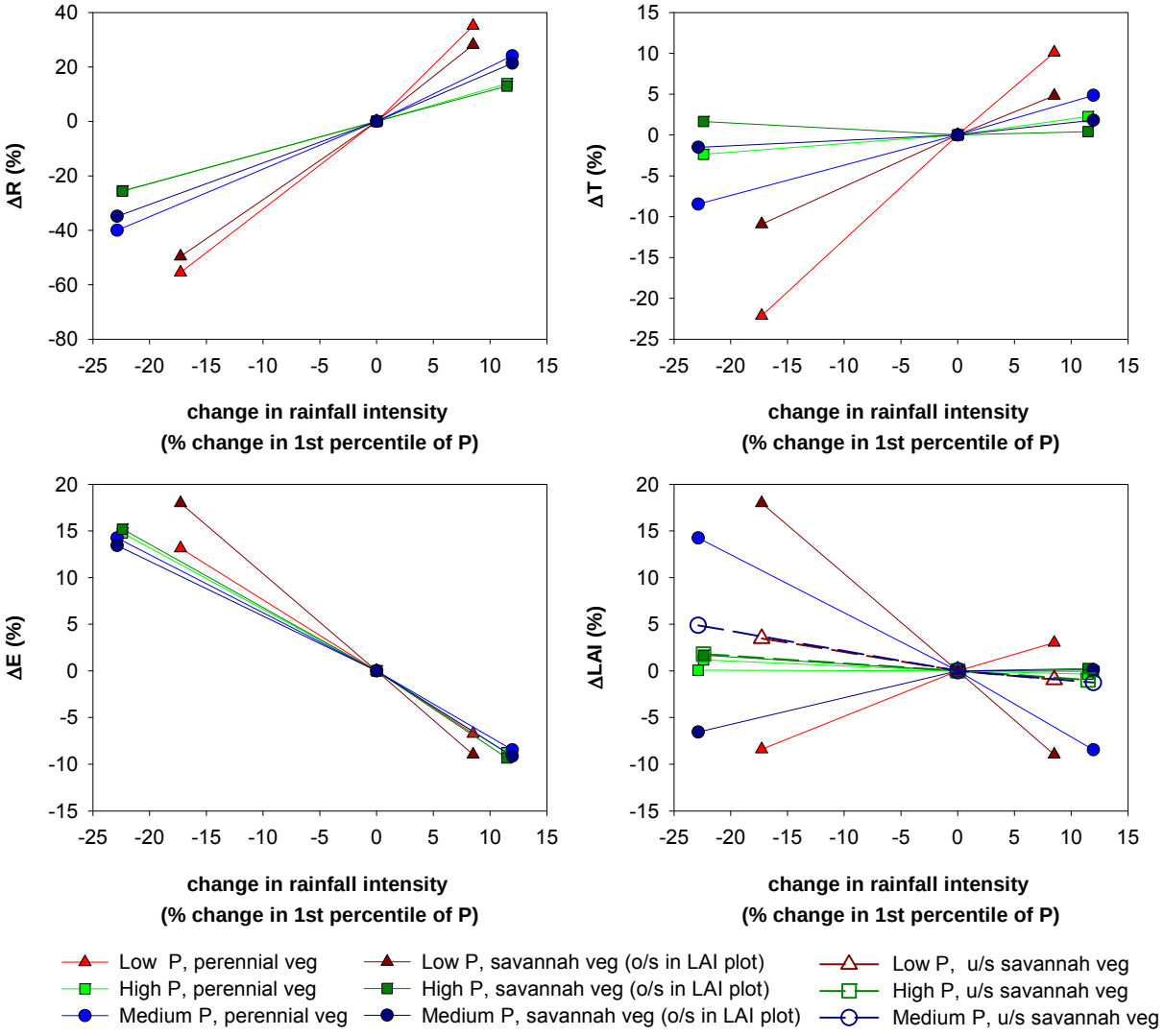

Figure 33. Sensitivity of recharge estimates for perennial and savannah vegetation on Kandasol soils to changes in daily rainfall intensity

4.2.7 Relationship to Scenario C

The sensitivity analysis has shown that after total rainfall, the next most important climate variables for recharge are rainfall intensity and temperature. The three global warming scenarios are defined by their increase in global temperature and so are quite similar, but the resultant changes in rainfall intensity are different between different GCMs. A probability of exceedance curve of daily rainfall and recharge was constructed for control points D, E and Q for perennial and savannah vegetation types on Kandasol soils; these are shown in Figure 34 and Figure 35. These figures show the changes in high intensity rainfall events and their effect upon recharge. Of particular interest is the model runs where the change in recharge is in the opposite direction to the change in rainfall (shown in red and blue on Figure 34 and Figure 35).

Through the MDBSY project the episodicity of rainfall was shown to be a useful predictor of changes in recharge. A useful metric for investigating the change in episodicity of rainfall is the proportion of total rainfall in the top 1 percent of daily records (Crosbie et al., 2009a):

$$E_P = \frac{\sum_{0<p<0.01} P_i}{\sum P_i} \tag{13}$$

where E_P is the episodicity of rainfall.

For the perennial vegetation at control point D, there was one model run where the rainfall increased but the recharge decreased; this model run had a reduced episodicity of rainfall when compared to that under Scenario A. For the perennial vegetation at control point E, there were two model runs where the rainfall decreased but the recharge increased; one of these model runs had the episodicity of rainfall increase and the other was almost the same as under Scenario A. For the perennial vegetation at control point Q, there was one model run where recharge increased from decreased rainfall and another where the recharge decreased from an increase in rainfall. In the case where the recharge increased the episodicity of the rainfall increased and the opposite was true for the case where the recharge decreased.

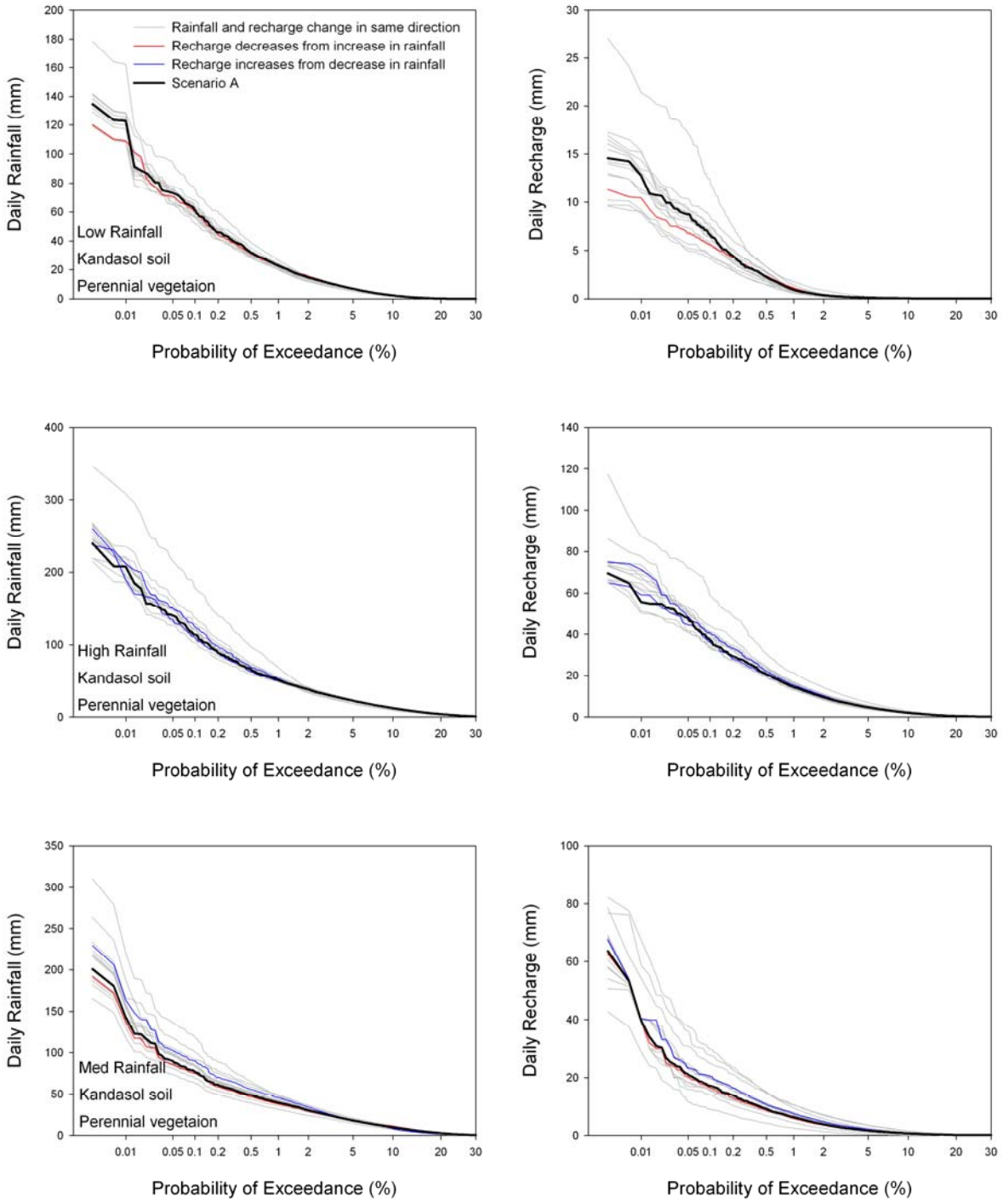

Figure 34. Probability of exceedance curves for daily rainfall and recharge for perennial grasses on Kandasol soils for the high global warming scenario for the 15 GCMs at control points D (low rainfall), E (high rainfall) and Q (medium rainfall)

For the savannah vegetation at point D there were five model runs where the recharge increased from a decrease in rainfall; in four out five of these cases the episodicity of rainfall increased. For the savannah vegetation at point E there were five model runs where recharge increased from a decrease in rainfall; in three out of the five cases the episodicity of rainfall increased. For the savannah vegetation at point Q there were four model runs where recharge increased from a decrease in rainfall; in all four cases the episodicity of rainfall increased.

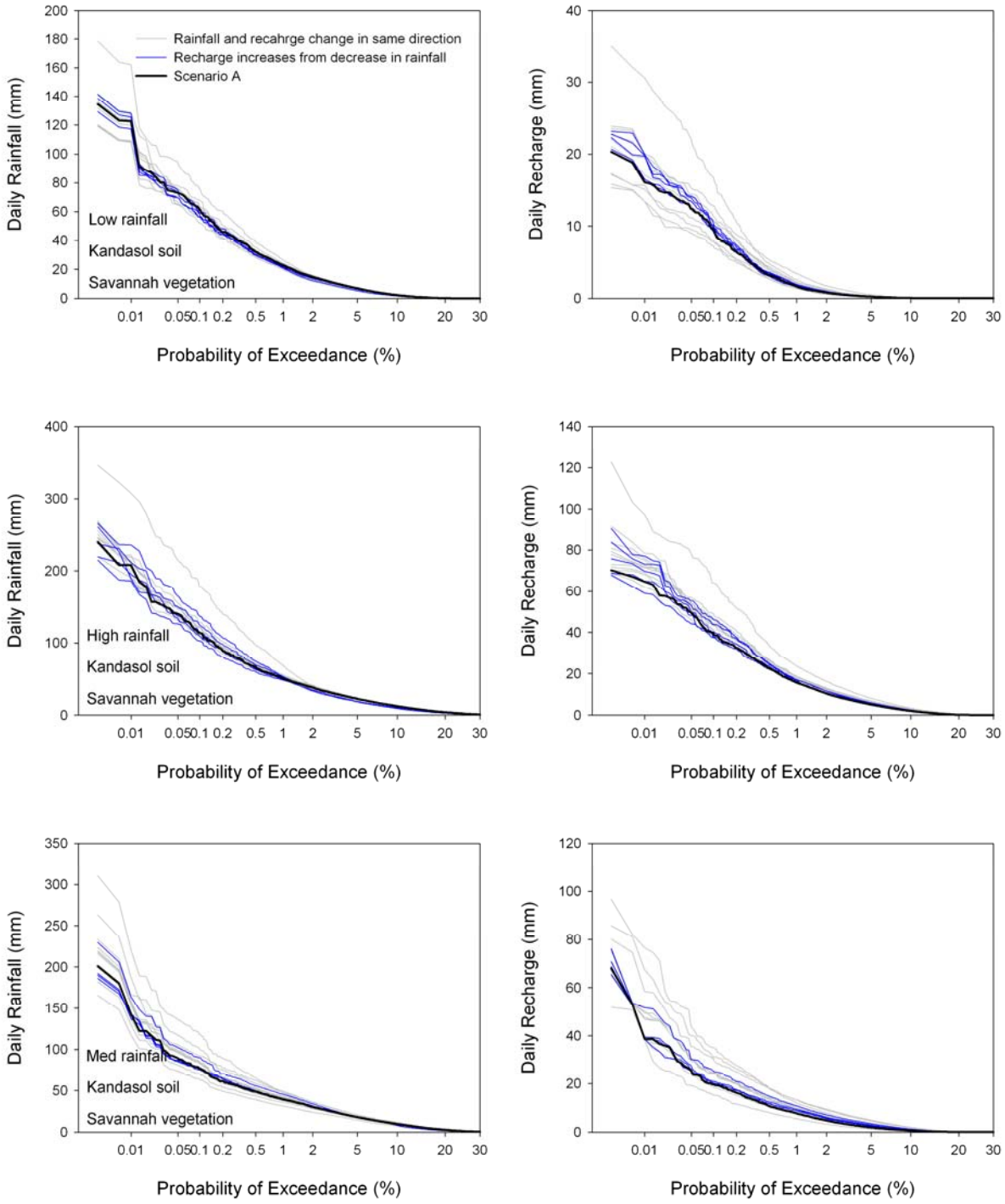

Figure 35. Probability of exceedance curves for daily rainfall and recharge for perennial grasses on Kandasol soils for the high global warming scenario for the 15 GCMs at control points D, E and Q

This analysis has shown that in most examples where recharge has increased from a decrease in rainfall that changes in rainfall intensity is at least partly the cause. In all examples shown where recharge decreased from an increase in rainfall the changes in rainfall intensity are at least partly the cause.

4.3 An assessment of the results in light of the performance of the GCMs

The analysis in this project assumes that each GCM is equally good. However, some GCMs are better than others at replicating the historical climate and this is used to judge their ability to predict a future climate. It is prudent to check the results obtained from assuming that each GCM is equally good to assuming that some are better than others. Post et al. (2009) presented the results of different studies examining the performances of the different GCMs as is relevant to the different sustainable yields projects around the country (Table 10). The best GCM was assessed to be GFDL which scored above the median in nine out 10 tests and the worst was NCAR_PCM which scored below the median in all tests.

Table 10. Weights for each GCM for use in weighted Pearson Type III distribution. The weights are 1 minus the failure rate identified by Post et al. (2009)

Model	Weight
cccma_t47	0.4
cccma_t63	0.5
cnrm	0.37
csiro	0.5
gfdl	0.9
giss_aom	0.37
iap	0.33
inmcm	0.5
ipsl	0.11
miroc	0.8
miub	0.75
mpi	0.7
mri	0.7
ncar_ccsm	0.62
ncar_pcm	0

A methodology for fitting the 15 RSF rasters for a global warming scenario to a weighted Pearson Type III distribution was presented by Crosbie et al. (2009b). This method allows a comparison to be made of the 10th, 50th and 90th percentiles of the RSFs at a pixel scale when the probability distribution is weighted for GCM performance or unweighted if all GCMs are assumed equal.

The difference between the weighted and unweighted cases is small (Figure 36). For the 10 percent exceedance case of the high global warming scenario (akin to Scenario Cwet) the greatest differences are in the Northern Coral region with a 0.06 increase in RSF and Van Diemen with a 0.04 RSF decrease (Table 11). This is not surprising as the GFDL model is the highest weighted and predicts more recharge for the Northern Coral region and less for the Van Diemen region, while the NCAR_PCM is the lowest weighted model and it predicts less recharge for the Northern Coral region and more recharge for the Van Diemen region (Figure 18). The 50 percent exceedance case of the medium global warming scenario (akin to Scenario Cmid) is very similar to the 10 percent exceedance case of the high global warming scenario with Northern Territory showing a decrease in RSF for the weighted case compared to the unweighted case, Western Australia showing very little change and the Queensland regions showing an increase in RSF. The 90 percent exceedance case of the high global warming scenario (akin to Scenario Cdry) shows a different pattern to the other two cases, for most of the NASY project area the weighted case shows either no change or a small decrease in RSF, South-West Gulf is the only region to show an increase in RSF for the weighted case when compared to the unweighted case. Overall, the differences between the weighted and unweighted cases are small and justify the decision to treat all GCMs as being equal.

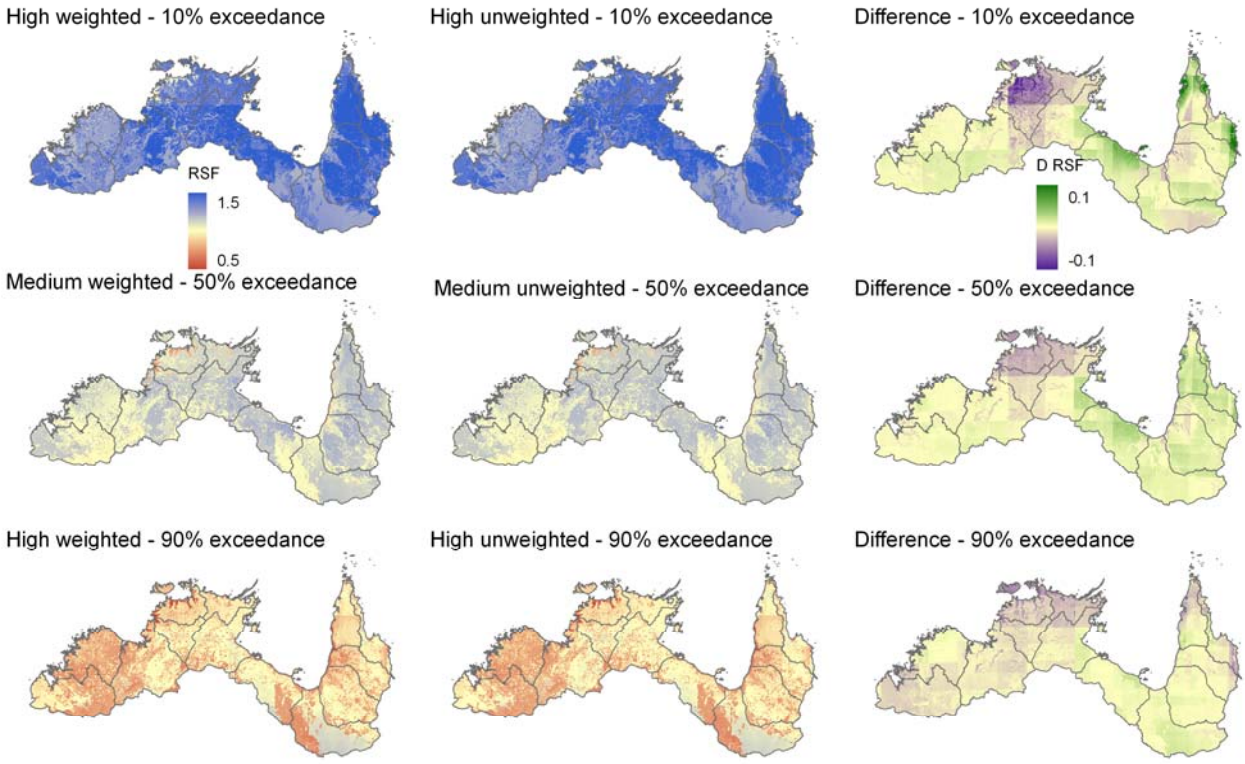

Figure 36. A comparison of the weighted and unweighted RSF rasters after being fitted to a Pearson Type III distribution. The plot shows the 10th and 90th percentile exceedance rasters for the high global warming scenario and the 50th percentile exceedance for the medium global warming scenario. The difference plots are the weighted minus the unweighted

Table 11. Comparison of the average RSFs calculated for each reporting region from the RSFs as output from the Pearson Type III distribution for the weighted and unweighted cases

Reporting Region	Unweighted			Weighted		
	H-10	M-50	H-90	H-10	M-50	H-90
Fitzroy (WA)	1.34	1.06	0.86	1.35	1.06	0.85
Kimberley	1.27	1.08	0.81	1.27	1.08	0.81
Ord-Bonaparte	1.43	1.11	0.89	1.43	1.11	0.88
Daly	1.41	1.13	0.94	1.38	1.11	0.93
Van Diemen	1.37	1.10	0.90	1.33	1.08	0.88
Arafura	1.41	1.13	0.95	1.39	1.11	0.93
Roper	1.45	1.14	0.96	1.45	1.13	0.95
South-West Gulf	1.42	1.11	0.92	1.44	1.13	0.93
Flinders-Leichhardt	1.37	1.05	0.82	1.38	1.06	0.82
South-East Gulf	1.48	1.12	0.91	1.48	1.13	0.91
Mitchell	1.48	1.12	0.89	1.49	1.13	0.89
Western Cape	1.48	1.12	0.93	1.51	1.13	0.92
Northern Coral	1.46	1.11	0.94	1.52	1.13	0.92

4.4 An assessment of the methodology

4.4.1 Limitations of the methodology

The method used in this study is very similar to that used in the MDBSY project and therefore suffers from the same limitations. The WAVES model has been used extensively around the world and shown to be able to reproduce the results from field trials; however, the way it has been used here has some limitations.

WAVES is a Richard's equation-based model that routes water through the soil matrix. There is no mechanism within the model to simulate recharge that bypasses the soil matrix. At a point scale, there is some evidence to suggest that preferential flow paths are an important mechanism for recharge within the project area (Wilson et al., 2006). This could be overcome within the model by increasing the hydraulic conductivity, however this approach has not been adopted.

The model assumed a 4 m soil column. In areas where there was no soil (i.e. rock outcrops) the results will be inaccurate because the model parameters were developed for soil not rock.

The soil parameters used (Table 2) were taken from a national database and do not seem appropriate in some cases. For example, the hydraulic conductivities for most soil types are higher than those used in the MDBSY project. The higher hydraulic conductivities used will lead to higher recharge being estimated. The effect this has upon the results are minimised by reporting the recharge for the different scenarios as RSFs, the absolute value of the recharge calculation is not given priority in the reporting.

The modelling assumes a free-draining lower-boundary condition; this will overestimate recharge in high watertable areas because the watertable will not limit the amount of rainfall that can be infiltrated.

The vegetation parameters used in WAVES were taken from literature values; there is insufficient detailed information on the vegetation of northern Australia to have confidence that the vegetation parameters used are correct. The effect this has upon the results is minimised by reporting the recharge for the different scenarios as RSFs, the absolute value of the recharge calculation is not given priority in the reporting.

4.4.2 Further work required

There are few field studies of recharge across northern Australia so there is no way to validate the historical estimates of recharge made here. The upscaled WAVES estimates of recharge were compared with independent estimates of net recharge and baseflow to test the accuracy of the modelling. The comparison was hampered by a lack of data and so the uncertainty was high in all methods. Better results could have been obtained had more field based data existed.

The modelling undertaken here demonstrates the impact vegetation has upon recharge. The Scenario C for this project was current development with a future climate; it was assumed that the vegetation was the same as historical. The modelling here suggests that under a future climate there is the possibility for ecological succession with changes in climate favouring some vegetation types over others. Investigating these changes was beyond the scope of this project, but could have changed the recharge results had they been incorporated.

5 Conclusions

This project used a similar methodology to that used in the MDBSY project to estimate the changes in diffuse groundwater recharge across northern Australia.

Under the historical climate (Scenario A) the results were very consistent between reporting regions with the median projection for the next 23 years being a 2 to 3 percent decrease in recharge with the extremes projecting between a 13 to 15 percent decrease in recharge to a 10 to 13 percent increase in recharge.

Under the recent climate (Scenario B) the majority of the reporting regions showed an increase in groundwater recharge with a maximum increase of 60 percent above the historical average for the South-West Gulf region. The South-East Gulf, Mitchell and Northern Coral were the only reporting regions to show a decrease in recharge under a recent climate.

Under the future climate (Scenario C) the median projection is for an increase in recharge in the next 23 years of between 2 and 15 percent depending upon reporting region. Under the wet extreme (Scenario Cwet), the projections for all reporting regions show an increase in recharge of between 21 and 54 percent. Under the dry extreme (Scenario Cdry), most reporting regions are projected to see a decrease in recharge of up to 13 percent except for the Western Cape and Northern Coral regions which show a small increase in recharge under Scenario Cdry.

The number of GCM-derived climate sequences projecting an increase or decrease in recharge can be informative for looking at trends. For the majority of northern Australia the trends in GCM outputs for rainfall show that between one-third and two-thirds of GCMs predict an increase for a 2030 climate relative to a 1990 climate. This is different to recharge where for most of northern Australia recharge is projected to increase for more GCMs than rainfall.

This counter-intuitive result was explained via a sensitivity analysis of the climate variables in WAVES. It was found that increased rainfall, temperature, CO_2 concentration and daily rainfall intensity lead to increased recharge and increased solar radiation and vapour pressure deficit lead to reduced recharge. After rainfall, it is changes in temperature and daily rainfall intensity that recharge is most sensitive to when modelled using WAVES. Both are projected to increase under a future climate and so the results of the modelling show that recharge increases under more future climate model runs than rainfall.

There is also the possibility that climate change could lead to ecological succession. Higher temperatures mean that the vegetation as modelled is pushed outside of its optimum temperature range; this presents an opportunity for different species to dominate. The implication of this observation is that the results presented here are for the current vegetation, there is the possibility that under a future climate the vegetation could change having an additional impact upon recharge.

References

Broadbridge, P. and White, I., 1998. Constant rate rainfall infiltration: A versatile non-linear model: I. Analytical solution. Water Resources Research, 24: 145-154.

BRS, 2003. Integrated Vegetation Cover (2003) Version 1, Bureau of Rural Sciences, Canberra.

Cartwright, I. and Simmonds, I., 2008. Impact of changing climate and land use on the hydrogeology of southeast Australia. Australian Journal of Earth Sciences, 55(8): 1009-1021.

Chapman, T.G. and Maxwell, A.I., 1996. Baseflow separation - comparison of numerical methods with tracer experiments, 23rd Hydrology and Water Resources Symposium, Hobart, Australia, pp. 539-545.

Crosbie, R.S., McCallum, J., Walker, G.R. and Chiew, F.H.S., 2008a. Diffuse groundwater recharge modelling across the Murray-Darling Basin. A report to the Australian government from the CSIRO Murray-Darling Basin Sustainable Yields project, Water for a Healthy Country Flagship. CSIRO, Canberra, http://www.csiro.au/files/files/pn7z.pdf.

Crosbie, R.S., McCallum, J.L., Walker, G.R. and Chiew, F.H.S., 2009a. The impact of climate change on the episodicity of groundwater recharge. Submitted to Hydrogeology Journal.

Crosbie, R.S., McCallum, J.L., Walker, G.R. and Chiew, F.H.S., 2009b. Modelling the climate change impact on groundwater recharge in the Murray-Darling Basin. Submitted to Hydrogeology Journal.

Crosbie, R.S., Wilson, B., Hughes, J.D., McCulloch, C. and King, W.M., 2008b. A comparison of the water use of tree belts and pasture in recharge and discharge zones in a saline catchment in the Central West of NSW, Australia. Agricultural Water Management, 95(3): 211-223.

CSIRO, 2009a. Description of methods. A report to the Australian Government from the CSIRO Northern Australia Sustainable Yields Project. CSIRO Water for a Healthy Country Flagship, Australia.

CSIRO, 2009b. Water in the Gulf of Carpentaria drainage Division: A report to the Australian Government from the CSIRO Northern Australia Sustainable Yields Project. CSIRO Water for a Healthy Country Flagship, Australia.

CSIRO, 2009c. Water in the Northern North-East Coast drainage Division: A report to the Australian Government from the CSIRO Northern Australia Sustainable Yields Project. CSIRO Water for a Healthy Country Flagship, Australia.

CSIRO, 2009d. Water in the Timor Sea drainage Division: A report to the Australian Government from the CSIRO Northern Australia Sustainable Yields Project. CSIRO Water for a Healthy Country Flagship, Australia.

Dawes, W., Zhang, L. and Dyce, P., 2004. WAVES v3.5 User Manual, CSIRO Land and Water, Canberra.

Dawes, W.R., Gilfedder, M., Stauffacher, M., Coram, J., Hajkowicz, S., Walker, G.R. and Young, M., 2002. Assessing the viability of recharge reduction for dryland salinity control: Wanilla, Eyre Peninsula. Australian Journal of Soil Research, 40(8): 1407-1424.

Donohue, R.J., McVicar, T.R. and Roderick, M.L., 2009. Climate-related trends in Australian vegetation cover as inferred from satellite observations, 1981-2006. Global Change Biology, 15(4): 1025-1039.

Eckhardt, K., 2005. How to construct recursive digital filters for baseflow separation. Hydrological Processes, 19(2): 507-515.

Eriksson, E., 1985. Principles and applications of hydrochemistry. Chapman and Hall Ltd, New York.

Evans, P., Arunakumaren, J., Burrows, W. and Raue, J., 2009. Groundwater modelling for the Darwin Rural Area, Northern Territory. A report to the CSIRO Northern Australia Sustainable Yields Project from EHA., Water for a Healthy Country Flagship, CSIRO, Canberra.

Grayson, R., Argent, R., Nathan, R., McMahon, T. and Mein, R., 1996. Hydrological recipes: Estimation techniques in Australian hydrology. CRC Catchment Hydrology, Melbourne, 125 pp.

Hingston, F.J. and Gailitis, V., 1976. The geographic variation of salt precipitated over Western Australia. Australian Journal of Soil Research, 14(3): 319-335.

IPCC, 2007. Climate Change 2007: The Physical Science Basis. Contribution of Working Group 1 to the Fourth Assessment Report of the Intergovernmental Panel on Climate Change. Cambridge University Press, Cambridge UK, 996 pp.

Isbell, R.F., 2002. Australian Soils Classification. CSIRO, Collingwood, Victoria, 144 pp.

Jeffrey, S.J., Carter, J.O., Moodie, K.B. and Beswick, A.R., 2001. Using spatial interpolation to construct a comprehensive archive of Australian climate data. Environmental Modelling & Software, 16(4): 309-330.

Johnston, R.M., Barry, S.J., Bleys, E., Bui, E.N., Moran, C.J., Simon, D.A.P., Carlile, P., McKenzie, N.J., Henderson, B.L., Chapman, G., Imhoff, M., Maschmedt, D., Howe, D., Grose, C., Schoknecht, N., Powell, B. and Grundy, M., 2003. ASRIS: the database. Australian Journal of Soil Research, 41(6): 1021-1036.

Keywood, M.D., Chivas, A.R., Fifield, L.K., Cresswell, R.G. and Ayres, G.P., 1997. The accession of chloride to the western half of the Australian continent. Australian Journal of Soil Research, 35: 1177-89.

Knapton, A., 2010. Groundwater modelling for the Tindall Limestone aquifer, Northern Territory. A report to the CSIRO Northern Australia Sustainable Yields Project from NRETAS, Water for a Healthy Country Flagship, CSIRO, Canberra.

Langkamp, P.J. and Dalling, M.J., 1983. Nutrient Cycling in a Stand of Acacia holosericea A. Cunn. Ex G. Don. III. Calcium, Magnesium, Sodium and Potassium. Australian Journal of Botany, 31(2): 141-149.

Li, L., McVicar, T.R., Donohue, R.J., van Neil, T.G., Teng, J., Potter, N.J., Smith, I.N., Kirono, D.G.C., Bathols, J.M., Cai, W.J., Marvanek, S.P., Chiew, F.H.S. and Frost, A.J., 2009. Climate data and their characterisation for hydrological scenario

modelling across northern Australia: a report to the Australian Government from the CSIRO Northern Australia Sustainable Yields Project, CSIRO Water for a Healthy Country Flagship, Canberra.

Lynne, V. and Hollick, M., 1979. Stochastic time variable rainfall runoff modelling, Hydrology and Water Resources Symposium, Perth, Australia, pp. 89-92.

McCallum, J.L., Crosbie, R.S., Walker, G.R. and Dawes, W.R., 2009. Impacts of climate change on groundwater: A sensitivity analysis of recharge. Submitted to Hydrogeology Journal.

Noller, B.N., Currey, N.A., Cusbert, P.J., Tuor, M., Bradley, P. and Harrison, A., 1985. Temporal variability in atmopheric nutrient flux to the Magela and Nourlangie Creek system, Northern Territory. Proceedings of the Ecological Society of Australia, 13: 21-31.

Petheram, C., McMahon, T.A. and Peel, M.C., 2008. Flow characteristics of rivers in northern Australia: Implications for development. Journal of Hydrology, 357(1-2): 93-111.

Post, D.A., Chiew, F.H.S., Teng, J., Vaze, J., Yang, A., Mpelasoka, F., Smith, I.N., Katzfey, J., Marston, F., Marvanek, S.P., Kirono, D., Nguyen, K., Kent, D., Donohue, R.J. and McVicar, T.R., 2009. Climate scenarios for Tasmania. Tasmania Sustainable Yields Project. A report to the Australian Government from the CSIRO Tasmania Sustainable Yields Project, CSIRO, Canberra.

Probert, M.E., 1976. The composition of rainwater at two sites near townsville, Qld. Australian Journal of Soil Research, 14(3): 397-402.

Salama, R., Hatton, T. and Dawes, W., 1999. Predicting land use impacts on regional scale groundwater recharge and discharge. Journal of Environmental Quality, 28(2): 446-460.

Slavich, P.G., Walker, G.R., Jolly, I.D., Hatton, T.J. and Dawes, W.R., 1999. Dynamics of Eucalyptus largiflorens growth and water use in response to modified watertable and flooding regimes on a saline floodplain. Agricultural Water Management, 39(2-3): 245-264.

Strack, O.D.L., 1999. Principles of the analytic element method. Journal of Hydrology, 226(3-4): 128-138.

Sun, Y., Solomon, S., Dai, A.G. and Portmann, R.W., 2006. How often does it rain? Journal of Climate, 19(6): 916-934.

Wang, H.X., Zhang, L., Dawes, W.R. and Liu, C.M., 2001. Improving water use efficiency of irrigated crops in the North China Plain - measurements and modelling. Agricultural Water Management, 48(2): 151-167.

Wetselaar, R. and Hutton, J.T., 1963. The ionic composition of rainwater at Katherine, NT. and its part in the cycling of plant nutrients. Australian Journal of Agricultural Research, 14(3): 319-329.

Wilson, D., Cook, P.G., Hutley, L., Tickell, S. and Jolly, P., 2006. Effect of land use on evapotranspiration and recharge in the Daly River catchment. Technical Report No. 17/2006D, Northern Territory Department of Natural Resources, the Environment and the Arts.

Xu, C., Martin, M., Silberstein, R. and Smetten, K., 2008. Identifying sources of uncertainty in groundwater recharge estimates using the biophysical model WAVES, Water Down Under, Adelaide, Australia.

Yang, Y.H., Watanabe, M., Wang, Z.P., Sakura, Y. and Tang, C.Y., 2003. Prediction of changes in soil moisture associated with climatic changes and their implications for vegetation changes: Waves model simulation on Taihang Mountain, China. Climatic Change, 57(1-2): 163-183.

Zhang, L. and Dawes, W., 1998. WAVES - An integrated energy and water balance model. Technical Report No. 31/98, CSIRO Land and Water.

Zhang, L., Dawes, W.R. and Hatton, T.J., 1996. Modelling hydrologic processes using a biophysically based model--application of WAVES to FIFE and HAPEX-MOBILHY. Journal of Hydrology, 185(1-4): 147-169.

Zhang, L., Dawes, W.R., Hatton, T.J., Hume, I.H., O'Connell, M.G., Mitchell, D.C., Milthorp, P.L. and Yee, M., 1999. Estimating episodic recharge under different crop/pasture rotations in the Mallee region. Part 2. Recharge control by agronomic practices. Agricultural Water Management, 42(2): 237-249.

Contact Us
Phone: 1300 363 400
+61 3 9545 2176
Email: enquiries@csiro.au
Web: www.csiro.au

Your CSIRO

Australia is founding its future on science and innovation. Its national science agency, CSIRO, is a powerhouse of ideas, technologies and skills for building prosperity, growth, health and sustainability. It serves governments, industries, business and communities across the nation.